Visualization of the intracellular trafficking of

incoming Adeno-associated virus type 2

Kerstin Lux
aus
Würzburg

2006

Erklärung

Diese Dissertation wurde im Sinne von § 13 Abs. 3 bzw. 4 der Promotionsordnung vom 29. Januar 1998 von Prof. Dr. Michael Hallek betreut und von Prof. Dr. Horst Domdey vor der Fakultät für Chemie und Pharmazie vertreten.

Ehrenwörtliche Versicherung

Diese Dissertation wurde selbständig, ohne unerlaubte Hilfe erarbeitet.

München, am 31.03.06

Kerstin Lux

Dissertation eingereicht am: 03.04.06

1. Gutachter: Prof. Dr. Horst Domdey
2. Gutachter: Prof. Dr. Michael Hallek

Mündliche Prüfung am: 23.05.06

Die vorliegende Arbeit wurde in der Zeit von April 2003 bis März 2006 am Genzentrum der Ludwig-Maximilians-Universität unter der Anleitung von Prof. Dr. Michael Hallek angefertigt.

Im Verlaufe dieser Arbeit wurden folgende Veröffentlichungen angefertigt:

Lux K., Goerlitz N., Schlemminger S., Perabo L., Goldnau D., Endell J., Leike K., Kofler D. M., Finke S., Hallek M., and Büning H. (2005). Green fluorescent protein-tagged adeno-associated virus particles allow the study of cytosolic and nuclear trafficking. *J Virol* 79(18), 11776-87.

Perabo L., Endell J., King S., **Lux K.,** Goldnau D., Hallek M., and Büning H. (2006). Combinatorial engineering of a gene therapy vector: directed evolution of adeno-associated virus. *J Gene Med* 8(2)**,** 155-62.

Büning H., Nieland. J, Perabo L., Goldnau D., **Lux K.,** and Hallek M. (2005). AAV anti-idiotype vaccine. Eingereicht als Erfindungsmeldung

Danksagung

Theorie ist wenn man alles weiß und nichts funktioniert.
Praxis ist wenn alles funktioniert und keiner weiß warum.
Hermann Hesse

Für meine Eltern

Summary

Understanding intracellular vector trafficking is crucial for the improvement of vector design strategies. While mechanisms of vector trafficking might not be of concern when experiments are successful, understanding vector-cell interactions becomes an important focus when gene expression does not reflect the dosage of input vector, or if the host has an unexpected response.

Besides biochemical studies, microscopic techniques are powerful tools for the study of viral infection. Labeling of viral capsids with chemical dyes requires highly pure viral preparations to avoid labeling of contaminating proteins. Since the required level of purity cannot be easily achieved for most retargeting vectors, we aimed to generate GFP tagged AAV capsids.

In this work it is demonstrated that the GFP incorporation into the viral capsid allows the generation of highly infectious GFP tagged particles which behave in cell entry and intracellular trafficking like wt AAV.

Applying FISH analysis and confocal microscopy for detection of the viral genome and the viral capsid, it was observed that only the genomes but no intact viral capsids are delivered into the nucleus. This suggests that uncoating occurs before or during nuclear entry, contradicting the previous model of AAV entry into the host cell. In addition, our data provide first experimental evidence that the phospholipase A2 domain previously identified on the viral capsid might play a role in nuclear entry rather than in endosomal escape of the virus.

In preliminary *in vivo* experiments, GFP tagged AAV could be detected also in infected animal tissue.

The amino acid position 587 which is usually used in our group to insert retargeting peptides does not tolerate larger polypeptides. Since this study revealed that large polypeptides like GFP can be inserted at the N-terminus of VP2, this cloning strategy is sought to be applied for the insertion of larger retargeting polypeptides such as single chain antibodies.

In another set of experiments the amino acid position 453 was found to be another useful retargeting site. Insertion of retargeting peptides at this site yielded viral mutants that were able to transduce target cells with higher efficiency than mutants carrying identical insertions at the 587 position.

1 Introduction

1.1 Adeno-associated Virus

Adeno-associated virus (AAV) was discovered 1965 when different groups described small, uniformly formed, virus like particles which were noticed during electron microscopical examination of simian adenovirus type 15 (SV15) (Atchison et al. 1965). These particles were 18-20 nm in diameter and showed an icosahedral symmetry (Mayor et al. 1965). Staining with acridin orange demonstrated that these particles contained DNA which contributed to the suggestion that those particles are viruses. The particles replicated only in cells that were coinfected with adenovirus. The authors named the particles adeno-associated virus (Atchison et al. 1965).

Today, AAV has been classified as a member of the *Parvoviridae*. With a diameter of only 18 to 30 nm the parvoviruses are among the smallest known viruses (latin: *parvum* = small). Viruses of this family contain a single-stranded DNA genome of approximately 5 kb and a non-enveloped icosahedral capsid. The family of *Parvoviridae* contains two subfamilies the *Densovirinae* which infects invertebrates and the *Parvovirinae* which is specific for vertebrates. These subfamilies are divided into three genera. The subfamily *Parvovirinae* includes the genera Parvovirus, Erythrovirus and Dependovirus. Adeno-associated viruses belong to the Dependovirus genus. Parvovirus B19 is the only human pathogen within the *Parvoviridae* (Erythrovirus genus) and causes Erythema infectiosum, hydrops fetalis and abortion (Brown 2000; Vafaie and Schwartz 2004). All other representatives of this family, including AAV, are not pathogenic for humans (Berns and Linden 1995; Blacklow 1988). On the contrary, AAV seems to be protective against bovine papillomavirus and adenovirus mediated cellular transformation (de la Maza and Carter 1981; Hermonat 1989; Khleif et al. 1991; Mayor et al. 1973) and to have cytotoxic effects in malignant cells (Raj et al. 2001).

In contrast to the Parvovirus and Erythrovirus genus, which are autonomous parvoviruses, AAV replication, and thus a productive infectious life cycle, depends on co-infection with unrelated helper viruses e.g. adenovirus (Ad), herpesvirus (HSV), human cytomegalovirus (HCMV), or papillomavirus (Berns 1990; Muzyczka 1992). In the absence of a helper virus AAV is able to establish a latent form of infection by stably integrating its genome into the the host cell genome. Helper viruses can be

partially replaced by chemical or physical carcinogens (Heilbronn et al. 1985; Yakobson et al. 1987,1989; Yalkinoglu et al. 1991). This leads to the conclusion that helper viruses induce specific changes in the host cell and thereby providing competence for AAV replication.

Until now, 11 serotypes which share different levels of sequence homology, have been identified (Gao et al. 2002, 2004; Mori et al. 2004). AAV1-4 and 6 have been detected as contaminants of adenoviral preparations. AAV5 was isolated from penile condylomata lata (human wart) (Bantel-Schaal and zur Hausen 1984), AAV6 seems to be a recombination between AAV1 and 2 (Xiao et al. 1999). AAV7, AAV8 and AAV9 have been detected in Rhesus monkey, AAV10 and AAV11 in Cynomolgus monkey (Gao et al. 2002, Mori et al. 2004). Sera epidemical studies suggest that AAV2, AAV3 and AAV5 are epidemic in humans, whereas AAV4, 7-11 are endemic in nonhuman primates (Gao et al. 2002). The natural occurrence of AAV1 and AAV6 is not known. Although the other serotypes have attracted increasing attention during recent years, AAV serotype 2 is still the best characterized serotype, being the first isolated and cloned.

1.2 Genome organization of AAV2

Wild type AAV2 contains a single stranded DNA genome of 4679 nucleotides (Srivastava et al. 1983). The genome can be divided into three functional subunits. These are the two open reading frames (ORF) *rep* and *cap* flanked by the inverted terminal repeats (ITR) (Carter and Samulski 2000). It contains three promotors (p5, p19 and p40) and a common polyadenylation signal (Fig. 1). The 5'-ORF *rep* encodes four Rep proteins, a family of multifunctional, non structural proteins. The different Rep proteins are named upon their molecular weight: Rep78, Rep68, Rep52 and Rep40. The larger Rep proteins are controlled from the p5, the smaller Rep proteins from the p19 promotor (Lusby and Berns 1982). Splicing of a common intron leads to Rep68, a splice variant from Rep78, and Rep40 from Rep52. The larger Rep proteins are important for site specific integration, control of replication and transcription (Chejanovsky and Carter 1989; Pereira et al. 1997; Philpott et al. 2002a/b). The smaller Rep proteins seem to be involved in accumulation and packaging of single stranded DNA into the preformed capsid (Dubielzig et al. 1999; King et al. 2001). The Rep proteins can act as transactivator of transcription in presence of helper virus functions and as repressor of

the three viral promotors in absence of helper virus (Kyostio et al.1994; Pereira et al. 1997).

The 3'-ORF *cap* encodes the three capsid proteins VP1, VP2 and VP3, which form the 60 subunits of the viral capsid in a 1:1:8 to 1:1:20 ratio (Kronenberg et al. 2001; Rabinowitz et al. 1999). All three capsid proteins are controlled by the p40 promotor and use the same stop codon. VP2 and VP3 are N terminal truncated variants of VP1. Synthesis of VP1 is regulated by alternative splicing whereas VP2 is initiated from an unusual translation initiation codon (ACG) (Becerra et al. 1985, 1988). The molecular weight of VP1, VP2 and VP3 is 90 kDa, 72 kDa and 60 kDa, respectively. VP3 alone is sufficient for capsid formation, but VP1 is required for viral infection (Warrington et al. 2004). VP2 seems not essential for capsids formation and infectivity (Lux et al. 2005; Warrington et al. 2004). Capsid assembly takes place inside the nucleus (Wistuba et al. 1995, 1997).

The 145bp long ITRs form hairpins of a T-shaped structure which contains Rep binding sites (RBS) and a terminal resolution site (TRS) which is a specific cleavage site for Rep proteins (Im and Muzcyczka 1990; McCarty et al. 1994; Snyder et al. 1990). They serve as origin of replication, contribute to the regulation of gene expression and are important for site specific integration and rescue of the provirus from the human chromosome 19 (Labow and Berns 1988; McLaughlin et al. 1988; Samulski et al. 1987).
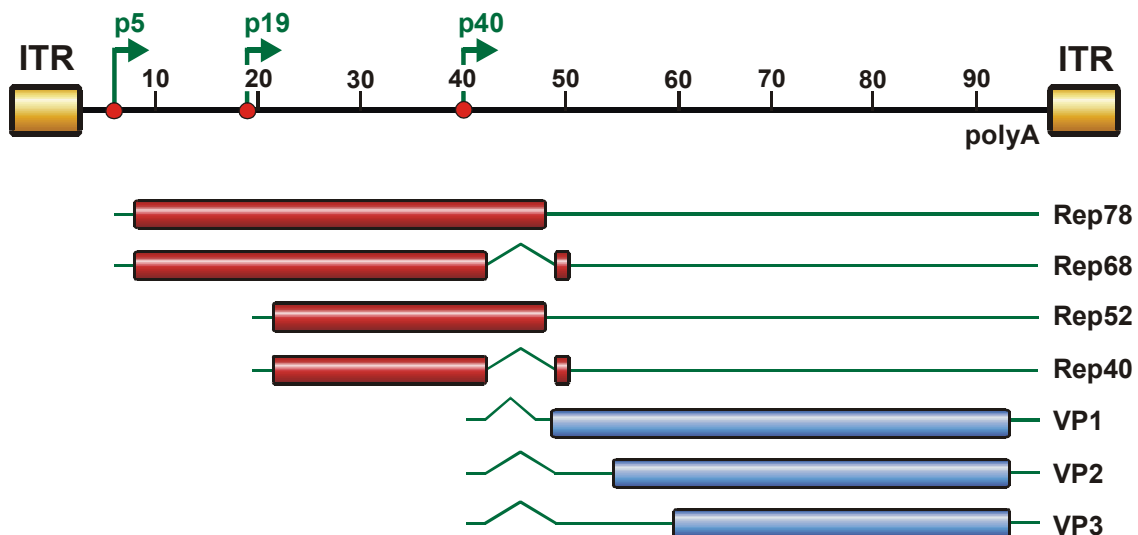
Figure 1. Map of the AAV genome. The AAV genome encompasses 4680 nucleotides, divided into 100 map units. Indicated are the two inverted terminal repeats (ITRs), the three viral promoters at map position 5, 19, and 40 (p5, p19, and p40) and the polyadenylation signal at map position 96 (poly A). The open reading frames are represented

by rectangles, untranslated regions by solid lines and the introns by nicks intercepting the solid lines. Large Rep proteins (Rep78 and Rep68) controlled by the p5 promoter and small Rep proteins (Rep52 and Rep40) driven by the p19 promoter exist in spliced and unspliced isoforms. The *cap* genes encoding the three different capsid proteins VP1, VP2, and VP3 are controlled by the p40 promoter.

1.3 Infectious biology of AAV

1.3.1 Virus cell interaction

Of all the serotypes, AAV2s infectious biology is the best characterized. However, a detailed understanding of intracellular trafficking, endosomal release or viral uncoating is still missing. Moreover, most experiments were performed within the same cell line, the human cervix carcinoma cell line HeLa. The current model of the infection process is depicted in figure 2.

Single Virus Tracing (SVT) studies characterized the motion of AAV2 outside the cell as normal diffusion with a diffusion coefficient of $D = 7.5 \ \mu m^2/s$. Approaching the cell membrane diffusion was decelerated, and finally stopped when AAV gets in contact with the cell membrane with a mean touching time of 62 ms. Most virions show multiple contacts to the cell before entering or being finally released from the cell. In average 4.4 repetitive touching events are observed. It is not clear whether these multiple touching events represent a binding and release process to viral receptors or adsorption to cellular structures (Seisenberger et al. 2001).

Heparan sulfate proteoglycan (HSPG) has been identified as the primary receptor of AAV2 (Summerford and Samulski 1998). HSPG binding residues are located within the VP3 region. 5 amino acids have been identified to be involved in HSPG binding: R484, R487, K532, R585 and R588. Mutational analysis showed that especially R585 and R588 are essential for the interaction with HSPG (Kern et al. 2003; Opie et al. 2003; Wu et al. 2000). Even though HSPG has been described as AAVs attachment receptor, it was shown that AAV2 is able to enter some cells in the absence of HSPG. It was proposed that HSPG is also the primary receptor for AAV3 whereas sialic acid was identified as the attachment receptor for AAV4 and 5 (Rabinowitz et al. 2002; Handa et al. 2000; Kaludov et al. 2001). The primary receptors for the other serotypes are not known yet. In addition to the attachment receptor, secondary receptors are required for viral infection. Three coreceptors have been described for AAV2 so far, fibroblast growth factor receptor I (hFGFR I), $\alpha_v\beta_5$-integrin and hepatocyte growth factor receptor

(HGFR) (Summerford et al. 1999, Qing et al. 1999, Kashiwakura et al. 2005). Human FGFR I was also shown to interact with AAV3 (Blackburn et al. 2006). For hFGFR I a function in enhancing the interaction of virion and HSPG was proposed (Qing et al. 1999). The function of HGFR is not known yet. Integrins are known to transduce signals between extra- and intracellular space. They influence the organization of the cytoskeleton and translate mechanical stimuli into biochemical signals (Blystone et al. 2004; Ingber et al. 2003). Blocking of $\alpha_v\beta_5$-integrin with antibodies can prevent internalization of rAAV2 into HeLa cells. Therefore, it was suggested that binding to $\alpha_v\beta_5$-integrin mediates endocytosis (Sanlioglu et al. 2000). For AAV5 platelet derived growth factor receptor (PDGFR) was identified as coreceptor (Di Pasquale et al. 2003). PDGFR was also discussed to act alone as a receptor for AAV5 because it is in itself a sialo-glycoprotein (Daniel et al. 1987).

1.3.2 Receptor mediated endocytosis of AAV

The endocytotic process was studied for AAV2 and 5. Following receptor binding AAV2 enters the cell by a receptor mediated endocytosis through clathrin coated pits in a dynamin dependent manner (Bartlett et al. 2000, Duan et al. 1999). Endocytosis seems to be a fast process with a half time of 10 min (Bartlett et al. 2000). Single Virus Tracing measurements showed an individual viral uptake even within milliseconds. AAV5 also was localized predominantly in clathrin coated vesicles. However, in rare situations, AAV5 was found to be endocytosed in noncoated vesicles, representing probably caveolae (Bantel-Schaal et al. 2002). Similar to ligand-receptor interaction, it was shown that receptor binding of AAV2 causes intracellular signal transduction. Binding to $\alpha_v\beta_5$ activates (in addition to mediate endocytosis) Rac1, a small GTP binding protein, stimulating thereby phosphoinositol-3 kinase (PI3K) which facilitates the rearrangement of microfilaments and microtubuli (Sanlioglu et al. 2000). Treatment of infected cells with nocodazole, which leads to depolymerization of microtubules, or with cytochalasin B, which disrupts microfilaments, reduces perinuclear accumulation of AAV2 (Sanlioglu et al. 2000).

1.3.3 Endosomal processing of AAV

Intracellular trafficking and endosomal processing are further complex steps which are known to be important for efficient cell transduction. These processes seem to be the rate limiting step in many cell types. For example, AAV2 is endocytosed in polarized

airway epithelial cells from the apical and the basolateral surface. Although the apical in contrast to the basolateral surface does not contain HSPG and $\alpha_v \beta_5$ integrin, only a 3 to 5 fold reduction in endocytosis was detected. However, transduction of cells from the apical surface is reduced >200-fold, indicating that in addition "postendocytotic" barriers exist for AAV mediated gene transfer (Duan et al. 2000). Recently, it was shown that several dependoviruses can penetrate barrier cells (epithelia and endothelia) by transcytosis. This process is cell type and serotype specific. For AAV5 it was shown that this transport pathway is distinct from transduction (Di Pasquale and Chiorini 2005).

Studies evaluating subcellular distribution of AAV2 following infection remain ambiguous and sometimes controversial. It was proposed that AAV2 is already released from the early endosome (Xiao et al. 2002) or might traffic through late endosome compartments (Douar et al. 2001, Hansen et al. 2001a). It was also shown that AAV2 colocalizes with transferrin (Duan et al. 1999). Transferrin is known to be recycled through the perinuclear recycling endosome (PNRE) (Ren et al. 1998, Sonnichsen et al. 2000). Therefore, it was suggested that this compartment might be involved in the processing of AAV. Recently a dose dependent trafficking was described, observing a predominant trafficking of AAV2 to the late endosome at low multiplicities of infection (MOI 100 genomes/cell) and trafficking of AAV2 to the PNRE at high MOI (10^4 genomes/cell). In addition, dose-response curves showed that viral movement through the PNRE is more competent for transgene expression than movement through the late endosome (Ding et al. 2006). Furthermore, it was proposed that AAV2 and 5 localize inside the golgi compartment (Bantel-Schaal et al. 2002, Pajusola et al. 2002).

1.3.4 Endosomal escape of AAV

In addition, to the unsolved question when and where AAV escapes from the endosome, the mechanism of endosomal release is not known. Acidification inside the endosomes seems to be essential in priming AAV for nuclear entry. This assumption is based on the observation that microinjection of AAV2 particles directly into the cytoplasm (instead of natural infection) did not result in gene expression (Ding et al. 2005). The same effect can be reached by the addition of inhibitors of acidification like bafilomycin A1 or ammonium chloride (Bartlett et al. 2000). It might be that this acidification leads to a conformational change inside the viral capsid. Interestingly, it has been shown that the

N-terminal region of VP1 contains a domain resembling secretory phospholipase A2 (sPLA2); a domain that was not known to exist in virus capsids (Zádori et al. 2001). A mutation in the catalytic center of the PLA2 motif of AAV2 causes a dramatic drop in infectivity (Girod et al. 2002). PLA2s are divided into three main types based on their biological properties: secretory Ca^{2+}-dependent PLA2 (sPLA2), cytosolic Ca^{2+}-dependent PLA2 and intracellular Ca^{2+}-independent PLA2. PLA2s are involved in physiological and pathological processes such as lipid membrane metabolism, signal transduction pathways, inflammation and degenerative diseases (Dennis 1997, Kramer and Sharp 1997, Balsinde et al. 1999). PLA2s catalyze the hydrolysis of phospholipid substrates at the 2-acyl ester (sn-2) position to release lysophospholipids and free fatty acids. The N-terminus of VP1 is located inside the AAV2 capsid and was shown to be exposed after heat shock (Kronenberg et al. 2005). This domain might be involved in endosomal escape or nuclear uptake.

1.3.5 Nuclear translocation of AAV

Viral translocation into the nucleus is, in contrast to endocytosis and trafficking to the perinuclear region, a slow and inefficient process. Perinuclear accumulation can be observed from 30 min p.i. on (Bartlett et al. 2000) and persist also many hours after gene expression has already started (Xiao et al. 2002). Only very few information is available about the mechanism of nuclear import. Having a diameter of 25 nm AAV can potentially pass the nuclear pore complex (NPC). However it is not clearly demonstrated whether AAV uses the NPC to enter the nucleus. It was shown that AAV interacts with nucleolin, a nuclear shuttle protein (Qiu et al. 1999). Others have suggested a nuclear entry independent of the NPC (Hansen et al. 2001b). Inside the VP2 region a nuclear localization sequence (NLS) is located which is important for capsid assembly (Hoque et al. 1999) but it is not known whether this NLS has a function for an incoming virus. There are also controversial data about the compartment in which uncoating (release of the viral genome out of the capsid) takes place and whether an intact capsid or only the DNA is shuffled into the nucleus. Some groups detected viral capsids inside the nucleus (Bartlett et al. 2000, Sanlioglu et al. 2000). Xiao and colleagues observed a great difference in the efficiency of nuclear translocation of the viral capsid dependent on presence or absence of a helper virus (Xiao et al. 2002). In the absence of adenovirus, only the viral genome seems to be transported into the nucleus,

while in presence of adenovirus, a shuffling of intact viral capsids into the nucleus was observed. By Single Virus Tracing directed motion (reminding of microtubule dependent movements) of viral capsids inside the nuclear area was observed. They suggested that those particles move inside nuclear invaginations and therefore inside the cytoplasm. Studies with nocodazole which inhibited such directed motions strengthened this hypothesis (Seisenberger et al. 2001). Our own studies showed no efficient transport of intact viral capsids, but of viral genomes into the nucleus independent of the presence of a helper virus. Data were generated by taking advantage of a new confocal microscopic software which allowed a more precise localization of signals within the z axis (Lux et al. 2005). With this method we detected also capsids within nuclear invaginations confirming the hypothesis made by SVT studies.

Another interesting aspect of AAV infection is the enhancement of transduction by proteasome inhibitors. This was shown for several serotypes in different cells (AAV2 (Duan et al. 2000; Yan et al. 2002), AAV1-4 (Hacker et al. 2005), AAV5 (Yan et al. 2002)). An effect of proteasome inhibitors was observed for AAV2 also *in vivo* in some organs from infected mice: Proteasome inhibitors augmented the transduction efficiency in lung from 0 to 10% and liver from 0.5 to 5% whereas inhibitors had no effect on transduction efficiency in muscle and heart muscle (Duan et al. 2000). Furthermore, it was shown that denaturated capsids of AAV2 and AAV5 are ubiquitinated in contrast to intact capsids which were no substrate for ubiquitination (Duan et al. 2000; Yan et al. 2002). This suggests that only AAV capsids that passed the endosomal processing, and thereby underwent a conformational change, are accessible for ubiquitination. (Yan et al. 2002).
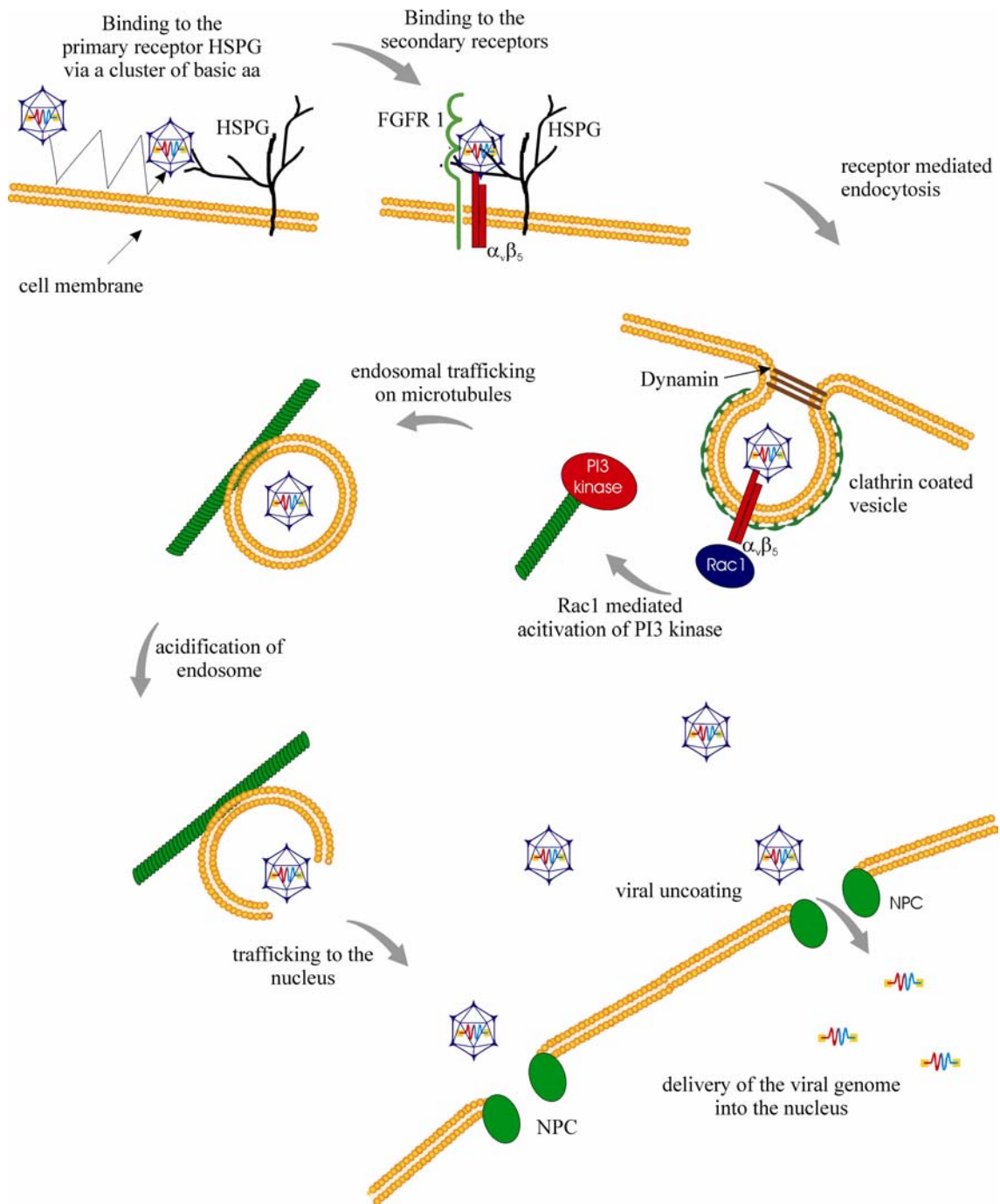
Fig. 2. The AAV infection pathway. AAV touches the membrane several times before entering the cell. Attachment to its primary receptor HSPG and the co-receptors FGFR and $\alpha_v\beta_5$ integrin is triggering a receptor-mediated endocytosis in a dynamin dependent manner into clathrin coated pits. This internalization is facilitated by the activity of Rac1. Activation of Rac1 subsequently stimulates PI3K pathways which regulate endosome trafficking along the cytoskeleton. The exact mechanism of endosomal release is not clear yet. Viral uncoating takes place before or during nuclear entry. Viral DNA enters the nucleus by an unknown mechanism. (Figure modified from Büning et al. 2003.)

1.3.6 Latent or lytic cycle

Upon nuclear entry, the presence or absence of a helper virus determines whether AAV enters a lytic or latent life cycle. In the absence of helper functions AAV enters a latent cycle which leads to integration of the viral genome into chromosome 19q13.3-qter. This locus is called AAVS1 (Kotin et al. 1992). Before viral integration, second strand synthesis and a basal expression of the Rep proteins are activated (Brister and Muzyczka 2000; Redemann et al. 1989). A complex of Rep78 and Rep68 was shown to bind to both, the Rep binding site (RBS) inside the viral ITRs and to a homologous sequence inside the AAVS1 locus, mediating thereby integration (Weitzmann et al. 1994; Linden et al. 1996). After super infection with a helper virus, the integrated genome is activated by entering the lytic cycle, leading to viral gene expression, rescue and replication of the AAV genome with subsequent production of viral progeny (Berns and Giraud 1996).

In the presence of helper virus during AAV infection, induction of gene expression and replication takes place directly.

1.4 Visualization of AAV

Besides conventional biochemical studies, microscopic techniques are emerging as powerful tools for the study of viral infection. A promising development for the investigation of AAV was the finding that viral particles can be labeled by cyanine dyes generating a stable *N*-hydroxysuccinimide (NHS)-ester with amino groups at the capsid surface (Bartlett et al. 2000). However, this labeling method is labor intensive and hampered by the low efficiency of the labeling reaction (on average one dye per capsid) (Seisenberger et al. 2001). High particle numbers need to be used for fluorescence microscopy studies to overcome this problem. This limitation was conquered by a new technique, Single Virus Tracing (SVT), recently described by our group (Seisenberger et al. 2001). This method is based on the detection of single molecules using an epifluorescent microscope and a laser beam as a light source, allowing the real time observation of single virus particles labeled with a single dye inside living cells. Although it is possible to merge the transmitted-light picture of the cell with the virus-tracking movie by the SVT method, a direct co-localization of virions and cellular organelles remains difficult. Additionally, highly pure viral preparations have to be used

to avoid labeling of contaminating proteins. This cannot be easily achieved for many AAV retargeting vectors, since many mutants lose the ability to bind heparan sulphate proteoglycans preventing the use of heparin affinity chromatography for purification.

Therefore, in this work an alternative strategy for the labeling of the AAV capsid by using the enhanced green fluorescent protein (GFP) was developed. GFP has been extensively used as a fusion protein to study intracellular trafficking and localization of proteins. It has an effective chromophore, which absorbs UV or blue light and emits green fluorescence. No further gene products or substrates are needed. Moreover, GFP does not seem to interfere with cell growth and function. GFP fusion proteins thus provide an attractive tool for biological studies including viral tracking (Desai and Person 1998; Elliott and O'Hare 1999; Glotzer et al. 2001; McDonald et al. 2002; Sampaio et al. 2005; Suomalainen et al. 1999; Ward 2004; Warrington et al. 2004).

During the preparation of this work Warrington and colleagues also generated GFP tagged AAV particles. However, their GFP tagged AAV particles showed a more than 10^4 fold reduction of particle to infectivity ratio in contrast to wt AAV (Warrington et al. 2004), which is not desirable if one aims to study mechanisms of viral entry with those particles.

1.5 AAV as a vector for gene therapy

Gene therapy can be defined as the transfer of genetic material into cells of an organism with the aim to cure a disease. There are two major approaches for somatic gene transfer: transfer by viral or non viral vectors (gene gun, lipofection, naked DNA). For the success of gene therapy, safety and efficiency are the most important aspects. There is still no vector system that fulfills both aspects perfectly. Viruses are parasites and have developed strategies to deliver genes into cells through an evolutionary process which leads to expression of these genes. Viral vector systems are generally efficient in transduction of cells but have in general more immunologic or toxic side effects and are often limited in the packaging capacity. In contrast non viral vector systems have no limited coding capacity and are safe, but suffer from low efficiency and selectivity.

The first phase I gene-based clinical trial, in 1990, was dedicated to the treatment of adenosine deaminase deficiency (Blaese et al. 1995). Until now 1145 clinical trials of gene therapy worldwide for the treatment of cancer, inherited or acquired genetic disorders and treatment of cardiovascular diseases or infectious diseases like AIDS have

been accepted. Severe throwbacks show that the ultimate success of gene therapy is not reached yet. Setbacks were caused by the case of Jesse Gelsinger, an ornithine transcarbamylase deficiency (OTCD) patient, who died in 1999 in a gene therapy trial after application of an adenoviral vector in consequence of multiple organ failure which was due to a strong cellular immune response against the vector. Furthermore, cases of leukemia were reported that developed in 3 of 16 X-linked severe combined immunodeficiency (XL-SCID) patients after treatment with retroviral modified hematopoietic precursor cells (Hacein-Bey-Abina et al. 2003). These cases demonstrate, that although remarkable progress has been reached in gene therapy the breakthrough of this treatment will depend on the development of safe and efficient vectors.

AAV has many features that make it attractive for use as a gene therapy vector. An ideal requirement of AAV as a vector system is its nonpathogenicity for humans (Berns and Linden 1995; Blacklow 1988; Blacklow et al. 1968; Blacklow et al. 1971). Moreover, AAV vectors are replication deficient due to the lack of viral genes in the vector genome. Furthermore AAV can transduce a broad variety of dividing and non dividing cells including differentiated tissues as the central nervous system, eye, lung, liver, muscle and haematopoietic system (Fisher et al. 1997; Fisher-Adams et al. 1996; Flannery et al. 1997; Flotte et al. 1993; Kaplitt et al. 1994; Snyder et al. 1997). AAV vectors have the potential to integrate specifically (Huttner et al. 2003) which is an advantage over retroviral vectors which showed the problem of insertional mutagenesis leading to the development of a leukemia-like blood disorder as mentioned above. A promising previous study could show expression of the AAV vector genome after more than one year after AAV application (Fisher et al. 1997). Furthermore, AAV capsids are relatively stable, allowing high titer purification of the virions. Up to 10^{10}-10^{11} infectious particles/ml of rAAV can be produced (Grimm et al. 1999).

But, as any other vector system, AAV also has some disadvantages. One is its low coding capacity. The optimal genome size for AAV vectors is between 4.1 and 4.9 kb (Dong et al. 1996). One major problem is the high prevalence of AAV specific antibodies (Ab) in the human population. 50 to 96% are seropositive for AAV Ab, and 18 to 67.5% of them have neutralizing antibodies, depending on age and ethnic group (Chirmule et al. 1999; Erles et al. 1999; Moskalenko et al. 2000). Animal experiments have shown that neutralizing antibodies greatly reduce or even prevent transgene expression after readministration of the vector (Fisher et al. 1997; Xiao et al. 2000; Xiao

et al. 1996). Thus many people carry antibodies against AAV before a possible gene therapy. The broad host tropism, initially seen as an advantage, is a disadvantage in systemic applications since the specific and selective transduction of respective cells of interest is not possible.

Although still some hurdles have to be overcome, AAV is overall a promising vector for gene therapy. Actually, there are 25 open gene therapy trials utilizing AAV worldwide. Most of them deal with monogenic or cancer diseases.

1.6 Retargeting of AAV vectors

To overcome the problem of low specificity of AAV infection, one main aim of our group is to modify the viral capsids to redirect the interaction of AAV to specific cell receptors. This process is called retargeting. Two approaches have been used to modify the natural tropism of AAV: genetic manipulation of the capsid gene (and therefore the capsid) and chemically cross linking of bifunctional antibodies (Fig. 3).

Pioneer work was done in our laboratory by Anne Girod (Girod et al. 1999). Since at that time the crystal structure of the AAV capsid was not known she did a sequence alignment of the AAV2 VP1 protein with the homologous capsid protein of CPV. Different sites which seemed to be located inside flexible regions at the outer surface of the capsid were tested for the insertion of retargeting peptides. The site of amino acid position 587 showed to be the most promising site for retargeting. This site became the position of choice for insertion of retargeting sequences for many other approaches (Grifman et al. 2001; Nicklin et al. 2001; Ried et al. 2002, Shi et al. 2001; Perabo et al. 2003, 2006).

Insertion of larger polypeptides inside the 587 position resulted in a markedly reduced packaging efficiency. Although still having to be proven as an efficient position for the insertion of targeting peptides, the N-terminus of VP2 (amino acid position 138) seem to be the most promising insertion site for larger peptides (Yang et al. 1998; Warrington et al. 2004; Lux et al. 2005).

In the approach of indirect targeting a linker module is used to mediate the interaction between cell and viral capsid. The interaction between virus and cell can be mediated by bispecific antibodies. To generate an universal targeting vector an immunoglobulin binding domain (Z34C) was inserted at the 587 position which enables the capsid to bind different antibodies via their Fc regions (Ried et al. 2002).
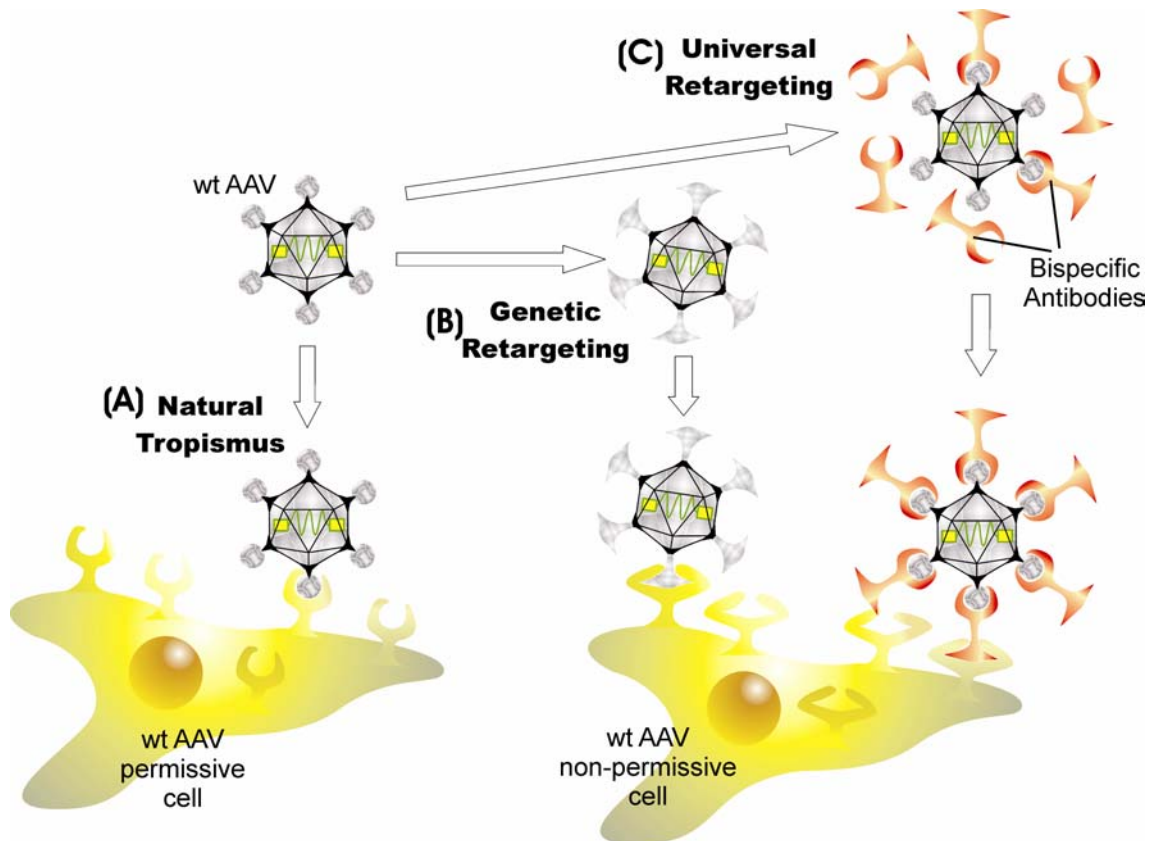
Fig. 3. Targeting strategies. Using wt tropism (A), AAV binds directly via structural motifs of the capsid to the cellular receptor. Retargeting can be mediated by a ligand which is genetically inserted into the capsid (B) or by interaction between cell and virus mediated by an associated molecule (e.g a bispecific antibody) (C).

1.7 Adenovirus free production of wt AAV and recombinant AAV vectors (rAAV)

For the production of wt AAV vectors two different plasmids are needed. The wt AAV plasmid encoding *rep* and *cap* flanked by the ITRs and an adenoviral helper plasmid coding for essential adenoviral helper genes (E2a, E4 and VA) but lacking the adenoviral structural genes (Collaco et al. 1999; Grimm and Kleinschmidt 1999; Xiao et al. 1998) (Fig. 4A). Both plasmids are transfected into 293 cells. AAV viral progeny can be harvested 48 h post transfection from the cell lysates and purified to high titers by either by gradient centrifugation (CsCl, Iodixanol) and/or column chromatography (Zolotukhin et al. 1999) (Fig. 4B).

For the generation of recombinant AAV vectors (rAAV) *rep* and *cap* are deleted, leaving only the ITR sequences of the parental virus, which are the only *cis* elements required for the production of viral particles (replication and packaging). The rep/cap

sequence can then be replaced by a marker gene (e.g. GFP) or a therapeutic gene. For the production of rAAV vectors *rep* and *cap* have to be submitted *in trans* cloned into a "helper plasmid"(Fig. 4A). In consequence, when generating rAAV, a triple transfection has to be performed: transfection of the vector plasmid (transgene flanked by the ITRs), the rep/cap (RC) helper plasmid and the adenoviral helper plasmid (Fig. 4C).

For the production of modified virions, mutations are introduced into the cap gene of wt plasmid if the wt genome is to be packaged or into the helper plasmid if a transgene is to be packaged.

A

B

C
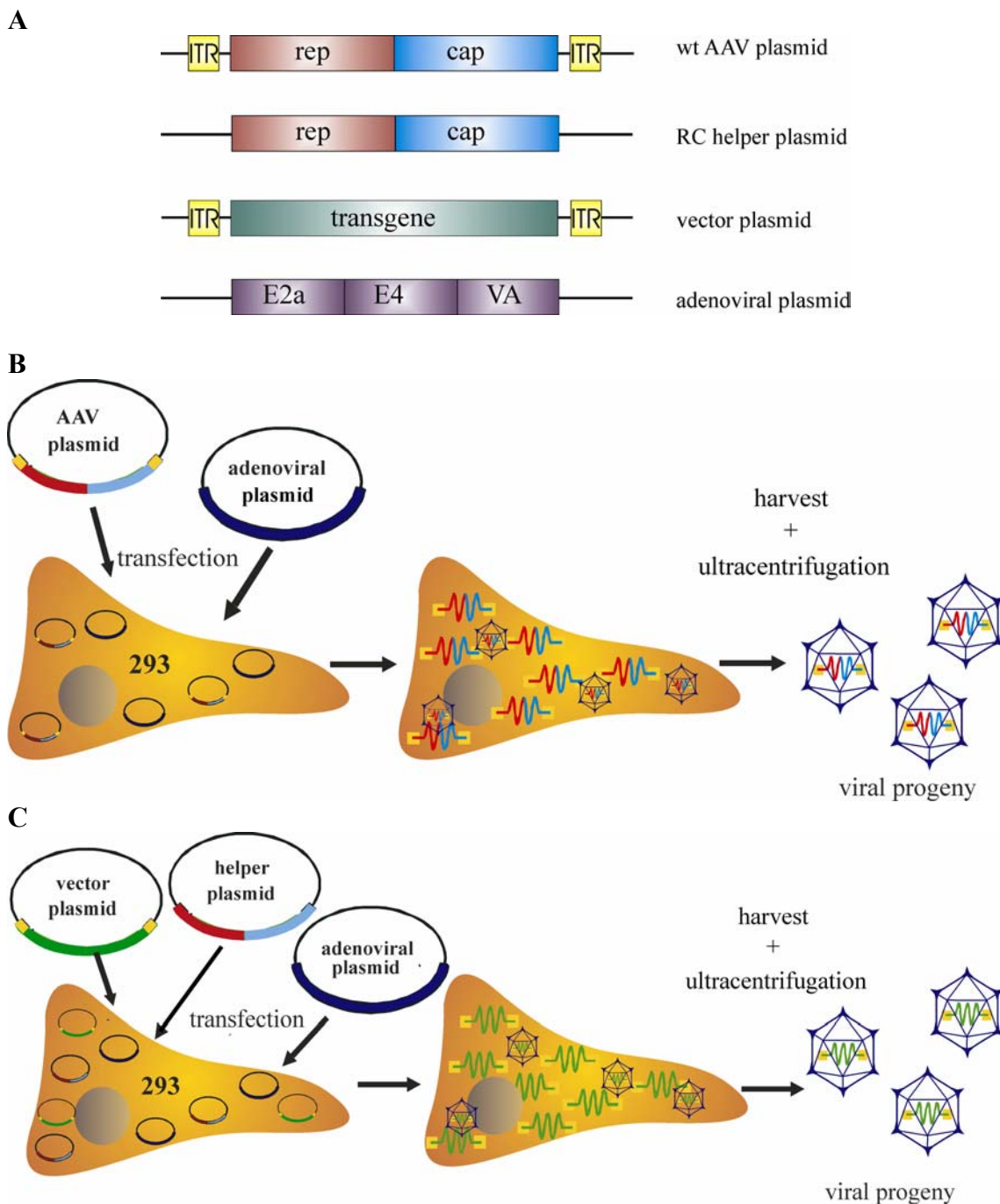
Figure 4. Packaging of AAV. (A) Plasmid constructs used for packaging of AAV. In contrast to the wild type AAV plasmid, which contains the viral *rep* and *cap* gene and the ITRs, the vector plasmid is devoid of all viral genes. Only the ITRs are left which flank the transgene and serve as packaging signal. The RC helper plasmid provides the regulatory (Rep) and the capsid proteins (Cap) required for replication of the ITR flanked transgene cassette and packaging into preformed capsids. The Ad helper plasmid codes for the adenoviral helper genes E2a, E4 and VA. For packaging of wt AAV (B) wt AAV plasmid and adenoviral helper plasmid are transfected into 293 cells; for packaging recombinant AAV (C) vector plasmid, RC helper plasmid, and adenoviral helper plasmid are transfected into 293 cells. After replication and assembly of viral particles cells are lysed and AAV virions are harvested and purified by iodixanol gradient centrifugation (B and C).

1.8 Aim of this work

As AAV has no clinical relevance because of its non pathogenicity in human, there was no great effort to elucidate its infectious biology. An increased interest for the understanding of AAV infectious biology has emerged as adeno-associated viruses have gained attention as a gene therapy vector in the last decade. While cell entry can be modified successfully by retargeting, it was shown that different post entry steps can limit AAV transduction of many cell types. Retargeting ligand insertions in the viral capsid could cause differences not only in cell entry but also in intracellular processing of these vectors in comparison to wt AAV. Understanding AAV infectious biology is essential to improve safety and efficiency of such vectors for the treatment of acquired and inherited diseases.

Visualization of several viruses by fluorescent proteins facilitated the investigation of different viral mechanisms. Our group has previously employed anorganic cyanine dyes to label the capsid and visualize viral entry of AAV. As this method is hampered in specific applications, for example the purity of viral preparations needed for chemical labeling cannot be easily achieved for many targeting vectors, an alternative labeling method was desirable. The aim of this work was to develop a novel and convenient technology to visualize the infectious pathway of AAV inside fixed or living cells. Therefore, enhanced green fluorescent protein (EGFP) was introduced into AAV particles by fusing it to the capsid protein VP2. Such modified capsids were characterized by detailed testing for capsid integrity, packaging, infectivity and trafficking in comparison to unmodified AAV capsids. In addition, we applied different imaging technologies (e.g. confocal microscopy and FISH) to investigate nuclear entry of AAV.

2 Results

2.1 Green fluorescent protein-tagged adeno-associated virus particles allow the study of cytosolic and nuclear trafficking

2.1.1 GFP fusion does not interfere with nuclear translocation of VP2

The enhanced green fluorescent protein (GFP) has been widely used as a fusion protein to monitor the cellular localizations of proteins (Chalfie et al. 1994). However, it is a relatively large protein for being inserted into a compact structure such as the AAV capsid. Based on the observation that large insertions are tolerated at the N-terminus of VP2 (Yang et al. 1998), we decided to generate a GFP-VP2 fusion protein to incorporate a fluorescent marker into the AAV capsid. For this purpose, the VP2 ORF was amplified by PCR and fused to the C-terminus of the GFP open reading frame (Fig. 5), with the human cytomegalovirus (CMV) promoter controlling transcription. To avoid translation from the natural VP2 start codon, the translation start codon was deleted.

To test the biological properties of this GFP-VP2 fusion protein, transient transfections of HeLa cells with pGFP-VP2 were carried out. As a control, HeLa cells were transfected with a GFP expressing plasmid lacking any known organelle homing signals (Ried et al. 2002). 48 h post transfection, cells were fixed and the nuclear lamina stained with an anti-lamin B antibody. Since VP2 contained a nuclear localization sequence (Hoque et al. 1999), GFP-VP2 was expected to be detectable in the nucleus, whereas the GFP lacking homing signals should be distributed throughout the whole cell. Figure 6 shows that this was indeed the case, allowing to conclude that the GFP fusion does not hamper the nuclear localization VP2.
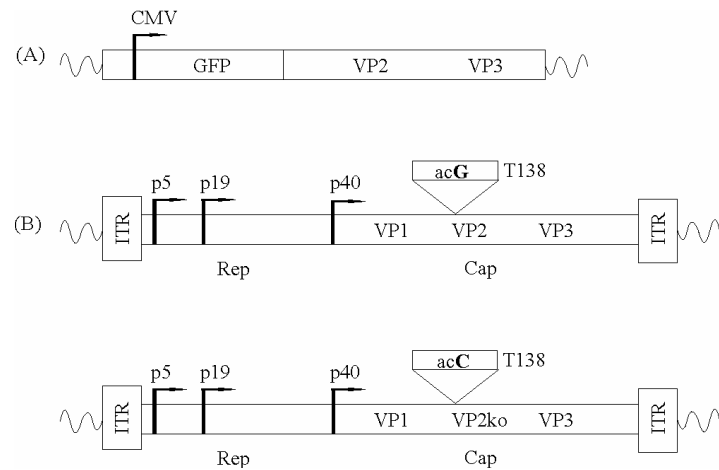
Fig. 5. Schematic representation of the plasmids. (A) The plasmid pGFP-VP2 encodes the GFP-VP2 fusion protein. VP2 was amplified by PCR from pUC-AV2 and cloned into the multiple cloning site of pEGFP-C3 (Clontech). During this step, the VP2 start codon was deleted. (B) To produce wild type AAV the plasmid pUC-AV2 was used (upper panel). A G-to-C substitution within the wobble position of the VP2 start codon (T138) was introduced, resulting in the plasmid pUC-AV2-VP2k.o. (lower panel). Due to the substitution, VP2 expression was abolished without altering the amino acid sequence of VP1.
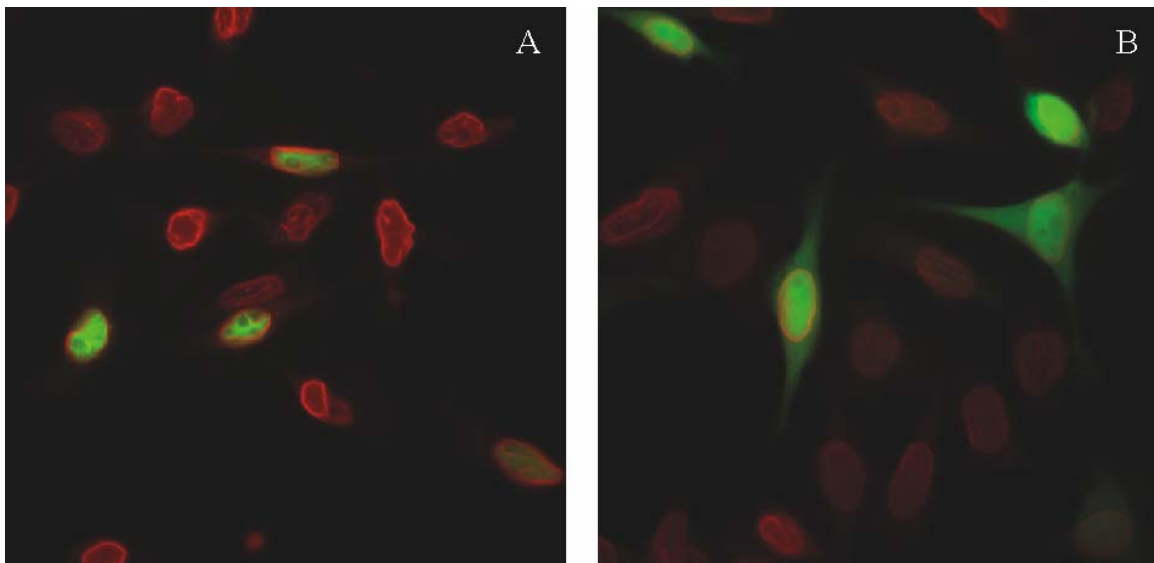
Fig. 6. Transient transfection of HeLa cells with GFP-VP2 and GFP expressing plasmids. Cells were transfected at 80% confluence with pGFP-VP2 (A) or pGFP (B) and fixed 48 h post transfection. The nuclear lamina was stained with Texas Red conjugated anti-lamin B antibody.

2.1.2 Substitution of VP2 by GFP-VP2 fusion protein results in infectious virions

In a prior study, scFv-VP2 fusion proteins used to generate viral particles resulted in viral progeny only when all three wild type AAV capsid proteins were provided during the packaging process (Yang et al. 1998). Since the GFP insertion was of similar size as scFv, we assumed that all three unmodified wild type capsid proteins had to be provided during the packaging process to obtain infectious GFP-tagged viral particles. The first step was therefore to determine the amount of VP2 which could be substituted by GFP-VP2 without interfering with the production of infectious AAV particles. We tested a 30% and 60% substitution of pUC-AV2 (coding for the AAV genome) by pGFP-VP2 during packaging. The viral preparations generated were named 30%-GFP-VP2-AAV and 60%-GFP-VP2-AAV, respectively. Wild type AAV was used as control. 48 h post transfection virus producing cells were harvested and cell lysates were purified by iodixanol step gradients. The 25% and the 40% phase of the gradient were harvested and genomic and capsid titers were determined. DNA containing viral particles with comparable titers were detected for the different viral preparations (25%-phase of the gradient: $2\text{-}5\text{x}10^{10}$/ml; 40%-phase of the gradient: $0.5\text{-}1\text{x}10^{11}$/ml). The amount of intact capsids was determined by ELISA using the anti-capsid antibody A20 (Wobus et al. 2000). As expected, a higher amount of empty capsids was obtained in the 25%-phase of the gradient. However, all the capsid titers showed comparable values (25%-phase of the gradient: $5\text{-}8\text{x}10^{13}$/ml; 40%-phase of the gradient: $0.4\text{-}1\text{x}10^{13}$/ml). Thus, neither capsid assembly nor DNA packaging was affected in the 30%- and the 60%-GFP-VP2-AAV preparations in comparison to the wild type control.

To investigate, if the GFP-VP2 fusion proteins were inserted into the AAV capsid and if the GFP-tagged virions retained infectivity, HeLa cells were incubated with the 30%- and 60%-GFP-VP2-AAV preparations, respectively. 2 h p.i. cells were washed intensively, detached from the plate by trypsin treatment and analyzed by flow cytometry. Treatment with trypsin removes all the proteins bound at the cell surface (Awedikian et al. 2005; Mizukami et al. 1996), thus only intracellular GFP signals should be detected. GFP positive cells were obtained in samples infected with both preparations. The highest amount of GFP positive cells (19.5%) was obtained with 60%-GFP-VP2-AAV, whereas 13.5% GFP positive cells were detected using the same amount of capsids of 30%-GFP-VP2-AAV. In contrast, no green cells were detected

when wild type AAV was used. To exclude pseudo-transduction, heparin inhibition controls were included. Heparin, a soluble analogue of the primary AAV receptor heparan sulphate proteoglycan (HSPG), blocks wild type AAV infection by binding to the viral capsid. Since the HSPG binding region of AAV is located in the VP3 region of the capsid proteins (Wu et al. 2000), the ability to bind to these molecules should be retained by the GFP-tagged virions. Incubation of both viral preparations with heparin inhibited cell transduction indicating that a viral infection and not pseudo-transduction was responsible for the GFP signal measured in the GFP-VP2-AAV infected cells.

These results demonstrate that GFP fusion proteins were incorporated into the AAV capsid of infectious virions and that the GFP signal provided by GFP-tagged virions was detectable by flow cytometry.

2.1.3 Production of GFP tagged AAV virions in the absence of wild type VP2

Since comparable titers were obtained for the 30%-GFP-VP2-AAV and the 60%-GFP-VP2-AAV preparations, we investigated the possibility to package a 100%-GFP-VP2-AAV preparation. A wild type AAV encoding plasmid containing a VP2 start codon mutation was generated (pUC-AV-VP2k.o.; Figure 5) and used to package 100%-GFP-VP2-AAV. In addition "VP1/VP3 only particles" (VP2 k.o.-AAV), 60%-GFP-VP2-AAV and wild type AAV were produced and purified by density gradient centrifugation. First, a Western blot analysis of our different preparations was performed (Fig. 7). Although only virions isolated from the 40% phase of the iodixanol gradient were used for the following studies, also the 25% phase of the gradient was analyzed by Western blot. For wild type AAV we obtained three signals corresponding to VP1, VP2 and VP3 (Fig. 7, lane 1) in a ratio of approximately 1:1:20. As expected, VP2 k.o.-AAV contained only VP1 and VP3 proteins (lane 2 and 3), whereas in the 100%-GFP-VP2-AAV preparation the GFP-VP2 fusion protein, VP1 and VP3 were detected (lane 4). The 60%-GFP-VP2-AAV was packaged in the presence of all three unmodified AAV capsid proteins; four protein bands (GFP-VP2, VP1, VP2 and VP3) were visible (lane 6).

Further, we performed a detailed titer analysis. Therefore, each virus mutant was packaged at least a second time. The capsid, genomic and infectious titers of these preparations were determined and empty-to-full and genomic particle-to-infectivity ratios were calculated to directly compare the different preparations for packaging efficiency and infectivity (Tab. 1). No significant difference between mutants (including wild type) was observed for genomic nor capsid titers which ranged between 1.3×10^{11} and 1.5×10^{12}, and 7.35×10^{12} and 1.36×10^{13} per ml, respectively. The ratios of empty-to-full capsids varied to nearly the same extent for different preparations of the same virus mutant (including wild type) as between the different mutants. This reveals that the deletion of VP2 or the substitution by GFP-VP2 does not interfere with capsid formation or viral genome packaging. The genomic particle-to-infectivity ratios were slightly increased for VP2 k.o.- and the 100%-GFP-VP2-AAV-preparations, but remained within the variation described for wild type AAV preparations (Girod et al. 1999; Grimm et al. 1999; Ried et al. 2002).

The results revealed that GFP-tagged virions with a 100 % substitution of VP2 by GFP-VP2 can be generated with high titers (2×10^9 infectious particles/ml).
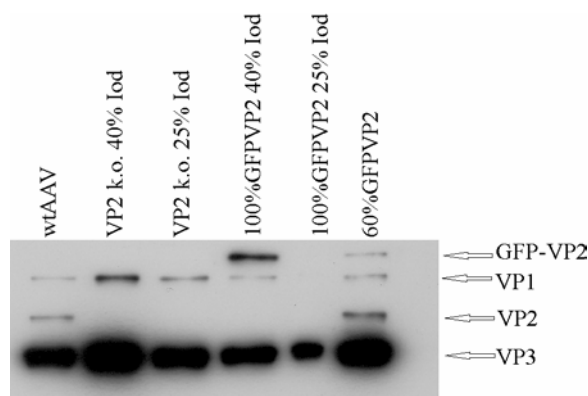
Fig. 7. Western blot analysis of iodixanol gradient purified AAV capsids. After iodixanol gradient centrifugation same amount of viral capsids (10^{10}) of wild type AAV (lane 1; 40% phase of iodixanol gradient), VP2 k.o.-AAV (lane 2: 40% phase of iodixanol gradient; lane 3: 25% phase of iodixanol gradient), 100%-GFP-VP2-AAV (lane 4: 40% phase of iodixanol gradient; lane 5: 25% phase of iodixanol gradient) and 60%-GFP-VP2-AAV (lane 7; 40% phase of iodixanol gradient) were separated by SDS-10% polyacrylamide gel electrophoresis and analyzed by Western blot using the B1 antibody.

TABLE 1. Characterization of the different viral preparations

Preparation[d]	Genomic particles/ml	Physical particles/ml	Infectious particles/ml	Empty/full ratio	Genomic particle/ infectivity ratio
Wild type AAV[a]	2.49×10^{11}	1.25×10^{13}	8.38×10^{9}	50.2	29
Wild type AAV[b]	1.04×10^{12}	1.19×10^{13}	1.67×10^{10}	11.4	62
VP2 k.o.-AAV[a]	1.30×10^{11}	9.39×10^{12}	1.31×10^{8}	72.2	991
VP2 k.o.-AAV[b]	1.17×10^{12}	1.41×10^{13}	4.19×10^{9}	12.1	278
60% GFP-VP2-AAV[a]	7.01×10^{11}	1.04×10^{13}	8.39×10^{9}	14.8	84
60% GFP-VP2-AAV[b]	2.15×10^{11}	1.25×10^{13}	2.10×10^{9}	58.1	102
60% GFP-VP2-AAV[c]	4.10×10^{11}	7.35×10^{12}	2.10×10^{9}	17.9	195
100% GFP-VP2-AAV[a]	3.00×10^{11}	1.36×10^{13}	1.31×10^{8}	45.3	2,288
100% GFP-VP2-AAV[b]	4.39×10^{11}	9.71×10^{12}	2.10×10^{9}	22.2	208
100% GFP-VP2-AAV[c]	1.50×10^{11}	1.09×10^{13}	1.05×10^{9}	7.2	1,431

[d] Titers were determined by quantitative PCR, A20 ELISA, and infectious titer assay, respectively (*a*, *b*, and *c* indicate viral preparations that were independently packaged)

2.1.4 Visualization of viral infection by GFP-VP2 tagged AAV particles

To determine, if GFP-tagged virions were suited for intracellular visualization, viral infections of HeLa cells followed by wide field fluorescent microscopic analysis 2 h p.i. were performed. GFP signals seemed to localize partly in the nucleus or perinuclear area in cells infected with the 60%- and 100%-GFP-VP2-AAV preparations (Fig. 8A and Fig. 8B). The fluorescent microscopy images obtained thus resembled published results with unlabeled or chemically labeled virions (Bartlett et al. 2000; Xiao et al. 2002). No signal was detected inside the cell when soluble heparin was used, demonstrating that the GFP signal was not due to pseudo-transduction (Fig. 8C).

A promising development in the field of fluorescent microscopy is live cell imaging. Infection of live HeLa cells with GFP-tagged AAV virions followed by live cell imaging microscopy allowed the visualization of virions undergoing cell membrane contact (Fig. 9 and movie 1 in supplement). Some of these virions touched the cell membrane multiple times similar to the observations, made previously by SVT (Seisenberger et al. 2001). As observed in fluorescent microscopy, most of the virions stacked to the membrane, again confirming previous SVT observations, which showed

that less than half of the virions enter the cell (Seisenberger et al. 2001). Furthermore, GFP-tagged virions seem to move inside the cytoplasm of infected cells and in the perinuclear area (Fig. 9 and movie 1 in supplement), suggesting the potential of this technology for real-time imaging studies.
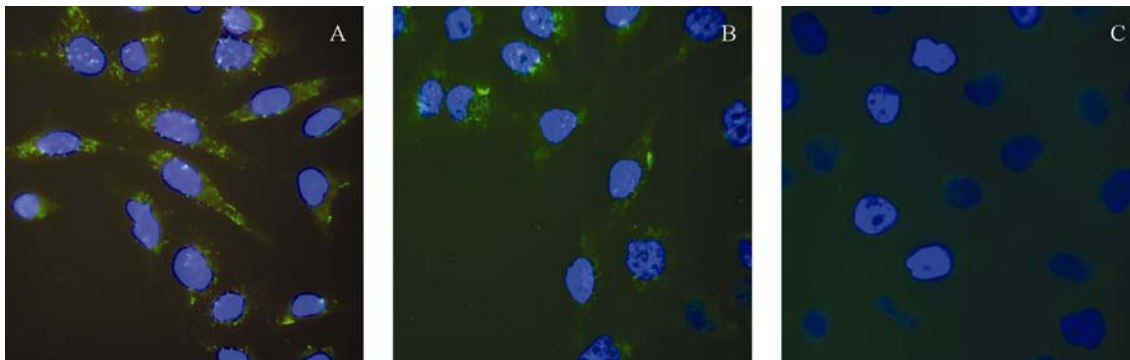
Fig. 8. GFP-tagged virions analyzed by wide field fluorescent microscopy. Cells were infected with 5×10^6 capsids per cell of 100%-GFP-VP2-AAV (A) and 60%-GFP-VP2-AAV (B and C) in the absence (A and B) or presence of heparin (C). Cells were fixed and nuclei were stained with Dapi.
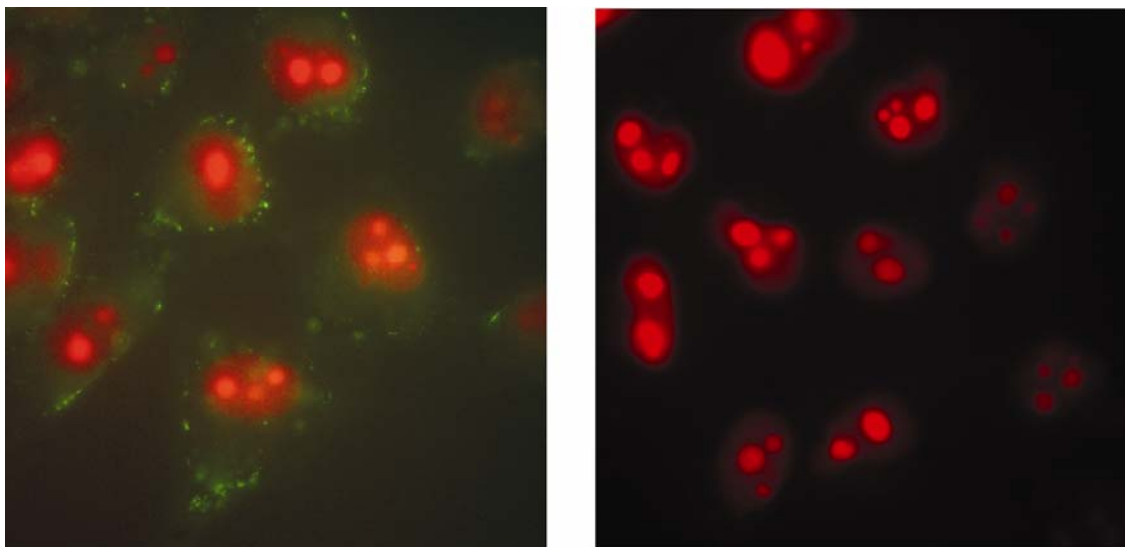
Fig. 9. Live cell imaging of GFP-tagged virions. HeLa-DsRed2Nuc cells were infected with 60%-GFP-VP2-AAV (10^6 capsids per cell). Cells were incubated for 20 min at 37°C and 5% CO_2. Then live cell movies were obtained under physiological conditions. (Left) The still image shown here was obtained from the movie 1 supplied in the supplemental material; (right) heparin control.

2.1.5 GFP-tagged virions within the cell are recognized by A20

To assess if the GFP signals within the cell are emitted from intact viral particles, cells were infected with 100%-GFP-AAV and fixed at 2, 4, 11 and 24 h p.i. Intact viral capsid were stained by A20 (A20 recognizes whole but not dissociated AAV capsids

(Bleker et al. 2005)) whereas an anti-lamin B antibody was used to visualize the nuclear membrane. Figure 10 shows one example obtained by confocal microscopy. GFP-tagged AAV particles recognized by A20 were detected within the cell and above the nuclear membrane. An almost 100% colocalization of the GFP-signals (Fig. 10, upper left) with A20 reactive AAV capsids (upper right) was observed (merge data are shown in Fig. 10, lower right). The few detectable non-colocalized signals were due to a very faint A20 signal which became visible after enhancing its excitation energy. Thus GFP signals visible within the cells emanate from intact virions.
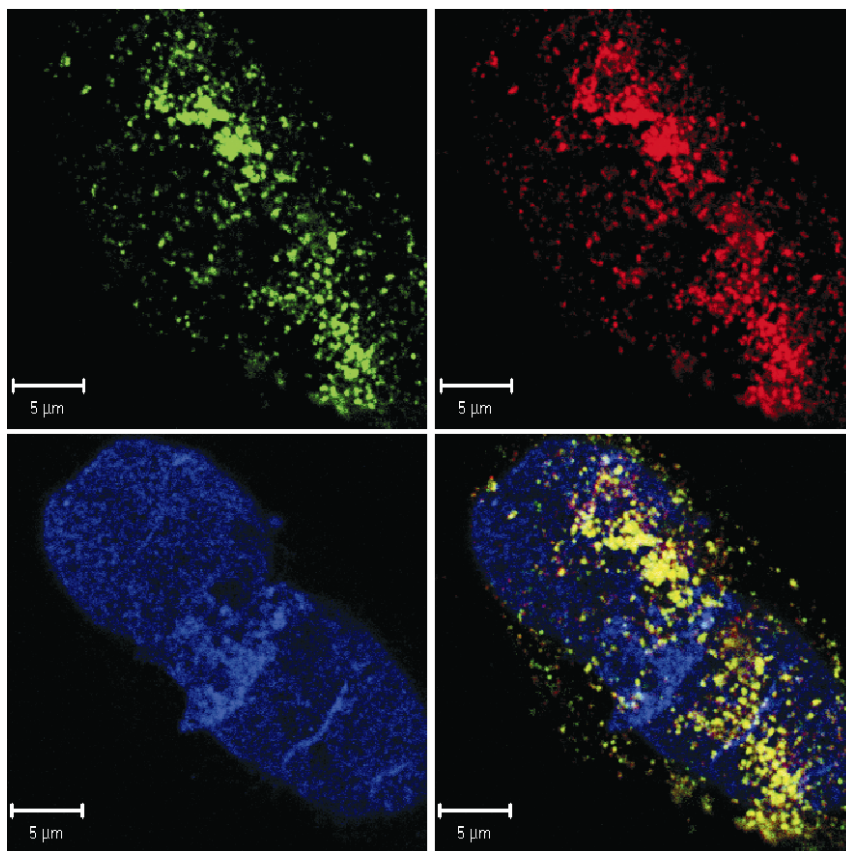
Fig. 10. Intact 100%-GFP-VP2-AAV particles within the cell. HeLa cells were infected with 100%-GFP-VP2-AAV (10^6 capsids per cell). At 4 h p.i., cells were fixed and stained with A20 (recognizes intact AAV capsids; RRX conjugated secondary antibody) and anti-lamin B antibody (nuclear membrane; Cy5 conjugated secondary antibody). (upper left panel: GFP staining; upper right panel: A20 staining; lower left panel: anti-lamin B; lower right panel: merge). Analysis was performed by confocal microscopy.

2.1.6 Viral capsids do not enter the nucleus efficiently

In order to analyze the time course of nuclear entry of AAV in more detail, HeLa cells were infected with 100%-GFP-VP2-AAV for 2, 4, 11 and 24 h with or without adenovirus type 5 coinfection (MOI of 5), and confocal laser scanning images were obtained. For each image, a series of horizontal sections was prepared by taking images each 0.2 μm (z-stack) and superimposed with the Leica confocal software. Figure 11B shows a typical image obtained 4 p.i. without adenovirus coinfection. Many GFP signals were visible in the nucleus of the infected cells (nuclear lamina stained in red by anti-lamin B antibody). This image leads to the assumption that GFP-tagged virions were efficiently transported into the nucleus in less than 4 hours, consistent with published results (Bartlett et al. 2000). However, the Leica confocal software enables the vertical sectioning of the superimposed pictures and allows to visualize a certain image plane within this stack. The investigator can determine if a certain signal emanates within, above or below the image plane and this enables the investigator to localize the object of interest more precisely. Using this technique, we could determine that in the absence of helper virus and up to 4 h p.i., the GFP signals (from the GFP-tagged virions) were localized above but not within the nucleus (Fig. 11C, top row). This is in contrast to results derived from the superimposed picture (Fig. 11B) indicating its limitations. At 24 h p.i. isolated signals were visible inside the nucleus (of Fig. 11C, arrows in top rows).

Moreover, in the superimposed picture of cells coinfected with adenovirus many GFP signals were observed in the nucleus 2 h p.i. Applying the new vertical sectioning method uncovered that most of the signals are localized above the nucleus (Fig. 11C, buttom row). With prolonged incubation time, the amount of coinfected cells showing a GFP signal inside the nucleus slightly increased (e.g. 4 h p.i.), but still the majority of signals were found outside the nucleus. Even after prolonged incubation (up to 11 h, data not shown) more than 90% of the GFP signals remained outside the nucleus.

Interestingly, 24 h p.i. many coinfected cells showed a diffused GFP distribution within the nucleus. This phenomenon was not observed in the absence of helper virus coinfection even after prolonged observation times (48 h, data not shown). Since this image resembles the image obtained after transfection with pGFP-VP2 (Fig. 11D), we analyzed the viral preparations used to infect the cells and the respective viral infected

cells by PCR. These analyses revealed that GFP sequences were packaged into the viral capsid, although the plasmid used to express GFP-VP2 during the packaging process contained no AAV inverted terminal repeats. It remains to be elucidated whether this is attributed to recombination or other events.
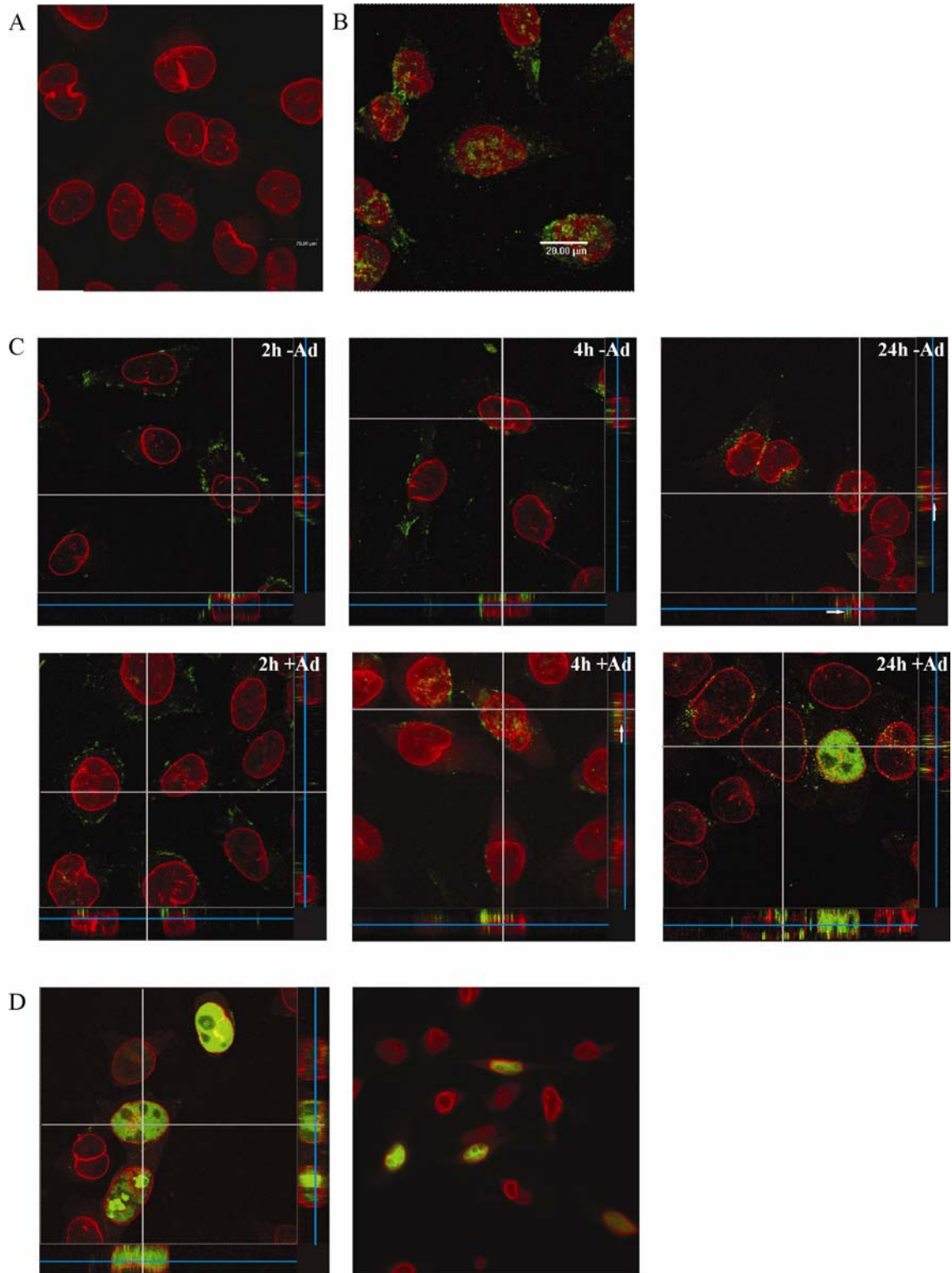
Fig. 11. Time course of AAV infection visualized by GFP-tagged AAV virions. HeLa cells were infected with 10^6 capsids per cell of 100%-GFP-VP2-AAV with or without adenovirus type 5 (MOI of 5) coinfection. In addition, a heparin control was included (A). At 2, 4 and 24 h p.i., cells were fixed and the nuclear lamina was stained with TexasRed conjugated anti-lamin B antibody. A series of horizontal sections (each 0.2 μm one image) were obtained for each image. With Leica confocal software all images of a series were superimposed. (B) Superimposed image of a series of sections 4 h p.i. in the absence of adenoviral coinfection. (C) Time course of infection with and without adenovirus (Ad5) coinfection. The square image of each panel shows one horizontal section of the stack. The vertical sections of the stack are depicted on the right and bottom of each panel. Arrows show GFP signals detected within the nucleus. (D) Comparison of images obtained 24 h p.i. in the presence of adenovirus (left) and after transfection of pGFP-VP2 (right).

To exclude that the observed results are due to inefficient nuclear transport of the GFP-tagged virions, the same experiments were performed with wild type AAV in Ad5 coinfected cells. For detection of viral capsids and viral capsid proteins A20- and B1-antibodies were used, respectively. A20 recognizes intact but not dissociated AAV capsids whereas B1 binds to amino acid 726-733 at the C-terminus of all 3 capsid proteins (Bleker et al. 2005). At 2, 4 and 11 h p.i. almost no B1 staining was detectable, in marked contrast to A20 staining (data not shown). At 4 and 11 h p.i., no difference was observed when comparing GFP-tagged with wild type virions (for an example at 11 h p.i., see Fig. 14B). At these time points only isolated intact capsids (recognized by A20) were found within the nucleus and the majority (over 90%) of the virions were visible outside the nucleus (Fig. 14B). At 24 h p.i. both antibodies were able to recognize their targets and resulted mainly in a nuclear staining (data not shown). This suggests that at this time point, new viral capsid proteins have been synthesized in the Ad5 coinfected cells and new capsids have been formed.

From this we propose that an adenoviral function augments the nuclear translocation of viral capsids. However, the low level of GFP or A20 signals detected within the nucleus suggests a very inefficient nuclear translocation. Thus, uncoating seems to occur before or during nuclear entry.

To further investigate this hypothesis, HeLa cells were infected by wild type AAV using 10x less virions per cell. Infections were performed with and without helper virus. Since viral replication in adenovirus coinfected cells is reported to start between 8 and 12 h p.i. (Mouw and Pintel 2000; Xiao et al. 2002), infections were stopped at 2, 4, and 11 h p.i. To visualize viral genomes FISH hybridization was performed. In addition, viral capsids and the nuclear lamina were stained by antibodies (Fig. 12A and 12B).

Viral genomes were detectable outside and within the nucleus at 11 p.i. (Fig. 12A and arrows in Fig. 12B). No colocalization of viral genomes and intact viral capsids was observed within the nucleus, whereas colocalizations were detectable in the perinuclear area and within the cytoplasm (red signals in Fig. 12A and in the merged image indicate intact capsids recognized by A20). In addition, empty capsids (no colocalization) were visible in the perinuclear area. Some of the FISH signals in the perinuclear area showed no colocalization with A20 and therefore with intact capsids. It has yet to be investigated if these signals emanate from free viral genomes or if they colocalize with one of the three VP proteins. The same image was obtained using a comparable amount of viral genomes in the absence of adenovirus, revealing that the observed viral genomes originate from incoming virions and are not the result of viral replication. Furthermore, it allows the assumption that a nearly comparable nuclear transport of viral genomes occurs with or without helper virus. Interestingly, viral genomes within the nucleus are already detectable at earlier time points (2 and 4 h p.i.) both in the presence and absence of Ad5 although 10x less virions per cell were used than for the capsid studies (Fig. 11 and 14). Under these conditions (10^5 instead of 10^6 capsids per cell) viral capsids are detected within the cell, but none of these localize within the nucleus (Fig. 12B).

To investigate if the viral DNA enters the nucleus naked or still associated to viral capsid fragments or one of the NLS containing VP proteins (VP1 and VP2), the same experiment was carried but using the B1 antibody instead of A20 to detect single viral capsid proteins. B1 recognizes the C-terminus of the three capsid proteins, which is thought to be buried within the intact capsid. Therefore, B1 recognizes only capsid fragments or single capsid proteins. No B1 signals whether outside nor inside the nucleus were detected (data not shown). This is still only a hint and no evidence for the hypothesis that complete uncoating takes place before entering the nucleus, since the failure of detection of B1 signals could be due to a sensitivity problem of detection of single proteins. Further investigations are ongoing at the moment.

However, all our current results strongly support the hypothesis that uncoating of AAV occurs during or before nuclear entry. However, at the current state it cannot be excluded that viral genomes within the nucleus are associated with one of the three viral capsid proteins.
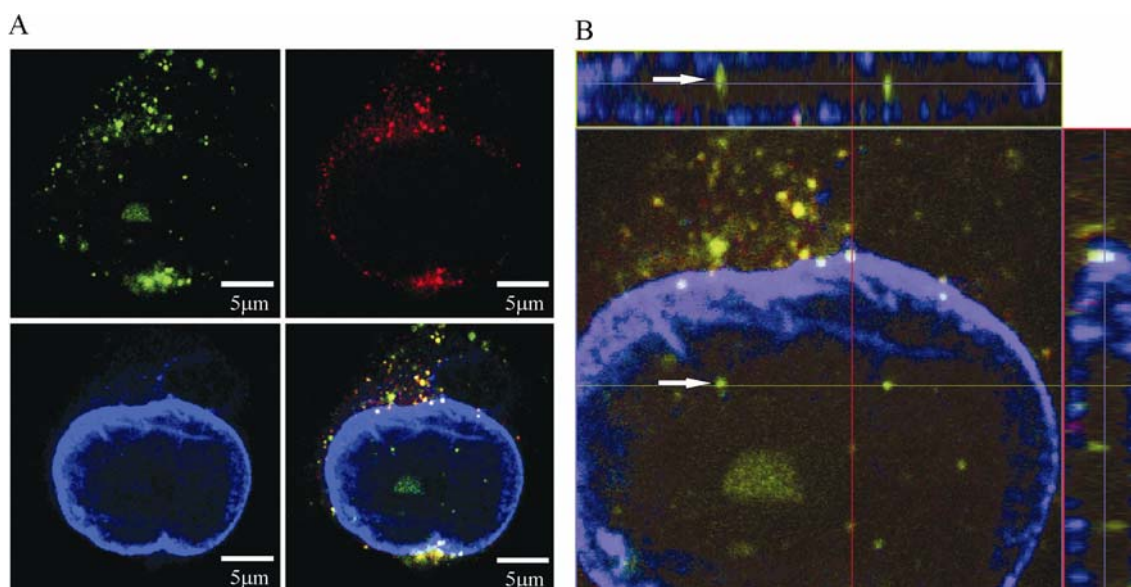
Fig. 12. Visualization of viral genomes by FISH. (A) HeLa cells were infected with wild type AAV (10^5 capsids per cell = 8,700 genomic particles per cell) and adenovirus type 5 (MOI of 5). Cells were fixed 11 h p.i. and FISH (green, Oregon green labeled DNA probe) was performed to visualize viral genomes, whereas intact capsids and nuclear membrane were stained using A20 (red; RRX conjugated secondary antibody) and anti-Lamin B antibody (blue: Cy5 conjugated secondary antibody), respectively. Analyses were performed by confocol microscopy and one image plane out of a z-stack is shown (top left: FISH; top right: A20; bottom left: anti-Lamin B; buttom right: merge). (B) Enlargement and vertical sectioning of merge shown in panel (A). The arrows show one example of a viral genome localized within the nucleus. The green signal indicates the viral genome visualized by FISH, using an Oregon green-labeled DNA probe; red signal indicates intact capsids visualized by A20 and RRX-conjugated secondary antibody; blue signal indicates nuclear lamina visualized by anti-lamin B and Cy5-conjugated secondary antibody.

2.1.7 Confirmation of viral uncoating observations utilizing GFP-VP2-AAV for nuclear entry analyses

For wild type AAV we could show that uncoating seems to take place during or before nuclear entry. If GFP-VP2-AAV behaves like wild type AAV2, viral genomes should be detected within the nucleus 2-4 h p.i., whereas viral capsid should be visible perinuclear. Therefore, HeLa cells were infected with 10^5 or 10^6 capsids per cell of 100%-GFP-VP2-AAV with or without adenovirus type 5 (MOI of 5) coinfection. Infections were stopped by fixing the cells 2, 4, 6, 8, and 11 h p.i. Viral genomes were detected by FISH utilizing a RRX labeled DNA probe, capsids were visible by the GFP-tag, whereas nuclear lamina was stained using an anti-Lamin B antibody (Cy5 conjugated secondary antibody). Figure 13 shows one representative example. In this experiment for both 10^5 and 10^6 capsids per cell only viral genomes and not capsids of GFP-VP2-AAV were detectable within the nucleus. In single cells viral genomes were

detectable from 4 h on. The number of FISH signals inside the nuclei increased with the time. Again, like for wild type AAV adenovirus coinfection had no influence on the course of infection. GFP-VP2-AAV capsids colocalized with FISH signals in the perinuclear area were detectable only when utilizing 10^6 capsids per cells. Utilizing 10xless capsids per cell resulted in a very weak GFP signal and thereby hampering colocalization studies.

A

B
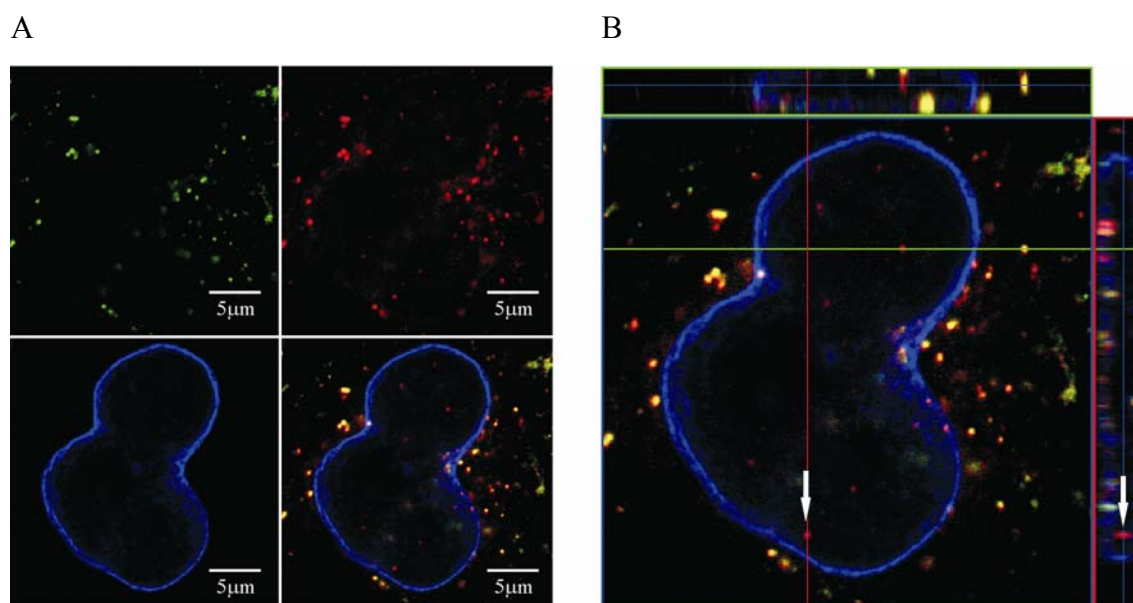
FIG. 13. Visualization of viral genomes by FISH . (A) HeLa cells were infected with 100%-GFP-VP2-AAV (10^6 capsids per cell = 105,000 genomic particles per cell). Cells were fixed 11 h p.i. FISH was performed to visualize viral genomes (red, Neutravidin-RRX conjugate from Molecular Probes which binds specifically to the biotin labeled DNA probe, labeled by a biotin nick translation kit from Roche), capsids were directly labeled by the incorporated GFP-VP2 fusion protein, and the nuclear lamina was visualized by an anti-Lamin B antibody (blue: Cy5 conjugated secondary antibody). Analyses were performed by confocol microscopy and one image plane out of a z-stack is shown (top left: GFP-VP2; top right: FISH; bottom left: anti-Lamin B; bottom right: merge). (B) Enlargement and vertical sectioning of merge shown in (A). The arrows show one example of a viral genome localized within the nucleus.

(viral genome: red, RRX labeled DNA probe; capsids: green, directly labeled by GFP-VP2, nuclear membrane: blue: anti-Lamin B recognized by Cy5 conjugated secondary antibody)

2.1.8 AAV is found in nuclear invaginations

Single particles have been shown to reach the nuclear area within seconds (Seisenberger et al. 2001) and a perinuclear accumulation of AAV was described to occur within 1-2 h p.i. (Bartlett et al. 2000; Xiao et al. 2002). Interestingly, we observed in addition AAV particles within tubular channels which extend deeply into the nucleoplasm (Fig. 14). This could first be assumed from SVT analysis. With SVT studies our group had observed that AAV moved very quickly on certain "pathways" through the nuclear area. We hypothesized that these pathways were nuclear invaginations, which are tubular structures derived from the nuclear envelope. The enclosed core is continuous with the cytoplasm and may function to bring larger proportions of the cytoplasm close to a nuclear pore (Fricker et al. 1997). In addition, a function of these nuclear channels in transport processes has been proposed (Dupuy-Coin et al. 1986). Within our current analysis, we observed AAV particles within nuclear invaginations (visualized by nuclear lamina staining), which verify our former assumptions (Seisenberger et al. 2001). These pictures were obtained for both, the GFP-tagged virions (Fig. 14A and C) and wild type AAV (Fig. 14B). The capsids were recognized in both cases by A20 revealing that intact viral capsids were detected within the nuclear invaginations. Although the significance of this colocalization has to be clarified, it explains the directed motion along defined pathways through the nuclear area observed by SVT.
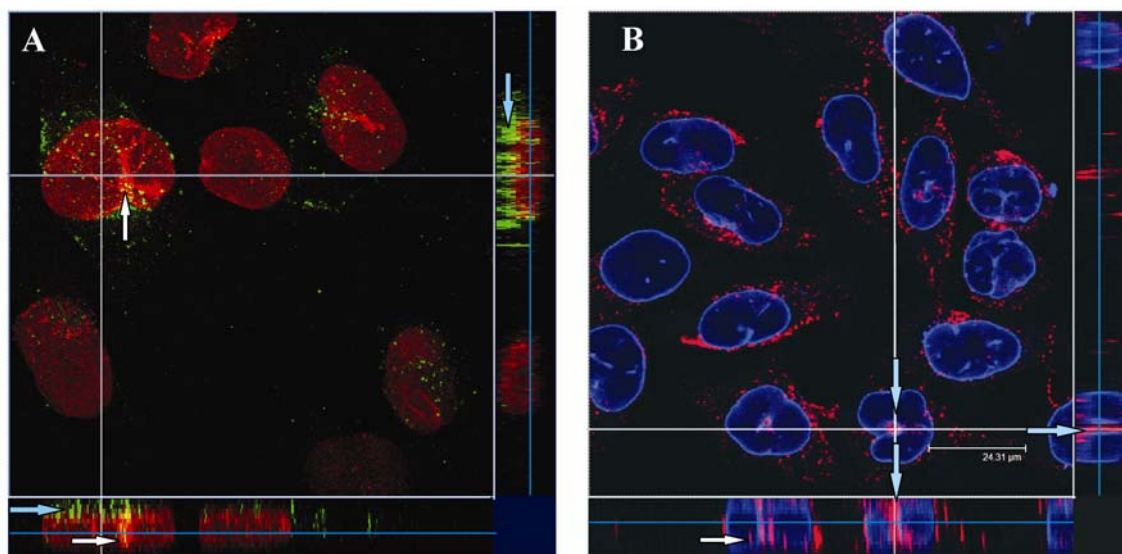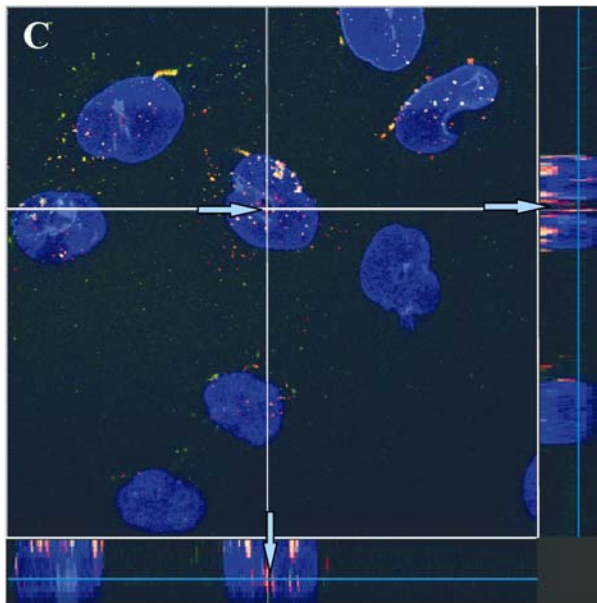
Fig. 14. AAV inside nuclear invaginations. (A) HeLa cells were infected with 10^6 capsids per cell of 100%-GFP-VP2-AAV. At 11 h p.i., cells were fixed, and the nuclear lamina was stained with TexasRed conjugated anti-lamin B antibody. Analysis was performed by confocal microscopy. A series of horizontal sections (each 0.2 μm) were obtained for each image. The square image shows one horizontal section of the stack. The vertical sections of the stack are depicted on the right and bottom of each panel. (white arrows: capsid in nuclear invaginations; blue arrows: capsid in perinuclear area). (B) HeLa cells were infected with 10^6 capsid per cell of wild type AAV and adenovirus type 5 (MOI of 5). At 11 h p.i., cells were fixed. Capsid and nuclear membrane were stained using A20 (red; RRX conjugated secondary antibody) and anti-Lamin B antibody (blue; Cy5 conjugated secondary antibody), respectively. Microscopical analyses were performed as described in legend to panel A. Under these conditions isolated signals of intact capsids were detectable inside the nucleus (white arrow). In addition, viral capsid within nuclear invaginations have been observed (blue arrows). (C) HeLa cells were infected with 10^6 capsid per cell of 100%-GFP-VP2-AAV and coinfected with adenovirus type 5 (MOI of 5). At 2 h p.i., cells were fixed. Capsids and nuclear membrane were stained using A20 (red; RRX conjugated secondary antibody) and anti-Lamin B antibody (blue: Cy5 conjugated secondary antibody), respectively. Microscopical analyses were performed as described in legend to panel A. GFP-tagged virions in nuclear invaginations were recognized by A20 (blue arrows).

2.1.9 GFP-VP2-AAV colocalizes with transferrin but not with dextran

Duan et al. described a colocalization of Cy3 labeled rAAV and transferrin which indicates that rAAV enters the cell via clathrin mediated endocytosis. The same entry pathway was proposed for Canine Parvovirus (CPV) which also colocalizes with transferrin but not with a fluid phase marker like dextran (Parker and Parrish 2000).

To give an additional example and to further prove the applicability of GFP-VP2-AAV to study the infectious biology of AAV we aimed to visualize AAV cell entry utilizing GFP-VP2-AAV and prelabeled transferrin and dextran. HeLa and PtK$_2$ cells were infected with 100%-GFP-VP2-AAV. PtK$_2$ cells were used since they are more

convenient for the online tracking of movements within cells. They have a very flat shape of 1-2 μm in the cell peripherie and only 5 μm in the nuclear area. In comparison the theoretical z resolution of a confocal microscope is about 0.5 μm. As a consequence this results in a more or less 2D situation and signals do not get lost quickly when they move in the z-axes. Therefore, PtK_2 cells are often used for monitoring movements by live cell imaging (e.g. Döhner et al. 2002). Prior to the colocalization experiment we were able to show that infection of PtK_2 cells with AAV leads to expression of viral protein. 1 μl of rAAV coding for GFP as a transgene leads to 99% positive HeLa cells and 78% positive PtK_2 cells detected by FACS analysis. Concomitant to infection either Alexa 633 labeled transferrin or Texas Red labeled Dextran (MW 3000) was added to the media. In these experiments GFP-VP2-AAV and transferrin or dextran, respectively, were initially bound to the surface of the cells by incubation at 4°C for 60 min and then shifted to 37°C, which initiates cellular uptake, by putting the multiwell chambers into the incubation chamber (37°C, 5% CO_2) of the live cell microscope. Subsequently, the distribution of AAV and transferrin or dextran were detected online up to 4 h post infection. We observed that GFP-VP2-AAV colocalizes with transferrin but not with dextran in both cell lines (Fig. 15). As it was shown for CPV, GFP-VP2-AAV colocalizes in a perinuclear vesicular compartment with transferrin.
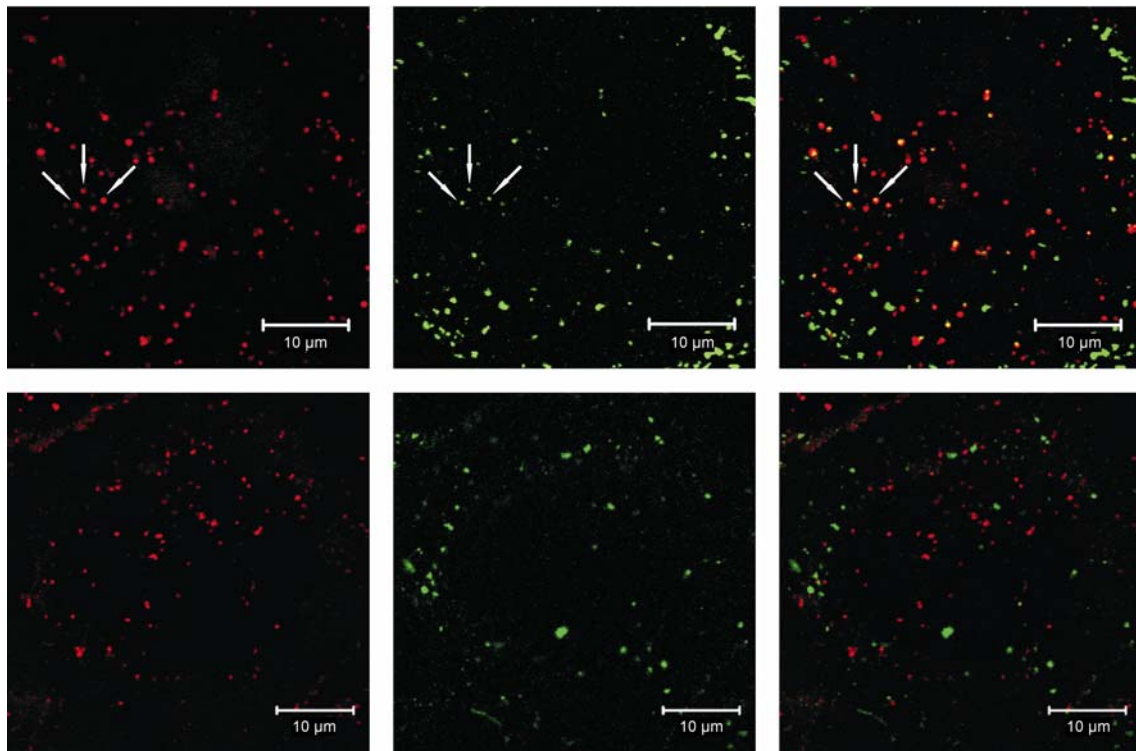
Fig.15. AAV colocalizes with transferrin. PtK$_2$ cells (male rat kangaroo kidney epithelial cells) seeded into glass bottom multiwell chambers from LabTek were infected with 100%-GFP-VP2-AAV; approximately 10^6 capsids/ cell. Additionally Alexa Flour 633 labeled transferrin in a final concentration of 0.5 mg/ml or Texas Red® labeled Dextran 3000 MW in a final concentration of 0.1 mg/ml was added to the media (Molecular Probes). Cells were incubated on ice to allow virus binding to the cells. Multiwell chambers were transferred directly after incubation on ice to a live cell microscope which was equipped with an incubation chambers allowing the observation of cells under physiological conditions (37°C, 5% CO$_2$). Upper row: codetection of transferrin (red, left image) and GFP-VP2-AAV (green, mid image) and merge (right image). Some colocalizations are marked by white arrows. The image was taken 3 h p.i. Lower row: Codetection of dextran (red, left image) and GFP-VP2-AAV (green, mid image) and merge (right image). No colocalization was observed. Image was taken 3.5 h p.i.

2.1.10 GFP-VP2-AAV shows directed movements inside cells similar to Cy5 labeled AAV

In previous studies performed in cooperation with Prof. Bräuchle and his group movements of incoming Cy5 labeled AAV were characterized by Single Virus Tracing (Seisenberger et al. 2001). Only a small part of AAV trajectories characterized inside the cells showed a directed motion, indicating microtubule dependent transport of the virus. This was surprising since experiments utilizing the microtubuli disturbing agent nocodazole had been shown to inhibit AAV infection. A possible reason for this discrepancy is very likely the temperature. Initial experiments were carried out at room temperature. However, Vihinen-Ranta et al. observed that a reduction in temperature to 18°C leads to depolymerisation of microtubules (Vihinen-Ranta et al. 1998). Based on this, an incubation chamber was obtained and measurements at 37°C were performed. HeLa cells were infected with Cy5 labeled AAV and movies were obtained with a time laps of 40 ms for each image as described by Seisenberger and colleagues. Under these conditions directed movements were the dominant kind of motion giving evidence for our hypothesis that measurements of microtubuli dependent movements cannot be performed by room temperature. Within our experiments at 37°C, velocity between 0.7 and 1.6 µm/sec were calculated by determining the distance and time of movement (see movies 2 and 3 in supplement).

GFP-VP2-AAV particles were invented as an alternative to the chemically labeling of AAV capsids. Therefore, we analyzed in cooperation with PD Sodeik (MHH, Hannover, Germany) whether GFP-VP2-AAV is suited for live cell imaging. The dynamics of GFP tagged virions in infected PtK$_2$ cells were analyzed by sequential fluorescence microscopic photography. To obtain movies pictures were taken with a time laps of 1 to 2 seconds and an exposure time of 0.5 seconds. For one movie a series

of 100 pictures was taken. To judge if the observed directed movements are due to microtubuli dependent transport processes, infection of cells incubated one hour prior to infection with nocodazole (50 µM final concentration) or cytochalasin D (0.1 µm final concentration) were performed in parallel.

Many particles performed small irregular, oscillatory movements without making large displacements. But also particles could be observed performing directed movements (Fig. 16 and movie 4 in supplement). Directed movements were observed only in the absence of nocodazole whereas cytochalasin D had no influence on directed movements. This indicates that the directed motion is microtuble and not actin filament dependent.

Directed movements were tracked by determining the xy-position of the fluorescent viral particles in each frame. From the xy displacements between each frame the velocity was calculated. The velocity of the directed motion within one track was mostly not homogenous. It can be observed that a particle shows directed movement then pauses at the same position to continue the track several seconds later. The maximum velocity calculated from 25 viral trajectories was 4.48 µm/sec. Approximately 50% of the particles moved with speeds of 0.5-1.0 µm/sec (Fig. 17). The average velocites of those tracks were in the range between 0.22-1.66 µm/sec. Directed movements observed in cells treated with cytochalasin D showed comparable velocities. The maximum speeds detected were in the range between 0.55-1.36 µm/sec whereas the average speeds was 0.27-0.49 µm/sec. Maximum velocities determined with GFP tagged AAV with conventional time laps microscopy were comparable with speeds observed in SVT measurements of chemically labeled AAV (Seisenberger et al. 2001). Furthermore velocities are within the range reported for movements of other viruses along microtubules: ~ 0.2-4 µm/sec (Suomalainen et al. 1999; Seisenberger et al. 2001; Lakadamyali et al. 2003; Sampaio et al. 2005; Wolfstein et al. 2006).
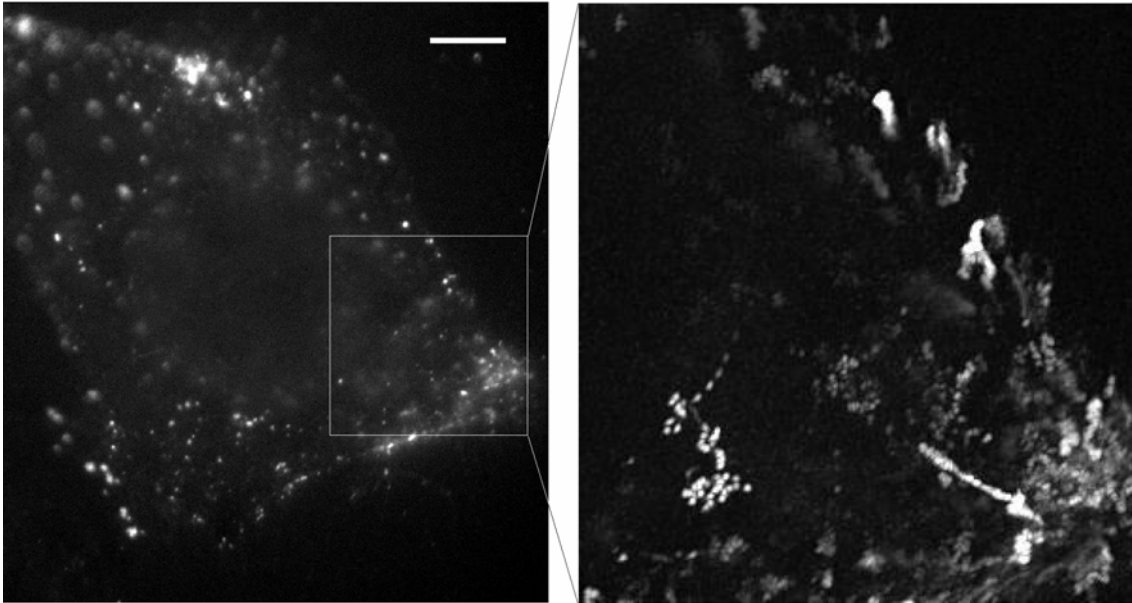
Fig. 16. Live cell imaging of GFP-VP2-AAV. Left: still image of a movie taken of a PtK$_2$ cell infected with approx. 10^6 capsids of 100%-GFP-VP2-AAV (white bar = 10 μm). Right: enlargement and z projection of the 100 single frames of the rectangular section (marked in the left image).
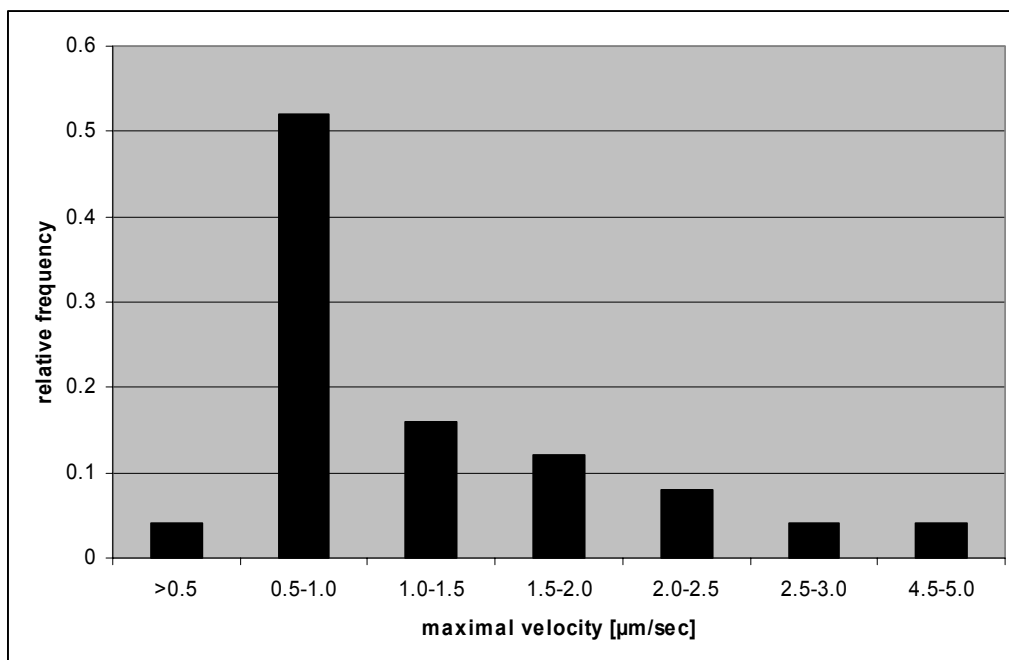
Fig. 17. Relative frequency of maximal velocities. Directed movements of 100%-GFP-VP2-AAV particles in infected PtK$_2$ cells were tracked by determining the xy-position of the fluorescent viral particles in each frame. From the xy displacements between each frame the velocity was calculated.

2.2 Application of GFP-VP2-AAV

2.2.1 Visualization of GFP-VP2-AAV *in vivo*

The great potential of direct labeling is the direct monitoring of the course of infection *in vivo*. Not only in living cells but also in living animals interesting information could be obtained. To assess if this is possible utilizing GFP tagged AAV capsids, such particles were subretinal injected into the eye of rats in cooperation with Dr. Rolling (University of Nantes, France) who is working on gene therapy of retinal degeneration (Fig 18). Gene therapy represents a possible approach for treating retinal degradation because the eye is easily accessible and allows local application of therapeutic vectors with reduced risk of systemic effects. An efficient long-term gene expression was already shown for AAV2 based vectors (Bennet et al. 1999; Ali et al. 2000).

Flatmounts of the neuroretina and sclera/choroid/RPE showed that GFP detection in the layers of photoreceptors and retinal pigment epithelium (RPE) is indeed possible (Fig. 19).
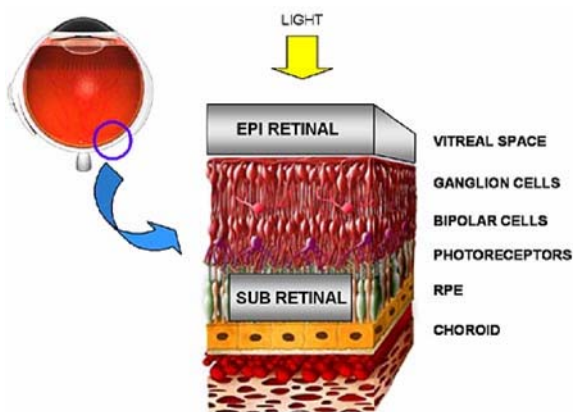
Fig. 18. Section of the eye showing the retina and its layers. The retina is the innermost of the three layers of the eye. It consists of the outer simple epithelial layer called the retinal pigmented epithelium (RPE) and the inner neurosensory retina. Between these two layers lies a potential space, the subretinal space, across which the two layers adhere. The retina is bound by the choroid externally, the vitreous internally, the ora serrata anteriorly, and is continuous with the optic nerve posteriorly.
www.bostonretinalimplant.org
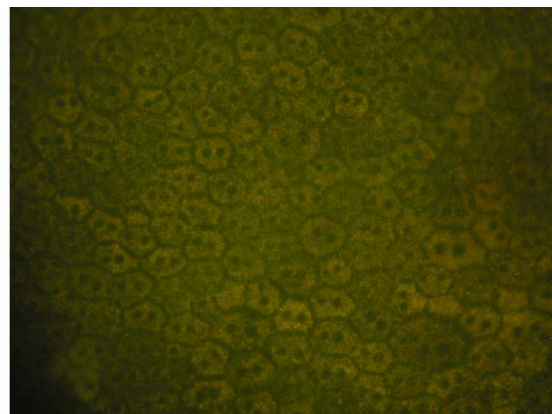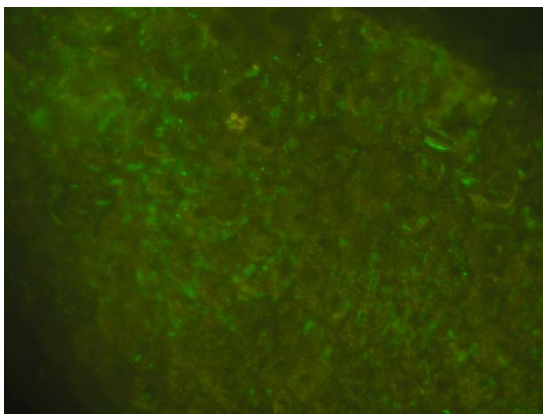
Fig. 19. GFP-VP2-AAV detected in the RPE. Wt Wistar rats were anesthetized with an intramuscular injection. For subretinal injection, the sclera and the choroid were punctured and a 33-gauge needle was then inserted in a tangential direction under an operating microscope. In one application, $6x10^{10}$ capsids were injected. 24 h p.i. a retinal flatmount was obtained. Therefore enucleated eyes were fixed with 4% paraformaldehyd for 40 minutes at room temperature. After washing, the eyes were cut through the pars plana and the anterior segment and the lenses were removed. The eye cup was cut peripherally into four sections under an operating microscope and flattened. The neuroretina was removed from the sclera/choroids/RPE with fine forceps and both cell layers were mounted on a glass side and examined by fluorescence microscopy.

Left image: Green fluorescent spots were detected in the layer of retinal pigment epithelium. Right image: negative control

2.2.2 Utilization of the VP2 N-terminus as insertion site for retargeting polypeptides

One major aim of our group is the generation of retargeting (= receptor/cell specific) vectors for gene therapy. Based on our characterization of GFP-VP2-AAV it can be assumed that the N-terminus of VP2 can be used for insertion of larger polypeptides. This is important for the field of AAV retargeting since larger peptides insertions within the capsid interfere with AAV packaging.

Therefore, a new PhD project was started with the aim of generating vectors specific for colorectal cancer cells and for Hodgkin Lymphoma. The sequences of single chain antibodies against CEA (colorectal embryonic antigen) and against CD30 (marker for Hodgkin Lymphom) were fused with the N-terminus of VP2. Therefore, the GFP sequence was replaced by the sequences for the single chain antibodies against CEA or CD30, respectively. Sequences of single chain antibodies were amplified from expression vectors provided by Prof. Abken (UKK, Köln, Germany). The natural binding site of AAV for its primary receptor heparan sulfate proteoglycan (HSPG) is located within the VP3 region and is not affected by insertion of polypeptides at the VP2 N-terminus. To avoid transduction of cells via the natural primary receptor of AAV2, crucial amino acid residues for HSPG binding were mutated in addition (R→A aa585/ R→A aa588). Until now we have observed that virions containing single chain antibodies can be packaged with comparable titers to wt AAV (Tab. 2). Transduction of HeLa could be successfully prevented by the mutation of the HSPG binding region. Currently, infection studies are being performed to determine the targeting specificity of these new vectors.

TABLE 2 Characterization of the different viral preparations

Preparation	Genomic particles/ml	Transducing particles/ml*
ssGFP-AAV2HaCEA	1.52×10^{12}	2.19×10^{9}
ssGFP-AAV(2)aCEA	3.46×10^{11}	n.i.
ssGFP-AAV2HaCD30	3.97×10^{12}	9.21×10^{8}
ssGFP-AAV(2)aCD30	4.65×10^{11}	n.i.
ssGFP-AAV2RC	1.29×10^{12}	4.44×10^{9}

* the infectious titer was determined on HeLa; n.i. = non infectious

ssGFP-AAV2HaCEA: rAAV2 with anti CEA inserted at the VP2 N-terminus;

ssGFP-AAV(2)aCEA rAAV2 with anti CEA inserted at the VP2 N-terminus and mutation of 2 residues important for the HSPG binding;

ssGFP-AAV2HaCD30: rAAV2 with anti CD30 inserted at the VP2 N-terminus;

ssGFP-AAV(2)aCD30: rAAV2 with anti CD30 inserted at the VP2 N-terminus and mutation of 2 residues important for the HSPG binding;

ssGFP-AAV2RC: wt AAV2 capsid

All vector contain ssGFP as a transgene. (Data kindly provided by Jorge Boucas)

2.3 PLA2 – an important domain within the AAV2 capsid

To continuously improve the vector system, a detailed understanding of functional domains within the AAV capsid proteins is important. It has been shown that the unique region of VP1 contains a secretory phospholipase A2 (sPLA2) domain; a domain that was not known to exist in virus capsids (Zádori et al. 2001).

A mutation in the catalytic center of the PLA2 motif of AAV2 causes a dramatic drop in infectivity. No differences in cell adhesion, entry or accumulation in the perinuclear area could be observed between wt and PLA2 mutant, however these mutants show a drastically reduced and delayed Rep expression (Girod et al. 2002). Based on these results, it can be assumed that the PLA2 activity is required for a step in the life cycle of AAV, following perinuclear accumulation, but prior to the onset of gene expression. This suggests that the PLA2 activity is may be required for endosomal escape or transfer of viral genomes into the nucleus.

2.3.1 Both wt AAV and PLA mutant seem to accumulate inside the endoplasmatic reticulum

To address this question we performed a costaining of viral capsids and the endoplasmatic reticulum (ER). HeLa cells were infected with 10^5 capsids per cell in parallel with wild type AAV and PLA2 mutant. The PLA2 mutant analyzed contains a substitution of the amino acids histidine (D) and aspartic acid (D) to alanin (A) and asparagin (N) at amino acid position 76 and 77, respectively, within the capsid protein VP1. These amino acids are located within the catalytic center of the phospholipase A2 domain. Infections were stopped by fixing the cells 2, 4 and 11 h p.i. Capsids and the ER were stained by antibodies (polyclonal Calreticulin (ABR) rabbit antibody). At all time points analyzed, both wt and PLA2 mutant capsids colocalized with the ER staining (Fig. 20).
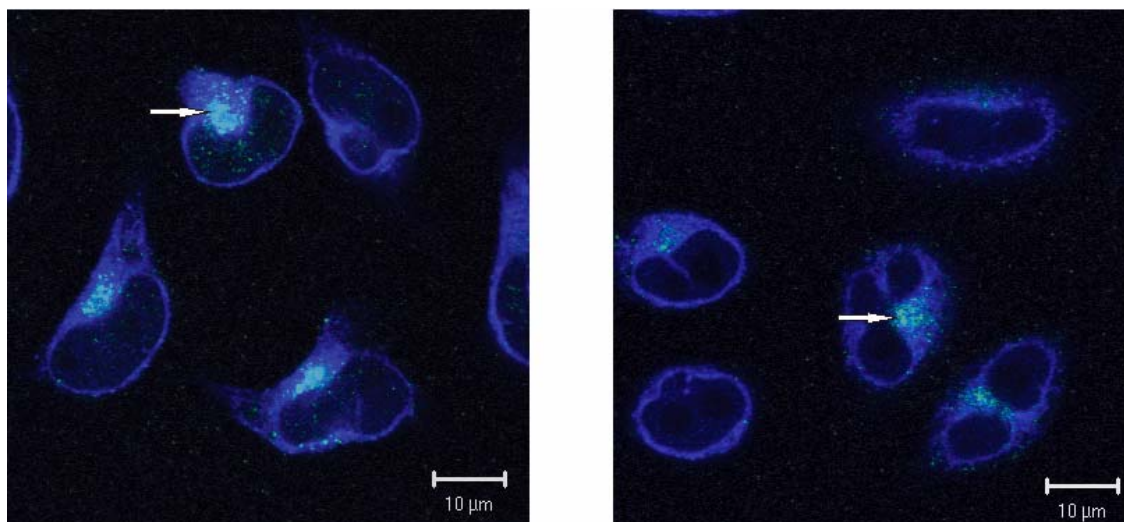
Fig. 20. Colocalization of viral capsids and ER signals. HeLa cells were infected with 10^5 capsids of wt AAV or PLA2 mutant per cell. Cells were fixed 4 h p.i. Viral capsids were stained with A20 and a FITC conjugated secondary antibody (green). The ER was stained with a calreticulin antibody and a secondary Cy5 conjugated antibody (blue). Analyses were performed by confocal microscopy and one image plane out of a z-stack is shown. Left: wt AAV infected cells. Right: PLA2 mutant infected cells. Arrows show accumulation of viral capsids within the ER.

However, the ER signal covers a relatively large area around the nucleus. To exclude that the capsids are localized only in the same region of the ER and not really within membrane stacks of the ER we wanted to get a higher resolution of this region of interest. Therefore, we started to establish an electron microscopic analysis of AAV inside infected cells in cooperation with Prof. Dienes (Institute for Pathology, University of Cologne). For that purpose same infections as described above were performed. Cells were fixed and then analyzed by electron microscopy (EM). The first results obtained by EM seemed to verify our immunofluorescence data: wt AAV and PLA2 mutant capsids localize within the ER structure (Fig. 21 and 23). For wt AAV, escape from a vesicular organelle was observed (Fig. 22). In addition, viral capsids of both wt and PLA mutant were also detected in the cytoplasm (outside of organelles) (Fig. 21, 22 and 23). The exact organelle from where viral capsids are released into the cytoplasm and if it is the same organelle for the wt and the PLA2 mutant cannot be concluded from these preliminary results. But the data favor the idea that also the PLA2 mutant is able to escape from endosomes or other vesicular compartments to which the capsids are transported, concluding that the phospholipase activity is not needed for viral escape from vesicular compartments. However, more data have to be obtained to strengthen this hypothesis. Furthermore, the current fixation protocols did not result in

an optimal recovery of cell structures. Therefore, a modified protocol and in addition immunogold staining against the viral capsid and cellular markers will be applied in the ongoing experiments to obtain a better depiction of intracellular membranes and viral capsids.
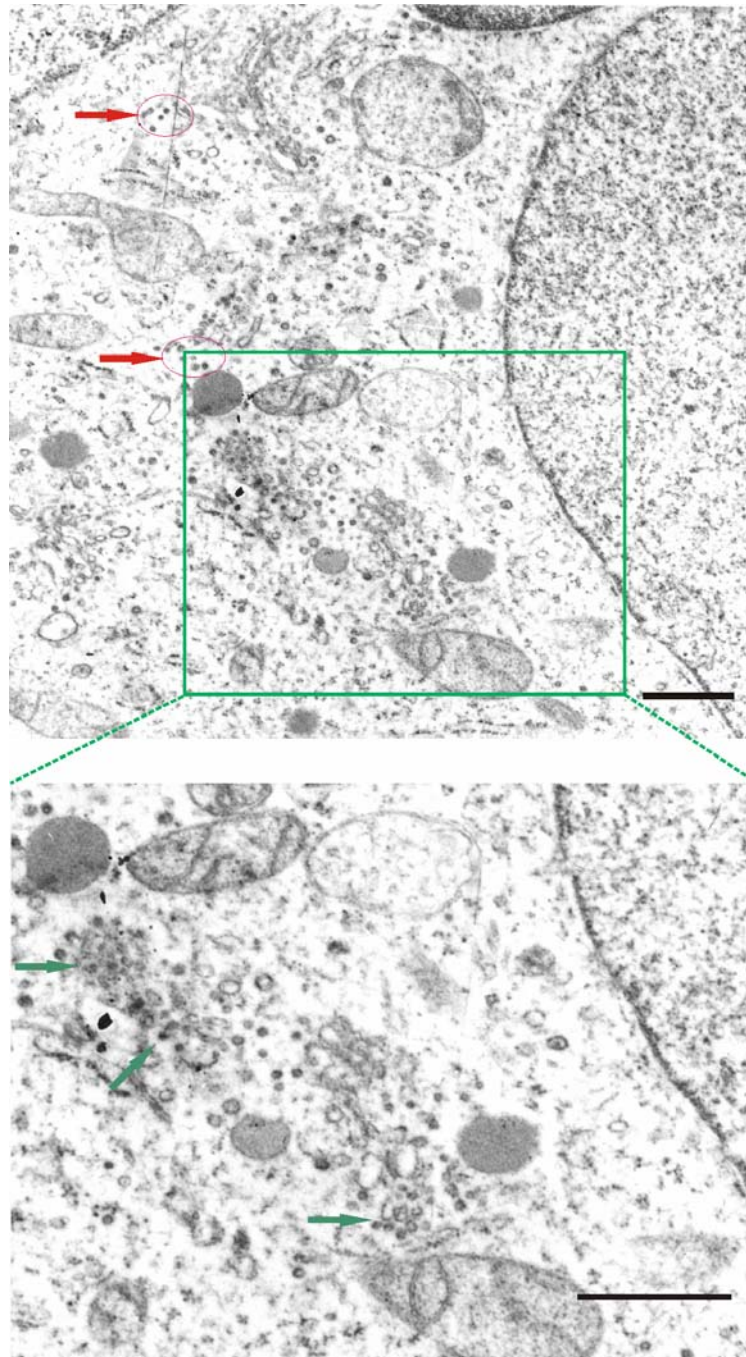
Fig. 21. Accumulation of wt AAV within membrane stacks. Electron micrographs of HeLa cells infected with wt AAV (10^6 capsids per cell) fixed 4 h p.i. Red circled particles show viral capsids outside of organelles (upper image) lower image: enlargement of green rectangle. Green arrows show wt capsids accumulated within membrane stacks. (scalebars = 142 nm)
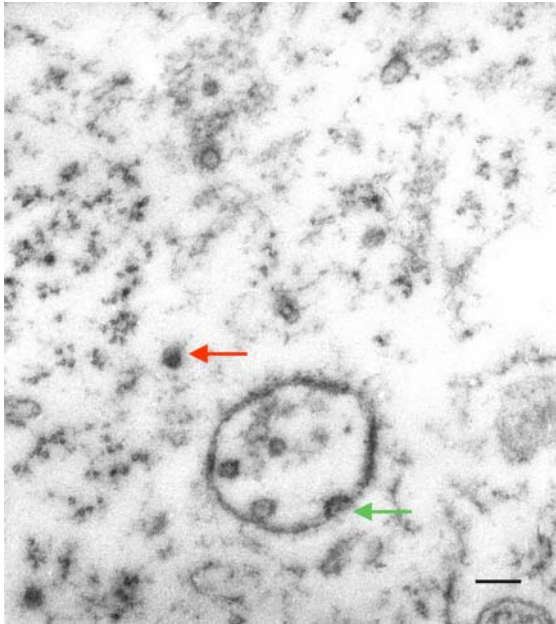
Fig. 22. Left image: viral escape out of a vesicular compartment. Electron micrograph of HeLa cells infected with wt AAV (10^6 capsids per cell) fixed 4 h p.i. Viral capsids are detected inside a vesicular compartment. Green arrow depicts a viral escape out of this organelle Red arrow shows a viral capsid free within the cytoplasm. (scalebar = 20 nm)

Fig. 23. Lower images: the PLA mutant accumulates within membrane stacks. Electron micrographs of HeLa cells infected with PLA mutant (10^6 capsids per cell) fixed 4 h p.i. (A) shows PLA mutant capsids within membrane stacks (green arrows). (B) shows viral capsids outside of organelles (red circled particles). (scalebars = 45 nm)
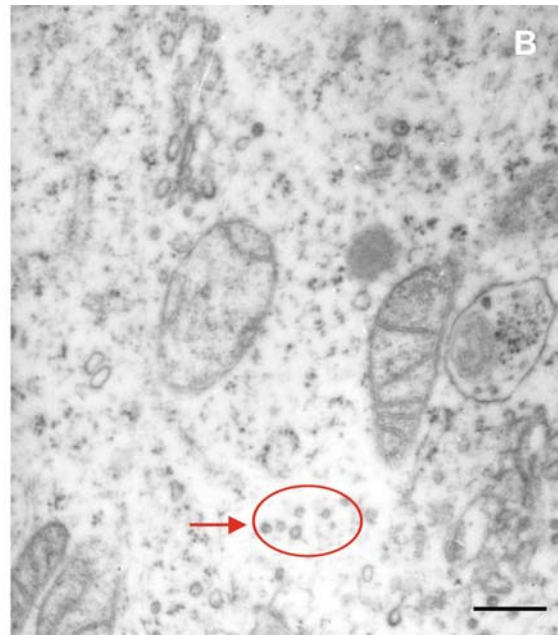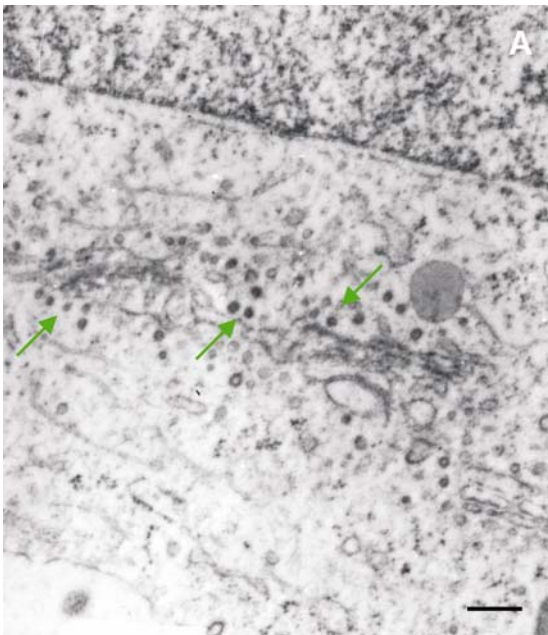
2.3.2 DNA signals from the PLA2 mutant cannot be detected inside the nucleus but inside nuclear invaginations

In further immunofluorescence experiments, we compared wt AAV and the PLA2 mutant regarding the distribution of viral DNA and capsids in the perinuclear area. HeLa cells were infected as described above and fixed 11 h post infection. Nuclear lamina and viral capsids were stained with antibodies, while DNA was visualized by FISH. We observed, in contrast to wt AAV no FISH signals (= no signal for viral DNA) from the PLA2 mutant within the nucleus. Outside the nucleus, the PLA2 mutant

behaved like wt AAV (FISH signals colocalized perfectly with capsid signals). Colocalizing signals of DNA and capsid were detected in close proximity to the nuclear membrane and inside nuclear invaginations (Fig. 24).
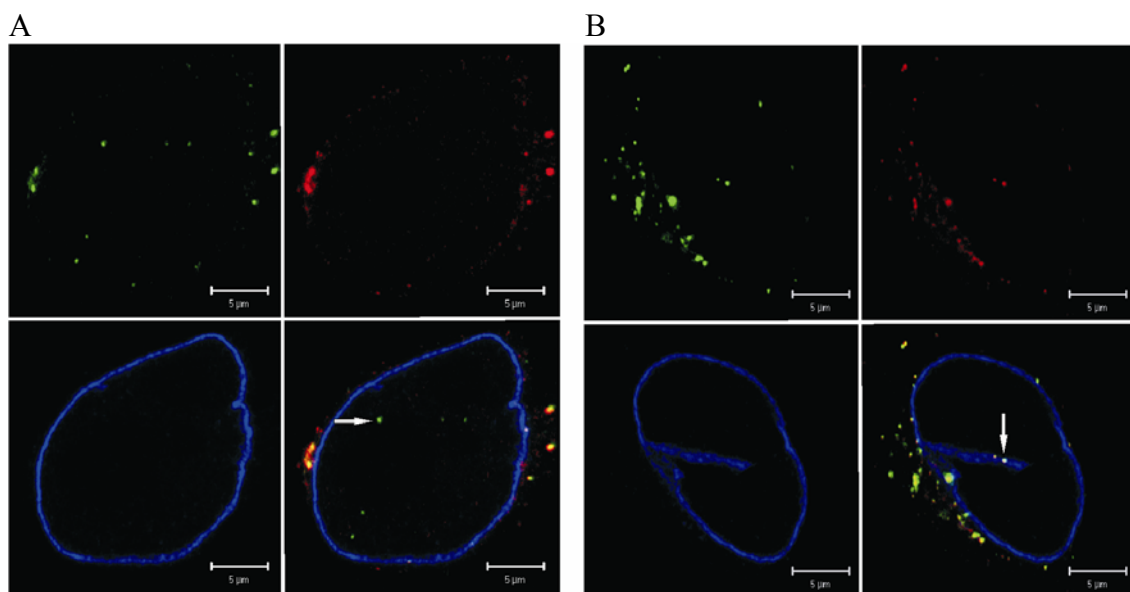
Fig. 24. Visualization of viral genomes by FISH. HeLa cells were infected with wt or PLA2 mutant (10^5 capsids per cell). Cells were fixed 11 h p.i. FISH (green, Oregon green labeled DNA probe) was performed to visualize viral genomes, intact viral capsids were stained with A20 (red, RRX conjugated secondary antibody). The nuclear lamina was visualized by an anti-Lamin B antibody (blue: Cy5 conjugated secondary antibody). Analyses were performed by confocal microscopy and one image plane out of a z-stack is shown (upper left: viral genomes; upper right: viral capsids; lower left: anti-Lamin B; lower right: merge). (A) wt AAV: the arrow shows one example of a viral genome localized within the nucleus. (B) PLA2 mutant: the arrow shows one example of a viral genome colocalized with viral capsid inside a nuclear membrane invagination. No FISH signals are detected within the nucleus.

2.3.3 The PLA2 mutant shows in contrast to wt AAV no DNA replication

To investigate if the PLA2 mutant is able to replicate its genome, HeLa cells were infected with wt AAV and PLA2 mutant, respectively, and coinfected with adenovirus type 5 at a multiplicity of infection (MOI) of 5. Since adenoviral proteins are necessary to assist AAV replication, HeLa cells were either coinfected or preinfected with adenovirus (1, 5 or 16 h) to evaluate if the time point of adenovirus infection makes a difference. For AAV infection 10^5 viral capsids per cell of wild type AAV or PLA2 mutant were utilized. 2, 4 or 6 h after AAV infection cells were fixed with 4% paraformaldehyd. Nuclear lamina was stained with an anti-Lamin B antibody and viral DNA was visualized by FISH. Interestingly, viral DNA replication was detected as an

accumulation of FISH signals inside the nucleus only in cells preinfected with adenovirus for 16 h, followed by 4 h wt AAV infection. No viral replication was detected under the same conditions for the PLA2 mutant (Fig. 25).
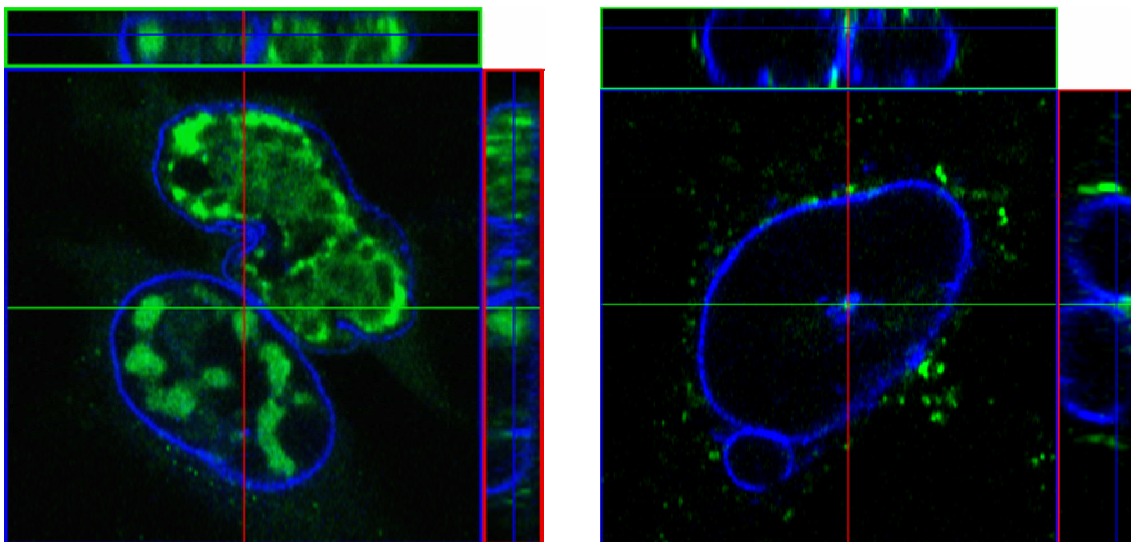
Fig. 25. Visualization of viral replication. HeLa cells were infected with adenovirus type 5 at a MOI of 5. 16 h post Ad infection cells were infected with wt or PLA2 mutant (10^5 capsids per cell). Cells were fixed 6 h post AAV infection. FISH hybridization (green, Oregon green labeled DNA probe) was performed to visualize viral genomes and the nuclear lamina was visualized by an anti-Lamin B antibody (blue: Cy5 conjugated secondary antibody). Analyses were performed by confocal microscopy. A vertical sectioning out of a z-stack is shown. (left panel) wt AAV infection; (right panel) PLA2 mutant. Replication was detected as bright accumulation of FISH signals inside the nucleus only after wt AAV infection.

2.3.4 Next steps of analysis of the PLA mutant

In following experiments we want to compare the wt AAV and the PLA2 mutant directly within the same cell. To distinguish the two different viruses inside the same cell, viral capsids should be tagged with different fluorescent proteins. As an alternative to GFP-VP2, monomeric DsRed was fused to the N-terminus of VP2 by cloning the VP2 PCR fragment at the C terminal cloning site of a DsRed expression vector from Clontech. Thus, DsRed labeled capsids can be generated in the same way as GFP labeled capsids. To generate a labeled PLA2 mutation containing capsid, the VP2 knock out was inserted into pHD/AN resulting in pHD/AN VP2ko. This plasmid has the same sequence as pUC-AV2 with exception of the HD/AN mutation. Thus, labeled capsids can be generated by transfecting 293 cells with pxx6, pGFP-VP2 or pDsRed-VP2 respectively and pHD/AN VP2ko instead of puc-AV2. At the moment DsRed-VP2-AAV and DsRed-VP2-HD/AN are being characterized.

2.4 Amino acid position 453 as an alternative insertion site

A sensitivity problem arises if chemical labeled AAV2 capsids, carrying only one dye per capsid are analyzed by confocal or fluorescent microscopy (not single virus tracing). Therefore, a higher number of fluorescent dyes incorporated into the viral capsids would be desirable allowing detection of a more physiological amount of virions per cell by conventional fluorescent and confocal microscopy. Therefore, we wanted to evaluate a different labeling method. Insertions within the VP3 region have the advantage of being displayed 60 times on the capsids, in contrast to approximately 5 to 10 times when the insertion is located in the VP1 or VP2 region. The 587 position, which is located within the VP3 region, was demonstrated to be a well suited site for insertion of retargeting sequences (Grifman et al. 2001; Nicklin et al. 2001; Ried et al. 2002; Shi et al. 2001; Perabo et al. 2003, 2006). However, insertions at the 587 position interfere with wild type AAV receptors binding and therefore cannot be used for insertions of fluorescence proteins in attempt to study infectious biology. Regarding the structure of AAV (Xie et al. 2002) we were attracted by the amino acid position 453 which is located on the top of the higher peak within the capsid (Fig. 26). We thought that an insertion at this site should be perfectly presented – like 587 – 60x at the capsids surface. However, several attempts to introduce larger polypeptides within the VP3 region were not compatible with viral packaging. Thus, fluorescent proteins like GFP derivates are too large to be inserted within that region. As an alternative we tried to incorporate an α-helical tetracystein-containing peptide (21 amino acids: GGWEAAAREACCRECCARAGG) into the 453 position. This peptide is specifically recognized by FLASH-EDT$_2$ (Fluorescein arsenical helix binder-1,2 Ethanedithiol adduct) which becomes strongly fluorescent after binding to the tetracystein peptide (Griffin et al. 1998). Moreover, we inserted as a control a NGR motif (11aa: ACVLNGRMECA) which, we already knew, is functional at the 587 site *in vitro*. The NGR peptide binds specifically to the tumorendothelial isoform of aminopeptidase N (APN), also known as CD13. APN is thought to play a role in chemokine processing and tumor invasion (Pasqualini et al. 2000). Curnis and coworkers showed that a tumor endothelium specific isoform of APN is upregulated on the very same tissue (Curnis et al. 2002). Insertions were cloned into the pRC plasmid. Thus generating the plasmids pRC NGR 453 or pRC FLASH 453.
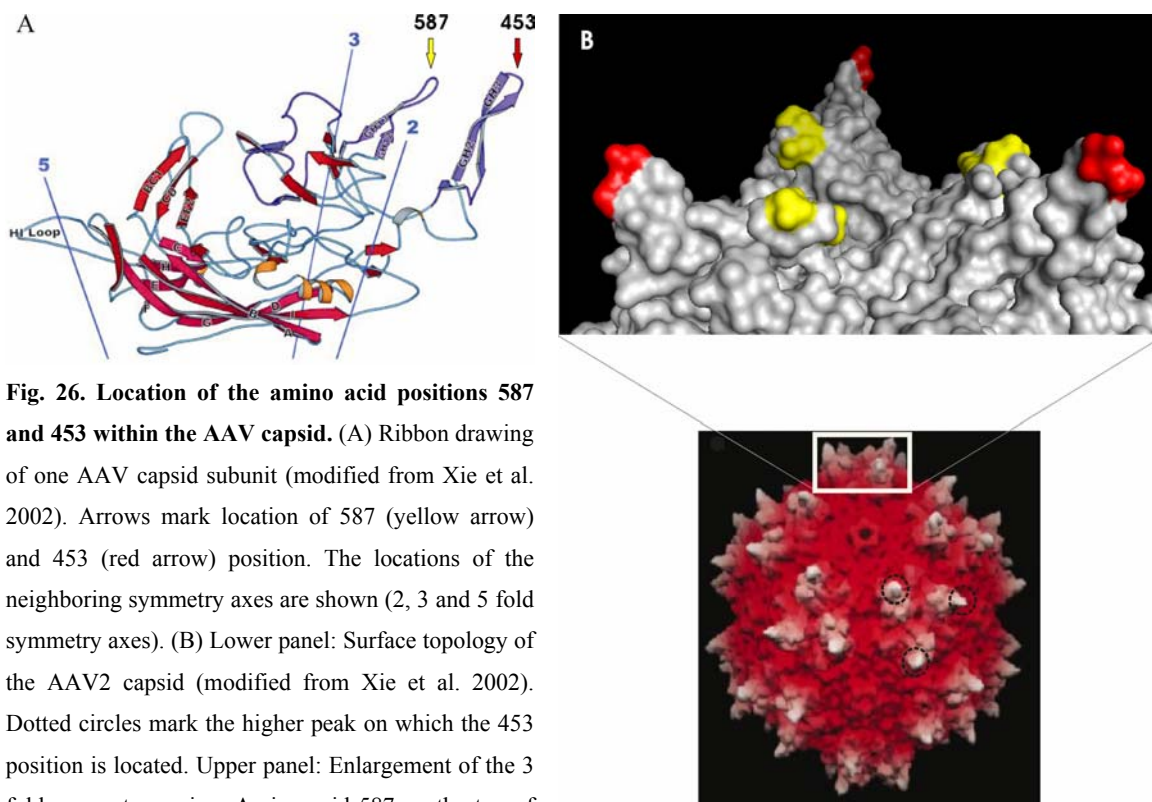
Fig. 26. Location of the amino acid positions 587 and 453 within the AAV capsid. (A) Ribbon drawing of one AAV capsid subunit (modified from Xie et al. 2002). Arrows mark location of 587 (yellow arrow) and 453 (red arrow) position. The locations of the neighboring symmetry axes are shown (2, 3 and 5 fold symmetry axes). (B) Lower panel: Surface topology of the AAV2 capsid (modified from Xie et al. 2002). Dotted circles mark the higher peak on which the 453 position is located. Upper panel: Enlargement of the 3 fold symmetry region. Amino acid 587 on the top of the lower peak is colored yellow and 453 on the top of the higher peak iscolored red.

2.4.1 Only the NGR not the FLASH peptide is tolerated at the 453 position

To control whether insertions at the new site allow the production of infectious virus, crude viral lysates were generated. Therefore, 293 cells were transfected with pxx6 (adenoviral helper plasmid), pGFP (plasmid encoding for the transgene) and either pRC (unmodified capsid), pRC NGR 453, pRC FLASH 453 or pOEN (negative control; stop codon inside the cap gene). Thus 293 cells should produce the following viral particles: RC-rAAV/GFP (wt viral capsids with GFP as transgene), NGR-453-rAAV/GFP (capsid with NGR insertion at the 453 site and with GFP as transgene) and FLASH-453-rAAV/GFP (capsid with FLASH insertion at the 453 site and with GFP as transgene). In the negative control where pOEN instead of pRC was transfected into 293 cells no viral capsids should be generated but free GFP protein. This allows us to distinguish between virus mediated transduction and GFP pseudotransduction. Cells were harvested 2 days post infection by trypsin treatment. Crude lysates were obtained by subjecting the cells to three freeze and thaw cycles. Crude viral lysates were used to infect HeLa cells thus determining the ability of the viral lysate to mediate GFP expression. HeLa cells were

screened for GFP expression at the microscope one and two days after infection. Only lysates containing wt AAV or the NGR 453 rAAV showed expression of GFP. Lysates of the negative control and FLASH 453 rAAV showed no GFP expression. From this we concluded that insertion of the α-helical tetracystein-containing peptide was not compatible with infectivity. A reason for this might be the formation of a helix interfering with the folding of the β-barrels which form the peak on which the 453 position is located. A larger spacer between peptide and capsids might be a solution for this problem. However, the NGR peptide at the 453 position showed potential as a new retargeting position within the capsids. For this reason we decided to analyze this in more detail.

2.4.2 NGR in 453 mediates an efficient transduction of HUVEC cells

Viruses were produced and purified by an iodixonal step gradient: RC-rAAV/GFP, NGR-453-rAAV/GFP and NGR-587-rAAV/GFP (contains NGR in aa position 587). Genomic particle titer was analyzed by DNA dot-blot hybridization. Gene expression of the different vectors was measured in HUVEC (human umbilical vein endothelial cells) and HFF (human foreskin fibroblast). HUVEC are used as a tumor endothelial model, because when primary HUVEC are kept in culture for longer time they start to develop a capillary like network, thus macroscopically indicating the switch to an angiogenic phenotype (Vailhe et al. 2001). Primary HUVEC were isolated from umbilical cords obtained from the new born clinic of the Ludwigs Maximilians-University. HHF were used as a non endothelial control for primary cells. HFF are reported to be permissive for AAV2 (Russell et al. 1994).

In a first attempt, to determine if the inserted NGR motif provides the vectors with targeting ability, HUVEC and HFF were infected with 10^4 genomic particles per cell. Additionally, infections on HUVEC were carried out in the presence of soluble heparin to check whether binding to the attachment receptor HSPG influences viral transduction. Infected cells were harvested 2 days post infection and GFP expression was measured by fluorescence activated cell sorting (FACS). With RC-rAAV/GFP 19.9% of HUVEC and 69.1% of HFF could be transduced. The NGR 587 mutant was able to transduce 14.5% of HUVEC and 7.95% of HFF whereas the NGR-453 mutant was able to infect 62.5% of HUVEC and 70.2% of HFF. For RC-rAAV/GFP a 7.2 fold,

for NGR-453-rAAV/GFP a 6.3 fold, but for NGR-587-rAAV/GFP only a 1.4 fold reduction in transduction was reached when incubating the vector with soluble heparin (Fig. 27). These results indicate that the insertion at 453 leads to an enhanced transduction of HUVEC, which points towards a successful new ligand-receptor interaction. Heparin inhibits wt and the 453 mutant nearly to the same extent while the inhibition of the 587 mutant was much lower. Furthermore HFF were transduced to the same extent from RC-rAAV/GFP (69.1%) and NGR-453-rAAV/GFP (70.2%) while transduction with NGR-587-rAAV/GFP was much lower (7.95%). This might indicate that HSPG is still used as a receptor by NGR-453, which is not astonishing since the heparin binding site is not affected within the 453 mutant.
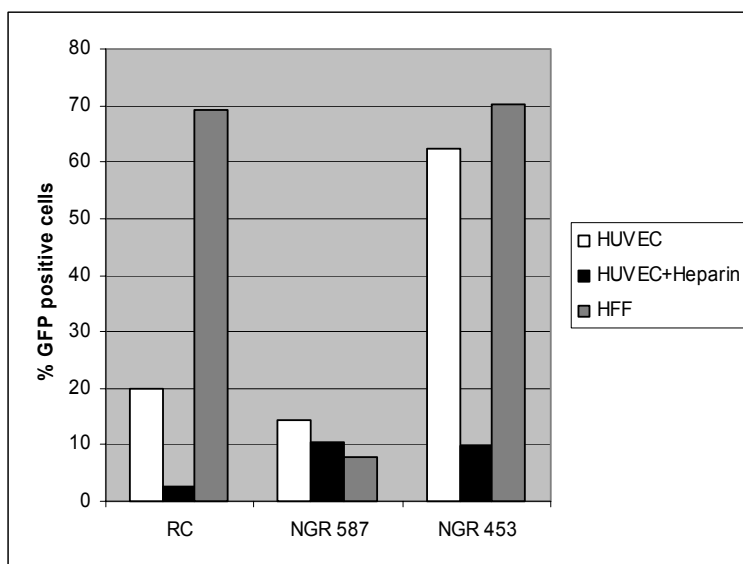
Fig. 27. Transduction efficiencies of NGR mutants. Transduction efficiencies of RC-rAAV/GFP (RC), NGR 587-rAAV/GFP (NGR 587) and NGR-453 rAAV/GFP (NGR 453) transduction of HUVEC in the presence (black bars) and absence of heparin (white bars) and of HFF (grey bars) determined by FACS.

2.4.3 The alternative retargeting peptide RGD-4C shows RGD mediated transduction

In parallel, *in vivo* studies were carried out in our group with the NGR-587-rAAV/GFP. They showed no hint that the NGR motif is able to redirect the respective targeting mutant towards tumor endothelia (unpublished results). For this reason we decided to exchange the NGR peptide for the RGD-4C peptide (11aa: ACDCRGDCFCA). The RGD-4C peptide binds specifically to $\alpha_v\beta_3/\alpha_v\beta_5$ integrins (Koivunen et al. 1995). A RGD motif was also selected in former work of our group using an AAV display on a human megakaryocytic cell line (M-07e) (Perabo et al. 2003). Virions containing such

RGD peptides at the 587 position were able to transduce M-07e but not Mec1 (B-cell chronic lymphatic leukemia cells in prolymphoid transformation). M-07e and Mec1 are both poorly transduced by wt AAV2. Insertions were cloned into the pRC plasmid, generating the plasmid pRC RGD 453. The four cysteins in the peptide are thought to build sulfate bridges in a way that the RGD becomes perfectly exposed.

RC-rAAV/GFP, RGD-4C-453-rAAV/GFP and RGD-4C-587-rAAV/GFP were packaged and purified by an iodixanol step gradient. Genomic titers were determined by quantitative PCR. HeLa, M-07e and Mec1 cells were infected using the same genomic particles per cell (approx. 10^4). To analyze whether the infection is mediated by the insertion, competition experiments were included. Therefore cells were preincubated with 300 µM soluble GRGDTP or GRGES peptides for 10 min. The RGD containing peptide should block RGD mediated cell entry by competing for integrin binding (receptors for RGD motif containing ligands). The RGE containing peptide is a nonspecific negative control. The transduction efficiencies were determined 3 days post infection by FACS (Fig. 28).

Interestingly, AAV with RGD-4C in 453 transduced M-07e cells more efficiently than RC rAAV (41% in comparison to 25%) and than RGD-4C in 587 (9%). Transduction of M-07e with RGD-4C containing virions was inhibited by GRGDTP peptides but not by unspecific GRGES peptides. Transduction of M-07e with RC-rAAV/GFP was not inhibited by both of the peptides. This indicates that the transduction of M-07e with RGD-4C containing virions is mediated by the RGD insertion and that the insertion site is important for enhancement of transduction.

In contrast, Mec1 cells were not infected by RGD-4C-453-rAAV/GFP (2%). RC transduced 25% and RGD-4C-587-rAAV/GFP 11% of Mec1.

RC-rAAV/GFP transduced 98% of HeLa and was not inhibited by soluble peptides. RGD-4C in 453 rAAV was able to transduce HeLa cells to 52%. Inhibition with RGD containing peptide reduced transduction efficiency only to 40%, which indicates that these virions, in which the HSPG binding is not affected by peptide insertion (in contrast to 587 insertions) are still able to enter cells through the HSPG mediated entry pathway in addition to RGD-4C. Infection of HeLa cells with RGD-4C-587-rAAV/GFP showed a lower transduction (21%), demonstrating that peptides at the 587 position interfere with natural receptor binding. Transduction was inhibited by GRGDTP soluble peptide to 7% indicating a RGD mediated entry also on HeLa cells.
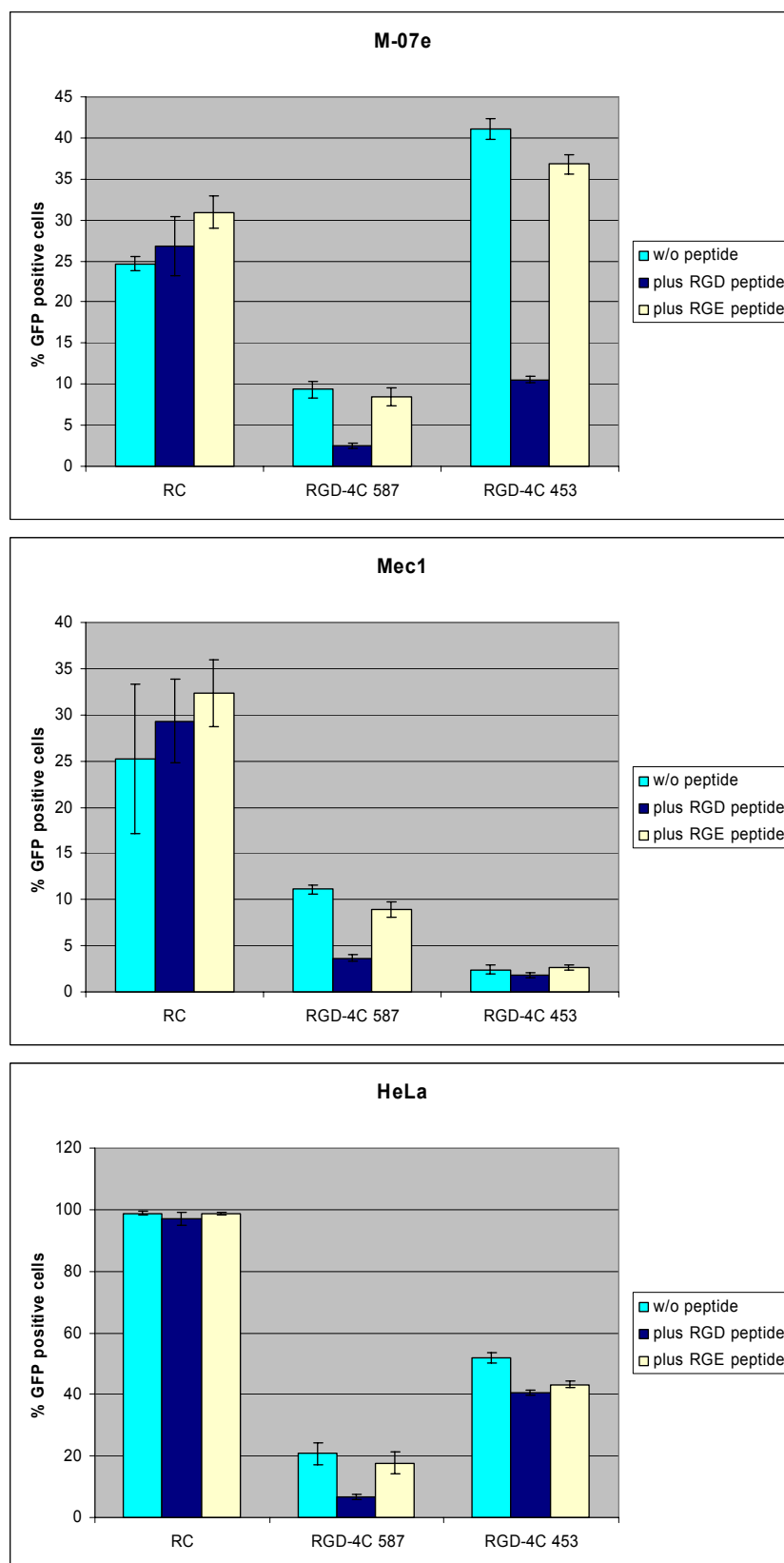
Fig. 28. Transduction efficiencies of RGD-4C mutants. Transduction efficiencies ± standard deviation in triplicate experiments as determined by FACS of RC rAAV/GFP (RC), RGD-4C 587 rAAV/GFP (RGD-4C 587) and RGD-4C 453 rAAV/GFP (RGD-4C 453) on M-07e, Mec1 and HeLa (cyan bars). Transduction rates were also assessed after pre-incubation of the cells with competing GRGDTP (blue bars) or unspecific GRGES (yellow bars)

3 Discussion

3.1 Incorporation of GFP-VP2 into the viral capsid allows the production of infectious particles

To track the intracellular trafficking of AAV and derived vectors in infected cells, we have tagged virions by incorporation of GFP-VP2 into the viral capsid. In a first step, chimeric virions containing VP1, VP2, GFP-VP2 and VP3 were produced. GFP-tagged AAV particles could also be generated without the addition of wild type VP2. This observation is in contrast to Yang et al. (1998), who showed that the AAV capsid is not able to tolerate large insertions at the N-terminus of VP2 without the simultaneous addition of wild type VP2. This discrepancy might be due to differences in the production and purification method: Yang et al. expressed the different VP proteins from three different plasmids controlled by the CMV promoter, and used a CsCl density gradient for purification. In addition, remaining helper virus was inactivated by heat. Using the natural AAV viral promoters and a helper virus-free production method allowed to efficiently generate particles with N-terminal VP2-fusions of different size (Loiler et al. 2003; Shi et al. 2001; Warrington et al. 2004; Wu et al. 2000). The largest insertion described so far is the 30 kDa GFP protein used by Warrington et al. and in our study. Interestingly, although Warrington and colleagues used the same amino acid position (aa 138) for the VP2 fusion, the genomic particle-to-infectivity ratio reported by Warrington et al. was remarkably higher (up to 130 fold less infectious) than ratios obtained for our GFP-tagged virions (Warrington et al. 2004). In addition an up to 30 fold higher amount of empty capsids was detected within their study. We observed a genomic particle-to-infectivity ratio between 84 and 195 for 60%-GFP-VP2-AAV, and between 208 and 2288 for the 100%-GFP-VP2-AAV, which is higher than ratios obtained for the wild type AAV within our study (29 and 62), but still in the range described for wild type preparations (Ried et al. 2002). Furthermore, no increase in the amount of empty capsids was detected. Since we used the same amino acid position for the fusion (aa 138), the differences observed must have been caused by other factors. One main difference could be the choice of the promoter responsible for the transcription of VP2. Warrington et al. used the natural p40 promoter, and translation was initiated from a modified and therefore stronger start codon (ATG instead of ACG),

which resulted in a more efficient VP2 and in the inhibition of VP3 initiation from this template. In our case, the viral CMV promoter was used to control the transcription of the fusion protein and the VP2 translation start codon was deleted. Warrington and colleagues performed a Western blot of their GFP-tagged virions. When comparing their Western blot results with the results obtained for our GFP-tagged virions packaged in the presence of pGFP-VP2 (Fig. 7), the most obvious difference was the amount of VP1 detected in the GFP-tagged virion preparations. While the preparations of Warrington and colleagues showed a clear reduction for the VP1 signal, the amount of VP1 in our preparations was comparable to wild type AAV. It is known that VP1 - possibly because of its phospholipase activity - is essential for AAV infectivity (Bleker et al. 2005; Girod et al. 2002; Kronenberg et al. 2005; Zádori et al. 2001). Therefore the reduced amount of VP1 within the preparations of Warrington et al. might be a reasonable explanation for the lower infectivity of the vectors produced by Warrington and colleagues and the discrepancy to our results. It remains unknown if the modification of the VP2 translation start codon as carried out by Warrington and colleagues or other factors are responsible for the VP1 reduction. However, our preparations yielded an up to 130 fold increased viral infectivity in comparison to Warrington et al., with an infectious titer of 10^9 per ml.

In addition, we could detect colocalization of A20 and GFP-VP2 derived signals by immunofluorescence within infected cells. Since A20 recognizes only intact capsids (Bleker et al. 2005), the integrity of AAV does not seem to be affected through the GFP-VP2 incorporation.

3.2 AAV capsids are not transported into the nucleus efficiently

According to the current model of AAV infection, AAV enters host cells by receptor-mediated endocytosis, which is a very fast process that occurs in approximately 60 ms (Seisenberger et al. 2001). Within the first 10 minutes, two-thirds of membrane bound virus particles are internalized (Bartlett et al. 2000). The endocytotic process and the subsequent trafficking steps are still poorly understood and may differ substantially in different cell types, and in some cases even in the same cell types (Duan et al. 2000; Hansen et al. 2001a). Different organelles have been proposed for the release of AAV

into the cytoplsm. Thereafter, the destiny of AAV remains unclear. Some studies have observed a perinuclear accumulation within 1-2 h p.i., which persisted in the absence of adenovirus coinfection for at least 16 h (Warrington et al. 2004; Xiao et al. 2002). In contrast, using laser scanning confocal microscopy, Bartlett observed AAV particles within the nucleus of infected cells already 2 h p.i. despite the absence of helper virus (Bartlett et al. 2000).

In this study, it was observed that intracellular trafficking of GFP-tagged virions occurs quickly at least in HeLa cells. This is in agreement with results obtained with SVT. This sensitive method allows the observation of single particles in a living cell. Due to this high sensitivity, it was possible to detect at least one AAV particle in the nuclear area of 50% of the cells 15 minutes p.i. In some cases, AAV reached the nuclear area within seconds (Seisenberger et al. 2001). In contrasts to this, the nuclear entry of intact AAV capsids is comparably slow. Although many virions were already accumulated in the perinuclear area before 2 h p.i. we observed in the absence of helper virus coinfection only isolated GFP signals from the GFP-VP2-AAV particles within the nucleus of cells at 11 and 24 h p.i. (no signal at 2 or 4 h p.i.). This result clearly contradicts results described by Bartlett et al., who observed in the absence of helper virus AAV particles inside the nucleus 2 h p.i. (Bartlett et al. 2000). This can be explained by the limited microscopic possibilities available at that time.

In adenovirus coinfected cells, a few GFP signals were observed within the nucleus 2 h p.i. (earliest time point observed), revealing that adenovirus is able to augment nuclear entry of AAV capsids. These results would confirm previous observations that described intact viral particles within the nucleus of coinfected cells in less than 1 h p.i. (Warrington et al. 2004; Xiao et al. 2002). However, the amount of AAV capsids we observed by applying the new vertical sectioning method for data analysis was much lower than described by (for example) Xiao et al. (2002). In all conditions and at all time points analyzed during this study, only very few GFP signals provided by the GFP-VP2-AAV particles could be detected within the nucleus. This was not due to the GFP-VP2-AAV virions used to analyze this step of the infectious biology, since the same image was obtained with wild type AAV visualized by A20 (Fig. 14). Even 11 h p.i. in the presence of helper virus, signals of intact capsids were detected inside the nucleus only in rare cases (cells were infected with 10^6 capsids/cell). The majority of AAV

capsids was detected in the perinuclear region. From this data it can be excluded that GFP tagged capsids are not transported into the nucleus due to the GFP incorporation.

3.3 Viral uncoating takes place before or during nuclear entry

From the experiments described above it was assumed, that the transport of intact viral capsids into the nucleus of infected cells is an inefficient process. Therefore, it might be an unspecific event, which is not needed for viral replication. We hypothesized, that viral uncoating takes place before or during nuclear entry independent of helper virus coinfection. This model was strengthened by the comparison of the amount of viral genomes with the amount of capsids detected within the nucleus at different time points of the infection in the presence and absence of helper virus: Neither in the presence nor in the absence of helper virus intact viral capsids were detected within the nucleus of cells infected with 10^5 instead of 10^6 viral capsids per cell. In contrast, under the same conditions, viral genomes were detected already 2 h p.i. within the nucleus with a slight increase in signals with prolonged observation times.

Almost no signals in the perinuclear region were observed, using an antibody specific for the C-termini of VP1, VP2 and VP3, which are buried within the intact capsid. Furthermore, no signals for dissociated capsid proteins were detected inside the nucleus. For parvovirus B19, it was recently shown *in vitro*, that the full length viral DNA is released from the capsids upon treatment with low pH (mimicking endosomal acidification) without capsid disassembly (Ros et al. 2006). This might be an explanation for not detecting dissociated capsid fragments or single capsid proteins in infected cells. A similar situation was seen for GFP-VP2-AAV. In cells infected with GFP-VP2-AAV only the viral genome was detectable inside the nucleus upon early time points after infection (4 h p.i.). GFP-VP2 signals were only detected in the perinuclear region. It is known that the VP2 region contains a nuclear localization signal (NLS), which is important during viral assembly, but it could not be proven that this NLS is also important for the incoming virus (Hoque et al. 1999). Moreover, it was shown in this study that VP2 knock out mutants are still infectious and furthermore, no GFP-VP2 signals of incoming virions are detected in the nucleus. However, it has to be considererd that VP1 also contains the VP2 region coding for the NLS.

In conclusion we can argue that the uncoating takes place before or during nuclear entry and is independent of helper virus coinfection. It still unclear, whether the AAV DNA is still associated with capsid proteins or needs the help of cellular proteins during nuclear entry.

3.4 Entry pathway and intracellular trafficking of GFP tagged AAV are not altered in comparison to wt AAV

AAV enters the cell through receptor mediated, clathrin dependent endocytosis (Bartlett et al. 2000; Duan et al. 1999). In this study, GFP-VP2-AAV colocalizes with transferrin, a marker for receptor mediated endocytosis, as seen for Cy3 labeled rAAV (Duan et al. 1999). This is a further evidence that the GFP tag does not interfere with the normal infectious pathway of AAV. Furthermore, colocalization of GFP-VP2-AAV and transferrin was observed in perinuclear compartments close to the nucleus. This suggests that AAV takes the same intracellular route as transferrin, trafficking through the perinuclear recycling endosome. In addition, GFP-VP2-AAV did not colocalize with the fluid phase marker dextran. This is congruent with observations of canine parvovirus (Parker and Parrish 2000).

Inhibition of viral infection with nocodazole was shown previously for AAV (Sanlioglu et al. 2000) indicating that AAV needs the microtubule network for intracellular trafficking. Velocities in the range of 1.8 and 3.7 µm/sec for directed movements were determined in previous work with Cy5 labeled AAV (Seisenberger et al. 2001). Live cell studies with GFP-VP2-AAV determined maximal velocities for single viral tracks with directed motion up to 4.5 µm/sec. Treatment of the cells with nocodazole abolished directed movements, whereas cytochalasin D had no effect on directed motion, thus giving evidence that the observed directed motions rely on microtubule transport. Microtubules are known to be the highways for long distance transport. Many viruses require microtubules during cell entry for efficient nuclear targeting, either for cytosolic transport of viral particles or for transport of particles inside vesicles. Among these viruses are herpes simplex virus (Sodeik et al. 1997), human immunodeficiency virus (McDonald et al. 2002), adenovirus (Suomalainen et al. 1999), parvoviruses (Seisenberger et al. 2001; Suikkanen et al. 2003), simian virus 40 (Pelkmans et al. 2001), influenza virus (Lakadamyali et al. 2003) or hepatitis B virus (Funk et al. 2004).

The velocities measured in this study are in agreement with published results for different viral particles moving along microtubules at speeds of 0.2-4 μm/sec (Suomalainen et al. 1999; Seisenberger et al. 2001; Lakadamyali et al. 2003; Sampaio et al. 2005; Wolfstein et al. 2006). About 50% of GFP-VP2-AAV particles moved with velocities of 0.5-1 μm/sec. This is slightly slower than measured by Single Virus Tracing. However, this can be due to a better time resolution of the SVT setup, which allowed to take images every 40 msec in contrast to a time laps of 1000 msec used when generating movies with the conventional microscope. Viral particles are difficult to track if the distance of a particle between two frames within a movie is too large. But even so, the velocities are comparable to velocities measured for other viral particles.

All together, these results, which demonstrate the integrity of the viral capsid, and time kinetics and intracellular viral trafficking comparable to wt or cyanine dye labeled capsids, prove that GFP tagged AAV can be used for live cell studies. Furthermore, preliminary data showed that GFP-VP2-AAV can be utilized for visualization of viral infections in animal tissue. This potential provides a novel method for monitoring viral infection within preclinical models.

In continuation of this work, the VP2 N-terminus is currently being tested as a retargeting site. Since this site tolerates large insertions such as GFP, we tested the insertion of larger retargeting polypeptides, such as single chain antibodies. It was shown, that also incorporation of polypeptides similar in the size of GFP allow the production of viral particles. Titers of these vectors were comparable to wt and GFP-VP2-AAV. Furthermore, transduction of wt AAV permissive HeLa cells, could be prevented successfully by introducing additional mutations inside the HSPG binding region. It is currently being tested, whether the incorporation of a single chain antibody redirect viral tropism.

3.5 PLA2 – an important domain within the AAV2 capsid

The unique region of VP1 plays a central role in parvovirus biology. Sequence alignment of the VP1 unique sequence of most parvoviruses including AAV2 identified a phospholipase A2 (PLA2) motif, resembling the catalytic domain of secreted PLA2 (sPLA2), an activity that was not known to exist in viruses (Zádori et al. 2001). PLA2 hydrolyses specifically the 2-acyl ester (*sn*-2) bond of phospholipids to generate

lysophospholipids and free fatty acids. Mutations of critical amino acid residues in the putative PLA2 of porcine parvovirus (PPV) resulted in strongly reduced PLA2 activity and virus infectivity (Zádori et al. 2001). Mutation in the catalytic center of PLA2 within the AAV2 capsid showed a drastically reduced and delayed Rep expression. PLA2 mutants were not affected in packaging. Binding to or entry into cells were both unaffected in those mutants. This suggests that the PLA2 activity is required for a step in the virus life cycle following perinuclear accumulation of virions, but prior to the onset of early gene expression. Moreover, it was shown that the loss in infectivity of the PLA2 mutant cannot be restored by complementing the PLA activity *in trans* (Girod et al. 2001). The PLA2 domain resides inside the capsid, but it was shown for AAV2 that VP1 is exposed after heat shock (Kronenberg et al. 2005). For minute virus of mice (MVM), another member of the parvovirus family, it was demonstrated that also low pH dependent endosomal processing leads to the externalization of VP1 (Mani et al. 2006).

Results of this study demonstrate that wt AAV2 and the PLA2 mutant are trafficked to the same perinuclear compartment or region. Evidence was provided by immunofluorescence costainings of the ER and the viral capsids. Wild type and mutant AAV accumulated both within the ER region stained with a specific antibody. In electron microscopy for this region of interest, accumulations within tubular-reticular structures characteristic for the ER were observed. Although unusual for viruses, it is known that simian vacuolating virus 40 (SV40) is sorted into the smooth ER bypassing the Golgi complex (Pelkmans et al. 2001; Norkin and Kuksin 2005). Viral capsids of AAV 2 and 5 localized inside the Golgi area was observed (Pajusola et al. 2002; Bantel-Schaal et al. 2002). For AAV2 this was observed by immunofluorescence at 2.5 h p.i. in contrast to 4 h p.i. which was the time point of observation in our study. Therefore, it could be possible that AAV passes the Golgi complex on its way to the ER. Several toxins (e.g. Shiga toxin) are routed from the endosome through the Golgi apparatus to the ER to be finally released into the cytosol, showing that this pathway in principal exists (Sandvig et al. 1992; Lauvrak et al. 2004, Saint-Pol et al. 2004). How SV40 transfers its DNA from the ER into the nucleus is not known, but it seems to involve a cytosolic phase, because neutralizing anti-SV40 antibodies injected into the cytoplasm inhibited the infection (reviewed by Greber and Fornerod 2005). Furthermore, SV40 enters the nucleus through the nuclear pore complex (Clever et al. 1991). To decide to

which organelle AAV2 is finally transported, more time points will have to be analyzed. In addition, other fixation protocols and immunogold staining will have to be performed.

Furthermore, free viral particles inside the cytoplasm were detected for both the wt AAV and the PLA2 mutant, suggesting that the PLA2 activity is not important for the release from membrane surrounded organelles. In addition, DNA containing viral particles (also of the PLA2 mutant) were detected in close vicinity of the nuclear membrane and inside nuclear invaginations. The only difference between the wild type and the PLA2 mutant observed until now, is that no viral DNA of the PLA2 mutant was detected inside the nucleus and in consequence no DNA replication was detected. From this preliminary data we suggest that the PLA2 activity might be involved directly in nuclear entry and not in release from membrane surrounded organelles.

3.6 Amino acid position 453 is an alternative insertion site

The knowledge of possible insertion sites within the capsid that do not interfere with capsid assembly and infectivity, is important for both the generation of labeled vectors and retargeting vectors. Quite an effort was done in this field. Insertion sites were found by insertional mutagenisis or with the help of a hypothetical model of the AAV2 capsid three dimensional structure, which was derived upon capsids protein amino acid sequence alignment between CPV and AAV2 (Wu et al. 2000; Shi et al. 2001; Girod et al. 1999). Position 587 is the most promising retargeting site based on this alignment model (Girod et al. 1999). Furthermore, different positions close to the 453 site were tested: 447 (Girod et al. 1999) 441, 459 (Shi et al. 2001). Insertion at these sites all interfered with viral transduction. Recently, the atomic capsids structure of AAV2 was determined by x-ray crystallography (Xie et al. 2002). Determining the location of the three positions 441, 447, 459 based on the new published structure, we observed that all are located within the two ß-barrels forming the highest peak of the AAV capsids and therefore probably interfere with the ß-sheet folding. Using this structural data, the 453 position was identified, which is located inside the linker sequence between the two ß-sheets, forming the peak (Fig. 26).

Originally we wanted to use this site to introduce an α-helical tetracystein-containing peptide which is specifically recognized by FLASH-EDT$_2$ (fluorescein arsenical helix binder-1,2 ethanedithiol adduct). This component becomes strongly fluorescent after

binding to the tetracystein peptide (Griffin et al. 1998). However, we observed that insertion of this α-helical peptide was not compatible with viral cell transduction. Reason for this might be that the spacer between peptide and capsids sequence was too short and therefore the folding of an α-helix interfered with capsid assembly. To overcome this a larger spacer flanking the peptide has to be tested.

Since our group is interested in generating vectors for gene therapy we tested this site for its ability to insert retargeting peptides. Both retargeting peptides, NGR and RGD-4C, at the 453 position mediated an enhanced transduction efficiency of target cells. However, the 453 insertion mutants still showed affinity for HSPG. This conclusion was drawn from the observed 6 fold reduction in transduction of HUVEC with NGR-453-rAAV in the presence of soluble heparin. This was not unexpected since the residues reponsible for HSPG binding are not touched by insertions at the 453 position. This was also observed for the RGD-4C insertion at the 453 site. HeLa cells were better transduced by RGD-4C-453-rAAV/GFP (52%) than by RGD-4C-587-rAAV/GFP (21%) and transduction was inhibited by soluble RGD peptides only to a minor extent (52% to 40%). For *ex vivo* application a better transduction of cells in comparison to the wt AAV would be sufficient. In systemic application however, the binding to the natural primary receptor is not desirable, for safety and efficiency reasons. Therefore, we decided to replace the essential arginines involved in HSPG binding at amino acid position 585 and 588 with alanines (in addition to the 453 insertion). The production of these viruses is in process. Furthermore, we are interested whether a double insertion mutant at 453 and 587 is functional. This would provide the opportunity to either insert more ligands at the capsid surface or to insert two different ligands to improve transduction of target cells.

However, the data provide evidence for the direction of the insertion mutants towards an alternative receptor. The NGR-453 mutant showed a 3 fold better transduction efficiency in comparison to RC-rAAV on HUVEC.

Concerning the targeting capability of 453 mutant another prove has been made: the RGD-4C insertion at the 453 position enhanced in comparison to RC-rAAV transduction of M-07e cells which are devoid of HSPG (41% in comparison of 25%). Transduction could be inhibited 4 fold by RGD containing but not RGE containing soluble peptides, showing that insertion at the 453 site mediates the M-07e transduction. Interestingly the RGD-4C peptide inserted into the 587 position transduced M-07e cells

poorly (9%) although it was shown in previous work in our lab that two different RGD containing peptides were fished on M-07e cells in an AAV display. Furthermore, it was shown that these fished RGD peptides inserted into the AAV capsid at the 587 position specifically transduce M-07e but not Mec1, demonstrating that the viral display selects peptides specific for the cells used during the selection (Perabo et al. 2003). From this it can be concluded that not only the RGD motif itself mediates efficient transduction, but the amino acid context of the RGD motif and the location of the insertion within the capsid is important for transduction. This indicates that insertion into the 453 position might be more efficient than the 587 or vice versa, depending on the inserted peptides. In summary, the 453 site seems to be a promising alternative and/or a additional position to the 587 site for insertion of retargeting peptides.

3.7 Conclusions and outlook

Different methods (Western blot, immunofluorescence microscopy and FACS analysis) showed that GFP-VP2 is incorporated into the viral capsid. A detailed titer analyses revealed that genomic particle and infectious titers are comparable to wild type titers. Also the behavior of GFP tagged AAV particles in intracellular trafficking, velocities of directed movements, colocalization with endocytotic marker and nuclear localization of the viral genome was indistinguishable to wt AAV visualized by antibodies or direct labeling with chemical dyes. Furthermore, first data demonstrated that GFP-VP2-AAV can be detected also in infected animal tissue. All together, GFP-VP2-AAV seems to be a promising alternative for chemical labeling of the viral capsid. This knowledge provides a platform for utilization of GFP-VP2-AAV for further studies of the infectious biology of AAV. Future projects will include the introduction of the GFP-VP2 fusion protein into viral capsids of different serotypes and retargeting mutants and studies on the intracellular trafficking in different cell types. Alternative fluorescent proteins such as DsRed will be tested to concomitantly trace the intracellular trafficking of different viruses. The knowledge derived from these studies should help to design better vectors for gene therapy.

Another major conclusion from the work presented here, is that uncoating takes place before or during nuclear entry. This conclusion was drawn from the inefficient transport of intact viral capsids of incoming AAV into the nucleus and the finding that in contrast

to viral capsids the viral genome can be detected inside the nuclei shortly after infection independently of helper virus coinfection.

Although the question of the function of the PLA2 domain is not solved, it seems that it is not required for endosomal release since both wt and PLA2 mutant capsids are found in the cytoplasm and inside nuclear invaginations. Since in contrast to the wt AAV no genome of the PLA2 mutant was detected inside the nucleus, we could narrow down the function of the PLA2 activity to a role in nuclear entry.

Concerning that AAV is routed within the same compartment like transferrin and that AAV is detectable inside the endoplasmatic reticulum (based on immunofluorescence and electron microscopic data), we complemented some possible details to the current entry pathway of AAV (Fig. 29). However many questions remain to be answered. What is the role of the ER in AAV infection? What is the mechanism of nuclear entry? Is the PLA2 activity needed for nuclear entry?

The desire to test another labeling method resulted in the detection of the 453 position as an alternative insertion site for the generation of AAV retargeting mutants. 453 is located at the top of the higher peak within the VP3 protein. Insertion of different targeting peptides showed a great enhancement in transduction of target cells. Since the HSPG binding site is not affected by insertion at the 453 site, in contrast to insertions at the 587 position (normally used for retargeting in our group), the wt tropism is not abolished which is desirable with regard to labeling. To improve this vector for ultilization in systemic application a HSPG binding knock out is generated in addition to the 453 insertion.
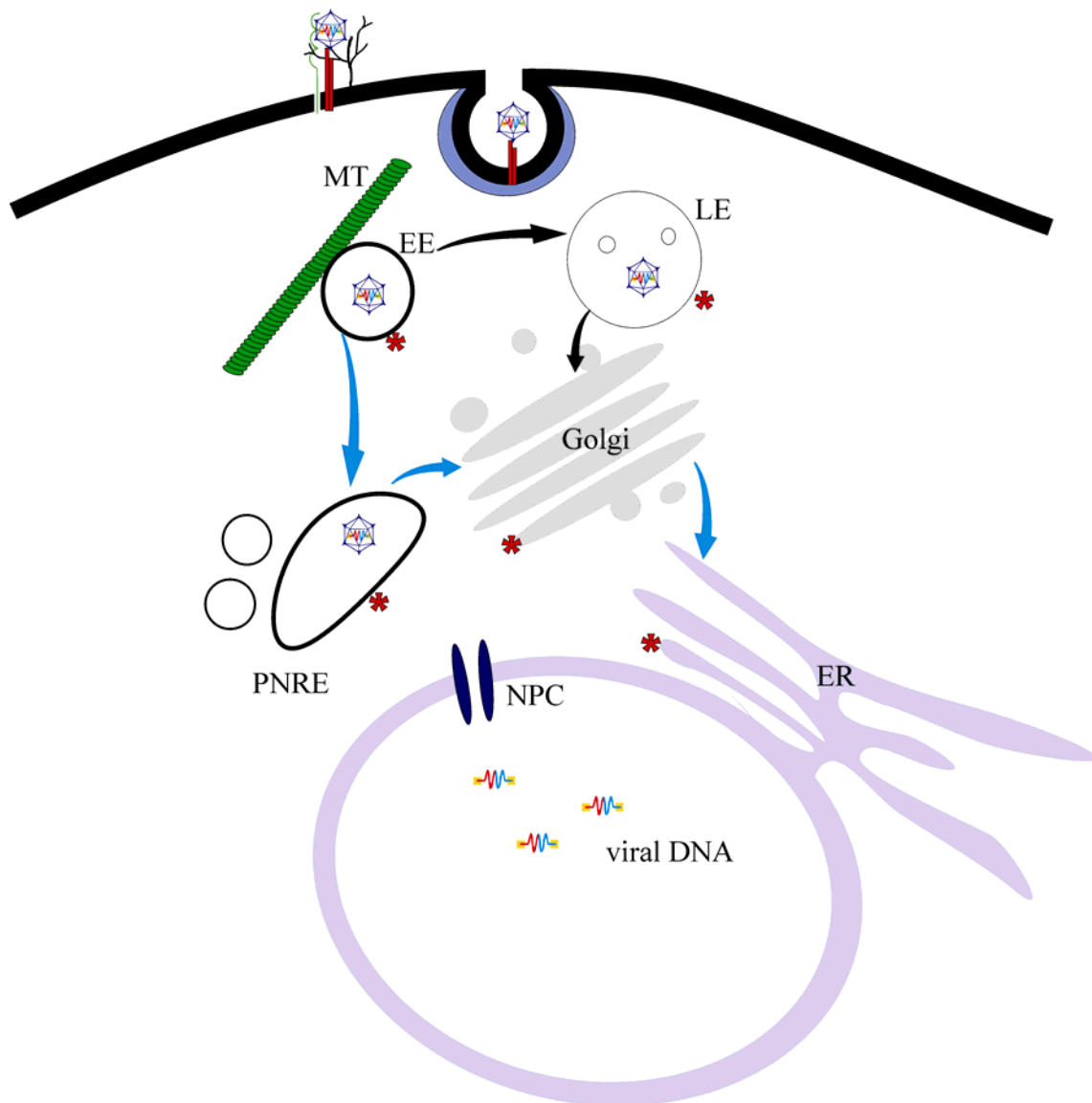
Fig. 29. Model of viral infection modified based on our current results. The potential intracellular pathways of AAV after receptor mediated endocytosis based on our own and other studies are depicted. Red asterisks mark potential sites where AAV is released into the cytoplasm. There is evidence that AAV is routed from the early endosome (EE) through the perinuclear recycling endosome (PNRE) (Xiao et al. 2002; Duan et al. 1999 and our own observations). From there it may enter the Golgi complex (Pajusola et al. 2002). From the Golgi AAV may be trafficked to the endoplasmatic reticulum (blue arrows) (own observations). Instead of being routed through the PNRE it may be trafficked to the late endosome (LE) (black arrows) (Douar et al. 2001; Hansen et al. 2001a). Once released into the cytosol uncoated viral DNA enters the nucleus (own observations) possibly through the nuclear pore complex (NPC).

4. Experimental procedures

4.1 Materials

4.1.1 Antibodies

Antibodies against cellular antigenes

- Polyclonal goat anti Lamin B antibody, IgG (Santa Cruz Biotechnology)
- Polyclonal rabbit anti calreticulin antibody, IgG (Affinity BioReagents)

Antibody against AAV2 proteins

- Rep76/3 (Rep-specific antibody), monoclonal mouse hybridoma supernatant (DKFZ Heidelberg, PD Dr. J. Kleinschmidt)
- A20 (AAV2-capsid antibody), monoclonal mouse hybridoma supernatant (DKFZ Heidelberg, PD Dr. J. Kleinschmidt)
- B1 (VP3-specific antibody), monoclonal mouse hybridoma supernatant (DKFZ Heidelberg, PD Dr. J. Kleinschmidt)

Secondary antibodies

- Texas Red conjugated donkey anti goat antibody (Dianova)
- Cy5 conjugated donkey anti goat antibody (Dianova)
- Cy5 conjugated donkey anti rabbit antibody(Dianova)
- FITC conjugated goat anti mouse antibody (Dianova)
- RRX conjugated goat anti mouse antibody (Dianova)
- Biotin-SP-conjugated rabbit anti mouse antibody (Dianova)
- AP conjugated anti Dig Antibody (Roche)
- Peroxidase conjugated anti mouse IgG (H+L) (Sigma)

4.1.3 Cell lines

Cell line	description	source
293	human embryonic kidney cells immortalized by adenoviral genes E1A and E1B	ATCC CCL 2; American Type Culture Collection, Rockville, Maryland
HeLa	human cervix epitheloid carcinoma	ATCC CCL 2
HeLa dsRed Nuc	HeLa stably transfected with SV40NLS::DsRed	generated by Nico Görlitz in our laboratory
HFF	human foreskin fibroblast (primary cells)	PomoCell GmbH, Heidelberg, Germany
HUVEC	human umbilical vein endothelial cells (primary cells)	isolated from umbilical cords
M-07e	human megakaryotic leukemia cell line	James D. Griffin, Boston, Massachussets
Mec1	B-cell chronic lymphatic leukemia cells in prolymphoid transformation	Federico Caligaris-Cappio, Torino, Italy
PtK$_2$	male rat kangaroo kidney epithelial cells (derived from metastatic site)	Beate Sodeik, Hannover, Germany

4.1.4 Viral strains (besides AAV)

Wild type adenovirus type 5 was generated in HeLa in the group of Prof. Hallek using the plasmid pTG3602 which encodes wt adenovirus 5.

4.1.5 Bacterial strains

Plasmids were amplified in *E. coli* TOP10F' and DH10B (Invitrogen).

TOP10F':

F' {*lac*Iᑫ*Tn10*(Tet^R)} *mcr*A Δ(*mrr-hsd*RMS-*mcr*BC) Φ80*lac*ZΔM15 Δ*lac*X74 *deo*R *rec*A1 *ara*D139 Δ (*ara-leu*)7697 *gal*U *gal*K *rps*L (Str^R) *end*A1 *nup*G

(Invitrogen Corp., Karlsruhe)

DH10B:

F' *mcr*A Δ(*mrr-hsd*RMS-*mcr*BC) Φ80*lac*ZΔM15 Δ*lac*X74 *rec*A1 *end* A1 *araD139* Δ (*ara-leu*)7697 *gal*U *gal*K λ-*rps*L *nup*G

(Invitrogen Corp., Karlsruhe)

4.1.6 Plasmids

Plasmid purification was performed using QIAGEN plasmid purification kits.

Plasmids from our or cooperating institutions:

pUC-AV2 (pwt)

wtAAV2 genome (*rep-cap* ORF flanked by ITRs) cloned into pUC19. Within the pUC19 backbone an ampicillin resistance gene is encoded. The plasmid was purchased from the MediGene AG (Martinsried) (Ried et al. 2002).

psub201(+)

contains like pwt the wtAAV2 genome: *rep-cap* ORF flanked by ITRs (Samulski et al. 1987).

pHD/AN

pHD/AN was generated by site specific mutagenisis of the *cap* gene within pwt, inducing a substitution of the amino acids histidine (D) and aspartic acid (D) to alanin (A) and asparagin (N) at amino acid position 76 and 77, respectively, within N-terminus of the capsid protein VP1. These amino acids are located within the catalytic center of the phospholipase A2 domain (Girod et al. 2002). The plasmid was obtained from the plasmid-bank of the group of Prof. Hallek.

pxx6

Adenoviral helper plasmid: expression plasmid of adenoviral helper proteins: VA, E2A, E4 and ampicillin resistance gene. pXX6 was kindly provided by R. J. Samulski (Chapel Hill, University of North Carolina, USA).

pGFP

The pGFP plasmid is an AAV vector plasmid in which the AAV ITR sequences flanking the hygromycin selectable marker gene controlled by the thymidine kinase promoter and the *Aequorea victoria* Green Fluorescence Protein (GFP) gene regulated by the cytomegalovirus promoter.

pRC

The pRC plasmid was constructed as previously described (Girod et al. 1999). Briefly, the 4.5 kb Xba I-fragment of psub201(+) (Samulski et al. 1987), containing the *rep* and *cap* ORFs of AAV was subcloned into the Pst I and BamH I sites of pSV40oriAAV. No ITRs are encoded (Chiorini et al. 1995).

pOEN

For the construction of plasmid pOEN, the HCMV promoter/enhancer cassette and the GFP open reading frame in the plasmid pEGFPC-1 (Clontech) were substituted with the wt AAV-2 genome encoding fragment of plasmid pUC-AV2. A DNA fragment encoding amino acids AAAstopA and the restriction sites NotI and AscI was inserted between amino acid position 587 and 588 by PCR mutagenesis (Perabo et al. 2003).

Generation of plasmids:

pUC-AV2-VP2k.o.

The plasmid pUC-AV2-VP2k.o. was obtained by PCR amplification combined with site directed mutagenesis of pUC-AV2, changing the ACG start codon into ACC using overlapping PCR fragments (VP2ko_for: 5´-GTTAAGACCGCTCCGGG-3´ and 4066: 5´-ATGTCCGTCCGTGTGTGG-3´; VP2ko_back: 5´-CCCGGAGCGGTCTTAAC-3´ and 3201: 5´-GGTACGACGACGATTGCC-3´) and ligation of the fragments by a second PCR step using the primers 3201 and 4066. The resulting fragment was digested with BsiWI and EcoNI and sticking end ligated into pUC-AV2.

pGFP-VP2

To obtain the plasmid pGFP-VP2 the sequence coding for VP2 was amplified from pSUB201[+] by PCR using the primer pair VP2-N 5´- CTCCGGGAAAAAAGAGG-3´ and VP2-C: 5´-TTACAGATTACGAGTCAGGTAT-3´, thereby deleting the VP2 start codon and ligated into pEGFP-C3 (Clontech), which was digested with Bgl II and filled in by Klenow polymerase. The plasmid pDsRed2Nuc was generated by deletion of the EGFP encoding region from pEGFP-Nuc (Clontech) and insertion of the DsRed2 gene, which was amplified by PCR (Primers: 5'-CGG AGT ACA TCA ATG G-3' and 5'-AGA TCC GGT GGA TCC TAC CT-3') from pDsRed2-N1 (Clontech) and cut with AgeI.

Plasmids with insertions at 453 or 587 position: pRC FLASH 453, pRC NGR 587, pRC NGR 453, pRC RGD 587, pRC RGD 453, pRC RGD 587

Peptide insertion at the 453 or 587 position within VP3 were generated by site directed mutagenisis of the *cap* ORF within pRC. Briefly, two primer pairs were designed, with overlapping inner primers of opposite priming directions which contain a 5' overlap encoding for the peptide insertions (primers see below) and two outer primers binding

in the pRC backbone up and downstream from the insertion site (453 and 587) (3201 5´-GGTACGACGACGATTGCC-3´, 4066: 5´-ATGTCCGTCCGTGTGTGG-3). In this way two overlapping PCR fragments were generated containing each one part of the peptide insertion sequence. In a second PCR step, using the two overlapping PCR fragments from the first PCR as templates and the primers 3201 and 4066, the two overlapping PCR fragments were ligated. The resulting fragment and the pRC backbone were cut with restriction enzymes BsiWI and XcmI and ligated. All cloning procedures were done using standard protocols (Maniatis et al. 1989).

Primers

FLASH_for 5'-TGT AGA GAA TGT TGT GCA CGA GCA GGA ACC ACC ACG CAG TCA AGG CT-3' and **FLASH_back** 5'-ACA CGC TTC TCG TGC TGC AGC TTC CCA TCC TCC TCC ACT TGG AGT GTT TGT T-3'

NGR 453_for 5'-GCC GCA TGG AGT GCG CGA CCA CCA GCG AGT CAA GGC T-3' and **NGR 453_back** 5'-CGT TCA GTA CGC ACG CTC CAG TTG GAG TGT TTG TT-3'

NGR 587: (OJE 007) 5'-CGC GTG CGT ACT GAA CGG CCG CAT GGA GTG CG-3' and **OJE 008** 5'-CGC GCG CAC TCC ATG CGG CCG TTC AGT ACG CA-3'

RGD4C 453_ for 5'-GCG TGT GAC TGC CGC GGA GAC TGC TTC TGT GCG ACC ACC ACG CAG TCA AGG CT-3' and **RGD4C 453_back** 5'-CGC ACA GAA GCA GTC TCC GCG GCA GTC ACA CGC TCC ACT TGG AGT GTT TGT T-3'

RGD4C 587: OJE 011 5'-CGC GTG TGA CTG CCG CGG AGA CTG CTT CTG TG-3' and **OJE 12** 5'-CGC GCA CAG AAG CAG TCT CCG CGG CAG TCA CA-3' 4066: 5´-ATGTCCGTCCGTGTGTGG-3´ and 3201: 5´-GGTACGACGACGATTGCC-3´

Synthetic Oligonucleotides

All synthetic oligonucleotides were obtained by Metabion in Martinried.

DNA sequencing

Sequence analyses for control of cloned plasmids were carried out by the sequencing unit of the Gene Center headed by Dr. Blum.

4.1.7 Chemicals and other Material

Aceton	Roth, Karlsruhe
Agarose	Sigma, Deisenhofen
Ampicillin	Sigma, Deisenhofen
Aqua bidest.	Millipore
ARES^{TM} DNA Labeling Kit	Molecular Probes, Oregon, USA
Benzonase	Merck, Darmstadt
Biomax Light Film	Kodak, New York, USA
Biotin conjugated Streptavidin	Dianova, Hamburg
Biotin Nick Translation Mix	Roche, Mannheim
Bovines Serumalbumin	AppliChem, Darmstadt
Canulas	Peske, Aindling
Cell culture plasticware	TPP, Trasadingen, Switzerland
Coverslips	Roth, Karlsruhe
Cy5 Monofunctional Dye	Amersham Pharmacia Biotech
Dextran conjugates	Molecular Probes, Oregon, USA
Dialyse Cassettes	Pierce, Rockford, USA
DIG DNA Labeling and Detection Kit	Boehringer Mannheim
DNA Pol I	New England Biolabs, Schwalbach
dNTPs	Boehringer Mannheim
Dulbecco´s MEM with Glutamax	Invitrogen, Karlsruhe
EDTA	AppliChem, Darmstadt
EndoFree® Plasmid Maxi Kit	Qiagen, Hilden
Ethidiumbromid	Roth, Karlsruhe
Fetal calf sera	Invitrogen Corporation
Filter 0,20μm,0,45μm	Peske, Aindling
Formaldehydlsg. min. 37%	Merck, Darmstadt
Formamid	Fluka ChemieAG, Buchs, Schweiz
Gelatine	Sigma, Deisenhofen
Glycine	Merck, Darmstadt
Heparin	B. Braun Melsungen AG
HEPES	Roth, Karlsruhe
HiTrap Heparinaffinity chromatography-column	Amersham Pharmacia Biotech
Iodixonal (Optiprep)	Sigma, Deisenhofen
Isopropanol	Roth, Karlsruhe
Maleic acid	Sigma, Deisenhofen
Methanol	Roth, Karlsruhe
Molecular weight marker:	
-1kb or 100bp ladder	
-λ DNA Hind III	New England Biolabs, Schwalbach
NeutrAvidin RRX conjugate	Molecular Probes, Oregon, USA
Nitrocellulose membrane	Schleicher & Schuell, Dassel
Objectholder	Medco, München
Parafilm	Roth, Karlsruhe
Paraformaldehyd	Sigma, Deisenhofen
PBS	Invitrogen Corporation
Penicillin/Streptomycin	Invitrogen Corporation

Permafluor   Immunotec, Heidelberg
Proteinase K   Merck, Darmstadt
Reaction tubes   Falcon and Eppendorf
Restriction enzymes   New England Biolabs, Schwalbach
Salines Sodium Citrate (SSC)   Merck, Darmstadt
Sodiumchlorid   Riedel-de Haën, Seelze
Sodiumdodecylsulfat (SDS)   Merck, Darmstadt
Transferrin conjugates   Molecular Probes, Oregon, USA
TMB   Sigma, Deisenhofen
Tris   Merck, Darmstadt
Triton®X-100   Sigma, Deisenhofen
Trypsin-EDTA   Invitrogen, Karlsruhe
Tween®20   Merck, Darmstadt

Standard Kits

DNeasy®Tissue Kit   Qiagen, Hilden

EndoFree® Plasmid Kits   Qiagen, Hilden

PCR Purification Kit   Qiagen, Hilden

Gel Extraction Kit   Qiagen, Hilden

Light-Cycler-FastStart DNS Master SYBR Green I   Roche, Mannheim

Buffer and Solutions

For buffers and solutions, please refer to the corresponding chapters.

4.2 Methods

4.2.1 Cell culture

All cells were maintained at as monolayer culture at 37°C and 5% CO_2 in adequate media and supplements (see table below). 100 U/ml penicillin and 100 mg/ml streptomycin were added to the media.

Cell line	media	Supplements (additional)
293	DMEM	10 % FCS, 2 mM L-glutamine
HeLa	DMEM	10 % FCS, 2 mM L-glutamine
HeLa dsRed Nuc	DMEM	10 % FCS, 2 mM L-glutamine
HFF	DMEM	10 % FCS, 2 mM L-glutamine
HUVEC	ECGM	2% FCS, 0,4% Endothelial Cell Growth Supplement
M-07e	RPMI	10 % FCS, Interleukine 3 (10 ng/ml), 2 mM L-glutamine
Mec1	Isocove's media	10 % FCS, 2 mM L-glutamine
PtK_2	MEM	10 % FCS, 0.1 mM NEAA, 2 mM L-glutamine

DMEM: Dulbecco´s modified Eagle´s medium (Invitrogen), ECGM: Endothelial Cell Growth Medium (PromoCell); RPMI 1640 media (Invitrogen) Iscove's media (PromoCell), MEM: minimal essential media (Invitrogen), FCS fetal calf sera (Invitrogen), NEAA non essential amino acids (Invitrogen)

Cell stocks

About 10^7 cells were suspended in cold freeze medium (50% FCS, 40% cultivation media, 10% DMSO), distributed in 1ml Cryo-tubes (Nunc) and cooled on ice for at least one hour. Stocks were then cooled in the -80°C freezer and later stored in liquid nitrogen.

For recultivation Cryo-tubes were thawed in warm water and cells were quickly suspended in the according medium. Cells were pelleted at 300g and resuspended in fresh medium to remove DMSO.

Isolation of primary HUVEC

Primary HUVEC were isolated from umbilical cords obtained from the Newborn Clinic at the hospital of the Ludwig-Maximilians-University (LMU, Großhadern, Germany) in agreement with the guidelines of the ethic commission of the hospital of the LMU. An isolation protocol described by Jaffe and colleagues was applied with some slight modifications (Jaffe et al. 1973). Briefly, umbilical veins were rinsed with PBS several times, and incubated with 0.2% collagenase type IV in PBS (Sigma) at 37°C for 10 minutes. HUVECs were harvested by rinsing the veins with PBS several times and collected in a 50 ml reaction tube. After centrifugation, cells were resuspended in Endothelial Cell Growth Medium (PromoCell).

4.2.2 Viral production and purification.

AAV particles were produced in HEK293 cells by the adenovirus free production method using pXX6 (Xiao et al. 1998) to supplement the adenoviral helper functions. Briefly, HEK293 cells were seeded at 80% confluence in 15cm^2 cell culture plates and cotransfected with the packaging plasmids by calcium phosphate precipitation with a total of 37.5 µg plasmid. For each plate a solution of 1ml CaCl (250mM), DNA and 1ml transfection buffer HBS (50mM HEPES, 280mM NaCl, 1.5 mM NaP) was prepared, incubated for 2 min and pipetted onto the plate while cautious mixing with the medium. 15-20 plates per vector were transfected for large scale production and 3-5 plates for small scale production.

For the production of wild type AAV pUC-AV2 and pXX6 were transfected in a 1:1 molar ratio. For the production of chimeric virions cells were transfected with pXX6, pUC-AV2 and pGFP-VP2, substituting 30% or 60% of pUC-AV2 with pGFP-VP2. For the production of the VP2 k.o.-AAV HEK293 cells were transfected with pUC-AV2-VP2k.o. and pXX6 in a 1:1 molar ratio. For the production of the 100%-GFP-VP2-AAV pUC-AV2-VP2k.o., pGFP-VP2 and pXX6 were transfected in 1:1:1 molar ratio. For the production of recombinant AAV (rAAV) pXX6 and pGFP were transfected with either pRC, pRC NGR 453, pRC NGR 587, pRC FLASH 453, pRC RGD4C 453 or pRC RGD4C 587 in 1:1:1 molar ratio respectively. 48 h post transfection cells were harvested and pelleted by low-speed centrifugation. Cells were resuspended in 150 mM NaCl, 50 mM Tris-HCl (pH 8.5), freeze-thawed several times, and treated with 50 U/ml Benzonase for 30 minutes at 37°C. To purify the viral preparation by iodixanol gradient centrifugation, the cell debris was spun down at 3700g for 20 minutes at 4°C and supernatant was loaded onto an iodixanol gradient containing a 60% iodixanol phase at the bottom, following by 40%, 25% and 15% iodixanol phase. Iodixanol solutions of different concentrations were layered beneath the virus containing solution. The gradient was centrifuged in an ultra centrifuge at 65.000rpm for 1.5h and at 18°C. The 40% and in some cases the 25% phase were then extracted with a canula by puncturing the tube underneath the 40% phase and allowing the solution to drip into a Falcon tube until the 25% phase was reached. The 25% phase was collected in a new Falcon tube.

15% Iodixanol :		25% Iodixanol :	
10xPBS	5 ml	10xPBS	5 ml
2 M MgCl2	25 µl	2 M MgCl2	25 µl
1 M KCl	125 µl	1 M KCl	125 µl
5 M NaCl	10 ml	Optiprep	20 ml
Optiprep	12.5 ml	0.5% Phenolrot	75 µl
0.5% Phenolrot	75 µl	Sigma Wasser	ad 50 ml
Sigma Wasser	ad 50 ml		

40% Iodixanol:		60% Iodixanol:	
10xPBS	5 ml	2 M MgCl2	25 µl
2 M MgCl2	25 µl	1 M KCl	125 µl
1 M KCl	125 µl	Optiprep	50 ml
Optiprep	33.3 ml	0.5% Phenolrot	25 µl
Sigma Wasser	ad 50 ml		

To generate highly pure viral preparations, a heparin affinity chromatography was performed in addition. The viral solution was loaded onto a 1ml HiTrap Heparin affinity column (Amersham) utilizing of a sterile peristaltic pump with a flow rate of 0.3 ml/sec. The column was washed with PBS substituted with 2 mM $MgCl_2$ and 1 mM KCl. The virus was eluted with PBS 1M NaCl.

4.2.3 Determination of AAV titers

Particle titer of vector stocks was determined by quantitative PCR (Theiss et al. 2003) or DNA dot-blot hybridization (Girod et al. 1999). Therefore, viral DNA was isolated from vector stocks according to the DNeasy kit protocol (Qiagen, Hilden, Germany). Capsid titer of vector stocks was determined by A20-ELISA as previously described (Girod et al. 1999). Infectious titer was obtained by infecting HeLa cells as monolayers on cover slips with serial dilutions of viral preparations in the presence of adenovirus type 5 (MOI 5). 72 h post infection Rep protein expression was determined by immunofluorescence staining (Wistuba et al. 1997). Briefly, cells were fixed in methanol and acetone for 5 min, respectively. After washing with PBS, unspecific reactions were blocked by incubation with 0.2% gelatine in PBS for 10 min. The cover slips were incubated for 1 h at room temperature with the anti-Rep antibody 76/3 (kindly provided by Dr. Jürgen Kleinschmidt, DKFZ Heidelberg, Germany), cover slips were washed and blocked again and incubated for 1 h with a secondary antibody (FITC conjugated goat anti-mouse; 1:100 in PBS; Dianova). Titers were calculated from the last limiting dilution of viral stocks that led to fluorescence positive cells.

4.2.4 Functional testing of GFP-VP2 fusion protein by transient transfection

HeLa cells (grown on coverslips) were transfected by calcium phosphate precipitation (Girod et al. 1999) at 80% confluence with the plasmid pGFP-VP2. As control, HeLa cells were transfected in parallel with pGFP (Hacker et al. 2001). 48 h post transfection cells were fixed for 30 minutes in 4% paraformaldehyde (PFA). The nuclear lamina was stained as described below using anti-lamin B antibody.

4.2.5 Western Blot

For the detection of viral capsid proteins 10^{10} capsids were separated on a SDS-polyacrylamide gel (10%) and blotted onto a nitrocellulose membrane. The membrane was then blocked with 0.2% I-Block (Sigma) in Tris buffered saline supplemented with Tween 20 (TBS-T) over night at 4°C. After incubation with B1 antibody (kindly provided by Dr. Jürgen Kleinschmidt (DKFZ Heidelberg, Germany); 1:10 in 0.2% I-Block) and three washing steps in TBS-T, the membrane was incubated for 1 h with a peroxidase conjugated anti-mouse IgG antibody (1:5000 in 0.2% I-Block, Sigma). The membrane was washed again, subsequently incubated for 5 min with SuperSignal West Pico Chemiluminescent Substrate (Pierce) and then exposed to Biomax Light Film (Kodak).

4.2.6 Fluorescence activated cell sorting (FACS) analyses

4×10^4 HeLa cells were seeded per well in a 24 well plate. 24 h later cells were infected with 8×10^7 capsids/cell in presence or in absence of 425 units of heparin/ml. The virus binding was carried out for 30 min. on ice. Thereafter, cells were shifted to 37°C for 1 h. Cells were harvested, resolved in 0.5 ml PBS and analyzed with a Coulter Epics XL-MCL (Beckman Coulter). A minimum of 5000 cells were analyzed for each sample. The percentage of positive cells is defined as the fraction beyond the region of 99% of the control of untransfected cells. Data were analyzed with the use of WinMDI 2.8 FACS software.

4.2.7 Immunoflourescence

4×10^4 HeLa cells per well were seeded onto 12 mm coverslips inside 24 well plates. 24 h later HeLa cells were infected with 1×10^6-5×10^6 capsids/cell with or without 425 units heparin/ml added to the medium. When indicated, cells were coinfected with adenovirus type 5 (MOI 5). The infection was carried out for 0.5 h on ice. Cells were then shifted to 37°C and incubated at 37°C and 5% CO_2 for the indicated time period.

Cells were washed with PBS and fixed for 0.5 h with 3% PFA in PBS at room temperature, washed again with PBS and the reminding PFA was quenched for 10 min with 50 mM NH_4Cl in PBS. Nuclear staining was obtained by Dapi (1 µg/ml in PBS) for 5 min or by anti-lamin B antibody staining. For antibody staining cells were permeabilized with 0.2% Triton X 100 in PBS for 10 min, blocked for 10 min with

0.2% gelatine in PBS and then incubated for 1 h at room temperature with first antibodies as indicated. As first antibodies polyclonal goat anti-lamin B IgG antibody (1:50 in PBS, Santa Cruz Biotechnology), monoclonal A20 or B1 hybridoma supernatant derived from mice (kindly provided by Dr. Jürgen Kleinschmidt, DKFZ Heidelberg, Germany) were used. After washing and blocking, the cells were incubated for 1 h with secondary antibodies. As secondary antibodies we used Texas Red or Cy5 conjugated donkey anti-goat-antibody (Dianova, diluted 1:50 or 1:100 in PBS, 0.2% gelatine) and Rhodamine Red-X (RRX) conjugated donkey anti-mouse (Dianova, diluted 1:200 in PBS, 0.2% gelatine). The cover slips were washed in PBS again, embedded in Vectashield mounting medium (Alexis) and examined.

4.2.8 Fluorescence in situ hybridisation (FISH)

Plasmid pRC (Hacker et al. 2001) which encodes Rep and Cap of AAV2 was linearized and labeled with 5-(3-aminoallyl)dUTPs by nick translation. Incorporated dUTPs were labeled with amino reactive Oregon Green 488 by ARES DNA labeling kit (Molecular Probes) according to manufacturers manual. Alternatively the linearized plasmid was labeled with biotin-16-dUTPs by biotin nick translation kit from Roche. To detect the AAV genome inside cells, HeLa cells were prepared as described above. Cells were infected with wild type AAV2 (10^5 capsids/cell), fixed with 3% PFA after indicated time points, quenched and permeabilized as described before. Nuclear lamina and viral capsids were stained by polyclonal goat anti-lamin B IgG antibody and monoclonal A20 hybridoma supernatant derived from mice (kindly provided by Dr. Jürgen Kleinschmidt, DKFZ Heidelberg, Germany). Cy5 conjugated donkey anti-goat antibody (Dianova) and Rhodamine Red-X conjugated donkey anti-mouse antibody (Dianova) were used as secondary antibodies. After antibody staining cells were washed with PBS. A hybridization mixture containing 1 ng/µl labeled DNA probe, 50% formamide, 7.3% dextran sulphate, 15 ng/µl salmon sperm DNA and 0.74x SSC was denatured for 3 min at 95°C and shock cooled on ice. Cover slips were inverted onto the denatured hybridization mixture (only the DNA probe was denaturated since the AAV genome is single stranded). Cover slips were sealed with rubber cement and hybridization occurred at 37°C over night. Rubber cement was removed and cover slips were washed 3x in 2x SSC at 37°C, 3x in 0.1x SSC at 60°C and 2x in PBS. If the direct labeled probe was used for hybridization, cells were embedded in Vectashield mounting medium (Alexis).

If the biotin labeled probe was used it was stained with RRX conjugated NeutrAvidin™ (10μg/ml) (Molecular Probes) for 1 h at room temperature. Cells were washed 2x in PBS and embedded in Vectashield mounting medium.

4.2.9 Microscopic tools

Wide field fluorescence microscopy

Images were acquired with an immunofluorescence microscope (Zeiss, Axioskop) equipped with filters specific for GFP and Dapi using a 40x (NA1.3) objective. Images were obtained with a CCD camera (Visicam, Visitron Systems) with MetaMorph Imaging System version 3.0.

Confocal microscopy

To localize the GFP-VP2 signal within the cell more precisely, images were obtained by confocal laser scanning microscopy using a Leica DM IRE2 microscope with a Leica TCS SP2 laser system or a Zeiss Axiovert 200M microscope with a Zeiss LSM 510 Laser Module, using a 63x (NA 1.4) objective and filter settings optimized for respective dyes. For each sample a series of 0.2 to 0.25 μm horizontal sections were made. The pinhole was adjusted to 1 airy unit. Images were processed by Leica confocal software or LSM 510 Meta software and Adobe Photoshop version 7.0.

Live cell imaging (Time-laps microscopy)

For live cell images $2x10^5$ HeLa-DsRed2Nuc cells were seeded onto the glass bottom of microwell dishes (35 mm; Mat Tek). 24 h later cells were infected with or without 425 units heparin/ml media with approx. 10^6 capsids per cell. Cells were incubated for 20 min at 37°C and then analyzed by live cell microscopy under physiological conditions. Live cell movies were obtained with an inverse Zeiss Axiovert 200M microscope with a 63x (NA1.4) objective using Zeiss filter sets (FS)10 for GFP and DsRed. Images were taken with a Zeiss Axiocam HRm using the Axiovision 3 software with a time laps of 30 seconds.

Determination of viral velocities with conventional time laps microscopy

Therefore PtK$_2$ were seeded onto cover slips. Prior to infection coverslips were directly clamped inside a POC-R (cell cultivation system from Zeiss). Cells were covered with

CO_2 independent media (Invitrogen) to which OSS (oxygen scavenging system 0.1 mg/ml glucose oxidase, 18 µg/ml catalase and 2.3 mg/ml glucose) was added to protect the cells from damage caused by photooxidative stress. CO_2 independent media had to be used, since no CO_2 regulation could be done. Cells were infected with approximately 10^6 capsids per cell of 100%-GFP-VP2-AAV. Cells were observed with an Axiovert 200 microscope from Zeiss equipped with a Xenon lamp and filter settings for GFP detection. Images were taken with Imago-QE camera from Photonics with the help of Till vision software. To obtain movies pictures were taken with a time laps of 1 to 2 seconds and an exposure time of 0.5 sec. For one movie a series of 100 pictures was taken. Movies were processed with Metamorph and ImageJ software. Directed movements were tracked by determining the xy-position of the fluorescent viral particles in each frame. From the xy displacements between each frame the velocity was calculated.

Single Virus Tracing (SVT) measurements

HeLa cells were seeded in 8 well chambers (LabTek). Before measurements normal DMEM was replaced by CO_2 independent media (Invitrogene). Cells were infected with Cy5 (Amersham) labeled wt AAV. Measurements were carried out at 37°C. Cy5 dyes are generating a covalent link with amino groups of amino acids within proteins. To avoid unspecific protein labeling of contaminating proteins Cy5 labeling was carried out with highly pure wt AAV preparations. Therefore virions were purified in addition to the iodixanol gradient by heparin affinity chromatography. Labeling reaction was carried out for 2h on ice. To get rid of the excess of free dye virions were was dialyzed against PBS.

For these measurements we used a Nikon TE300 microscope equipped with a PentaMax CCD Camera (Visitron) and a HeNe Laser (633nm, 35 mW, Coherent). To generate movies, images were taken every 40 ms. For one movie 200-400 images were taken. Movies were processed with Metamorph imaging software determining xy-position of the fluorescent viral particles in each frame. From the xy displacements between each frame the velocity was calculated.

Transmission electron microscopy

$4x10^4$ HeLa cells per well were seeded on coverslips within a 24 well plate. 24 h later cells were infected with 10^6 capsids per cell. The virus binding was carried out for 30 min. on ice. Thereafter, cells were shifted to 37°C for 4 h. Cells were fixed with 2.5% glutaraldehyd in Cacodylate buffer (100 mM, pH 7.2) at room temperature for 30 min. Cells were then washed with Cacodylate buffer and post fixed with 1% Osmiumtetraoxid in Cacodylate buffer for 30 min to 1 h. Cells were washed again in Cacodylate buffer and then dehydrated with increasing ethanol concentrations (50%, 70%, 90%; each concentration twice) for 5 min and finally with 100% ethanol p.a. twice for 10 min and 20 min. Cells were incubated with propylenoxid (2 x 15 min) and then infiltrated with increasing concentrations of Araldit. Araldit/Propylenoxid 1:2 at room temperature for 1 hour, Araldit/Propylenoxid 1:1 at 4°C over night and then for max. 2 h in 100% Araldit. Samples are transferred into resign filled casting molds. Polymerization occurred over night at 40°C and hardening at 70°C for 36-40 h. Ultratomes (50 nm) were generated with UltracutE (Reichert-Jung). Electron micrographs were obtained with a transmission electron microscope (TEM, Zeiss EM 902).

4.2.10 Animal studies

Wt Wistar rats were anesthetized with an intramuscular injection. For subretinal injection, the sclera and the choroid were punctured and a 33-gauge needle was then inserted in a tangential direction under an operating microscope. In one application $6x10^{10}$ capsids were injected. 24 h p.i. a retinal flatmount was obtained. Therefore, enucleated eyes were fixed with 4% paraformaldehyd for 40 minutes at room temperature. After washing the eyes were cut through the pars plana and the anterior segment and the lens were removed. The eye cup was cut peripherally into four sections under an operating microscope and flattened. The neuroretina was removed from the sclera/choroids/RPE with fine forceps and both cell layers were mounted on a glass side and examined by fluorescence microscopy.

4.2.11 Determination of transduction efficiencies

$2x10^4$ cells were seeded in 48 well plates and transduced with the respective rAAV/GFP vector, harvested 48 hrs p.i., washed and resuspended in 0.5 ml PBS. The percentage of GFP expressing cells was determined by flow cytometry with a Coulter Epics XL-MCL

(Beckman Coulter, Krefeld). A minimum of 5000 cells were analyzed for each sample. Transduction efficiency of the retargeting mutants was also determined in the presence or absence of 300µM of GRGDTP or GRGES peptides (Bachem, Bubendorf), or 425 units/ml soluble heparin (Braun, Melsungen).

5. Abbreviations

aa	amino acid	CLL	chronic lymphocytic leukemia
AAV	adeno-associated virus	CMV	cytomegalovirus
AAV2	adeno-associated virus serotype 2	CPV	canine parvovirus
AAVS1	AAV integration site 1	CTL	cytotoxic T-lymphocyte
	(located in human chromosome 19)	Cy3, Cy5	indocarbocyanine dyes
Ab	antibody	Da	Dalton
Ad	adenovirus	DMEM	Dulbecco's Modified Eagle Medium
		e.g.	for example (Lat.: exempli gratia)
Amino acids:		ELISA	enzyme-linked immunosorbent assay
A (Ala)	alanine	EM	electron microscope
C (Cys)	cysteine	ER	endoplasmatic reticulum
D (Asp)	aspartate	FACS	fluorescence-activated cell sorting
E (Glu)	glutamate	FCS	fetal calf serum
F (Phe)	phenylalanine	FGFR	fibroblast growth factor receptor 1
G (Gly)	glycine	Fig.	figure
H (His)	histidine	FISH	fluorescence *in situ* hybridization
I (Ile)	isoleucine	FITC	fluorescein isothiocyanate
K (Lys)	lysine	FPV	feline panleukopenia virus
L (Leu)	leucine	GFP	green fluorescence protein
M (Met)	methionine	h	hour
N (Asn)	asparagine	HSPG	heparan sulfate proteoglycan
P (Pro)	proline	ITR	inverted terminal repeat
Q (Gln)	glutamine	kb	kilobases
R (Arg)	arginine	min	minute
S (Ser)	serine	MOI	multiplicity of infection
T (Thr)	threonine	MVM	minute virus of mice
V (Val)	valine	MT	microtubule
W (Trp)	tryptophan	n.i.	non infectious
Y (Tyr)	tyrosine	NLS	nuclear localization signal
		NPC	nuclear pore complex
Bases:		nt	nucleotide
A	adenin	ori	origin of replication
C	cytosin	ORF	open reading frame
G	guanin	p.i.	post infection
T	thymin	PLA2	phospholipase A2
		PNRE	perinuclear recycling endosome
B19	human B19 parvovirus	rAAV	recombinant AAV
bp	base pair	RBS	Rep binding site
BSA	bovine serum albumin	Rep	viral regulatory protein
CEA	colorectal cancer antigen	RPE	retinal pigment epithelium
ch	chromosome	rpm	rounds per minute

RRX	Rhodamine Red-X
RT	room temperature
sec	second
SDS	sodium dodecyl sulfate
Stav	streptavidin
SVT	Single Virus Tracing
TRS	terminal resolution site
VP	viral protein (AAV capsid protein)
w/o	without
wt AAV	wild type AAV

6. References

Ali, R. R., Sarra, G. M., Stephens, C., Alwis, M. D., Bainbridge, J. W., Munro, P. M., Fauser, S., Reichel, M. B., Kinnon, C., Hunt, D. M., Bhattacharya, S. S., and Thrasher, A. J. (2000). Restoration of photoreceptor ultrastructure and function in retinal degeneration slow mice by gene therapy. *Nat Genet* 25(3)**,** 306-10.

Atchison, R. W., Casto, B. C., and Hammon, W. M. (1965). Adenovirus-Associated Defective Virus Particles. *Science* 149**,** 754-6.

Awedikian, R., Francois, A., Guilbaud, M., Moullier, P., and Salvetti, A. (2005). Intracellular route and biological activity of exogenously delivered Rep proteins from the adeno-associated virus type 2. *Virology* 335(2)**,** 252-63.

Balsinde, J., Balboa, M. A., Insel, P. A., and Dennis, E. A. (1999). Regulation and inhibition of phospholipase A2. *Annu Rev Pharmacol Toxicol* 39**,** 175-89.

Bantel-Schaal, U., Hub, B., and Kartenbeck, J. (2002). Endocytosis of adeno-associated virus type 5 leads to accumulation of virus particles in the Golgi compartment. *J Virol* 76(5)**,** 2340-9.

Bantel-Schaal, U., and zur Hausen, H. (1984). Characterization of the DNA of a defective human parvovirus isolated from a genital site. *Virology* 134(1)**,** 52-63.

Bartlett, J. S., Wilcher, R., and Samulski, R. J. (2000). Infectious entry pathway of adeno-associated virus and adeno-associated virus vectors. *J Virol* 74(6)**,** 2777-85.

Becerra, S. P., Koczot, F., Fabisch, P., and Rose, J. A. (1988). Synthesis of adeno-associated virus structural proteins requires both alternative mRNA splicing and alternative initiations from a single transcript. *J Virol* 62(8)**,** 2745-54.

Becerra, S. P., Rose, J. A., Hardy, M., Baroudy, B. M., and Anderson, C. W. (1985). Direct mapping of adeno-associated virus capsid proteins B and C: a possible ACG initiation codon. *Proc Natl Acad Sci U S A* 82(23)**,** 7919-23.

Bennett, J., Maguire, A. M., Cideciyan, A. V., Schnell, M., Glover, E., Anand, V., Aleman, T. S., Chirmule, N., Gupta, A. R., Huang, Y., Gao, G. P., Nyberg, W. C., Tazelaar, J., Hughes, J., Wilson, J. M., and Jacobson, S. G. (1999). Stable transgene expression in rod photoreceptors after recombinant adeno-associated virus-mediated gene transfer to monkey retina. *Proc Natl Acad Sci U S A* 96(17)**,** 9920-5.

Berns, K. I. (1990). Parvovirus replication. *Microbiol Rev* 54(3)**,** 316-29.

Berns, K. I., and Giraud, C. (1996). Biology of adeno-associated virus. *Curr Top Microbiol Immunol* 218**,** 1-23.

Berns, K. I., and Linden, R. M. (1995). The cryptic life style of adeno-associated virus. *Bioessays* 17(3)**,** 237-45.

Blackburn, S. D., Steadman, R. A., and Johnson, F. B. (2006). Attachment of adeno-associated virus type 3H to fibroblast growth factor receptor 1. *Arch Virol* 151(3)**,** 617-23.

Blacklow, N. R. (1988). Adeno-associated virus in humans. *Parvovirus and Human disease***,** 165-174.

Blacklow, N. R., Hoggan, M. D., Sereno, M. S., Brandt, C. D., Kim, H. W., Parrott, R. H., and Chanock, R. M. (1971). A seroepidemiologic study of adenovirus-associated virus infection in infants and children. *Am J Epidemiol* 94(4)**,** 359-66.

Blacklow, N. R., Hoggan, M. D., and Rowe, W. P. (1968). Serologic evidence for human infection with adenovirus-associated viruses. *J Natl Cancer Inst* 40(2)**,** 319-27.

Blaese, R. M., Culver, K. W., Miller, A. D., Carter, C. S., Fleisher, T., Clerici, M., Shearer, G., Chang, L., Chiang, Y., Tolstoshev, P., and et al. (1995). T lymphocyte-directed gene therapy for ADA- SCID: initial trial results after 4 years. *Science* 270(5235)**,** 475-80.

Bleker, S., Sonntag, F., and Kleinschmidt, J. A. (2005). Mutational analysis of narrow pores at the fivefold symmetry axes of adeno-associated virus type 2 capsids reveals a dual role in genome packaging and activation of phospholipase A2 activity. *J Virol* 79(4)**,** 2528-40.

Blystone, S. D. (2004). Integrating an integrin: a direct route to actin. *Biochim Biophys Acta* 1692(2-3)**,** 47-54.

Brister, J. R., and Muzyczka, N. (2000). Mechanism of Rep-mediated adeno-associated virus origin nicking. *J Virol* 74(17)**,** 7762-71.

Brown, K. E. (2000). Haematological consequences of parvovirus B19 infection. *Baillieres Best Pract Res Clin Haematol* 13(2)**,** 245-59.

Buning, H., Nicklin, S. A., Perabo, L., Hallek, M., and Baker, A. H. (2003). AAV-based gene transfer. *Curr Opin Mol Ther* 5(4)**,** 367-75.

Carter, P. J., and Samulski, R. J. (2000). Adeno-associated viral vectors as gene delivery vehicles. *Int J Mol Med* 6(1)**,** 17-27.

Chalfie, M., Tu, Y., Euskirchen, G., Ward, W. W., and Prasher, D. C. (1994). Green fluorescent protein as a marker for gene expression. *Science* 263(5148)**,** 802-5.

Chejanovsky, N., and Carter, B. J. (1989). Mutagenesis of an AUG codon in the adeno-associated virus rep gene: effects on viral DNA replication. *Virology* 173(1)**,** 120-8.

Chiorini, J. A., Wendtner, C. M., Urcelay, E., Safer, B., Hallek, M., and Kotin, R. M. (1995). High-efficiency transfer of the T cell co-stimulatory molecule B7-2 to lymphoid cells using high-titer recombinant adeno-associated virus vectors. *Hum Gene Ther* 6(12)**,** 1531-41.

Chirmule, N., Propert, K., Magosin, S., Qian, Y., Qian, R., and Wilson, J. (1999). Immune responses to adenovirus and adeno-associated virus in humans. *Gene Ther* 6(9)**,** 1574-83.

Clever, J., Yamada, M., and Kasamatsu, H. (1991). Import of simian virus 40 virions through nuclear pore complexes. *Proc Natl Acad Sci U S A* 88(16)**,** 7333-7.

Collaco, R. F., Cao, X., and Trempe, J. P. (1999). A helper virus-free packaging system for recombinant adeno-associated virus vectors. *Gene* 238(2)**,** 397-405.

Curnis, F., Arrigoni, G., Sacchi, A., Fischetti, L., Arap, W., Pasqualini, R., and Corti, A. (2002). Differential binding of drugs containing the NGR motif to CD13 isoforms in tumor vessels, epithelia, and myeloid cells. *Cancer Res* 62(3)**,** 867-74.

Daniel, T. O., Milfay, D. F., Escobedo, J., and Williams, L. T. (1987). Biosynthetic and glycosylation studies of cell surface platelet-derived growth factor receptors. *J Biol Chem* 262(20)**,** 9778-84.

de la Maza, L. M., and Carter, B. J. (1981). Inhibition of adenovirus oncogenicity in hamsters by adeno-associated virus DNA. *J Natl Cancer Inst* 67(6)**,** 1323-6.

Dennis, E. A. (1997). The growing phospholipase A2 superfamily of signal transduction enzymes. *Trends Biochem Sci* 22(1)**,** 1-2.

Desai, P., and Person, S. (1998). Incorporation of the green fluorescent protein into the herpes simplex virus type 1 capsid. *J Virol* 72(9)**,** 7563-8.

Di Pasquale, G., and Chiorini, J. A. (2005). AAV transcytosis through barrier epithelia and endothelium. *Mol Ther*.

Di Pasquale, G., Davidson, B. L., Stein, C. S., Martins, I., Scudiero, D., Monks, A., and Chiorini, J. A. (2003). Identification of PDGFR as a receptor for AAV-5 transduction. *Nat Med* 9(10)**,** 1306-12.

Ding, W., Zhang, L., Yan, Z., and Engelhardt, J. F. (2005). Intracellular trafficking of adeno-associated viral vectors. *Gene Ther* 12(11)**,** 873-80.

Ding, W., Zhang, L. N., Yeaman, C., and Engelhardt, J. F. (2006). rAAV2 traffics through both the late and the recycling endosomes in a dose-dependent fashion. *Mol Ther*.

Döhner, K., Wolfstein, A., Prank, U., Echeverri, C., Dujardin, D., Vallee, R., and Sodeik, B. (2002). Function of dynein and dynactin in herpes simplex virus capsid transport. *Mol Biol Cell* 13(8)**,** 2795-809.

Dong, J. Y., Fan, P. D., and Frizzell, R. A. (1996). Quantitative analysis of the packaging capacity of recombinant adeno- associated virus. *Hum Gene Ther* 7(17)**,** 2101-12.

Douar, A. M., Poulard, K., Stockholm, D., and Danos, O. (2001). Intracellular trafficking of adeno-associated virus vectors: routing to the late endosomal compartment and proteasome degradation. *J Virol* 75(4)**,** 1824-33.

Duan, D., Li, Q., Kao, A. W., Yue, Y., Pessin, J. E., and Engelhardt, J. F. (1999). Dynamin is required for recombinant adeno-associated virus type 2 infection. *J Virol* 73(12)**,** 10371-6.

Duan, D., Yue, Y., Yan, Z., Yang, J., and Engelhardt, J. F. (2000). Endosomal processing limits gene transfer to polarized airway epithelia by adeno-associated virus. *J Clin Invest* 105(11)**,** 1573-87.

Dubielzig, R., King, J. A., Weger, S., Kern, A., and Kleinschmidt, J. A. (1999). Adeno-associated virus type 2 protein interactions: formation of pre-encapsidation complexes. *J Virol* 73(11)**,** 8989-98.

Dupuy-Coin, A. M., Moens, P., and Bouteille, M. (1986). Three-dimensional analysis of given cell structures: nucleolus, nucleoskeleton and nuclear inclusions. *Methods Achiev Exp Pathol* 12**,** 1-25.

Elliott, G., and O'Hare, P. (1999). Live-cell analysis of a green fluorescent protein-tagged herpes simplex virus infection. *J Virol* 73(5)**,** 4110-9.

Erles, K., Sebokova, P., and Schlehofer, J. R. (1999). Update on the prevalence of serum antibodies (IgG and IgM) to adeno- associated virus (AAV). *J Med Virol* 59(3)**,** 406-11.

Fisher, K. J., Jooss, K., Alston, J., Yang, Y., Haecker, S. E., High, K., Pathak, R., Raper, S. E., and Wilson, J. M. (1997). Recombinant adeno-associated virus for muscle directed gene therapy. *Nat Med* 3(3)**,** 306-12.

Fisher-Adams, G., Wong, K. K., Jr., Podsakoff, G., Forman, S. J., and Chatterjee, S. (1996). Integration of adeno-associated virus vectors in CD34+ human hematopoietic progenitor cells after transduction. *Blood* 88(2)**,** 492-504.

Flannery, J. G., Zolotukhin, S., Vaquero, M. I., LaVail, M. M., Muzyczka, N., and Hauswirth, W. W. (1997). Efficient photoreceptor-targeted gene expression in vivo by recombinant adeno-associated virus. *Proc Natl Acad Sci U S A* 94(13)**,** 6916-21.

Flotte, T. R., Afione, S. A., Conrad, C., McGrath, S. A., Solow, R., Oka, H., Zeitlin, P. L., Guggino, W. B., and Carter, B. J. (1993). Stable in vivo expression of

the cystic fibrosis transmembrane conductance regulator with an adeno-associated virus vector. *Proc Natl Acad Sci U S A* 90(22)**,** 10613-7.

Fricker, M., Hollinshead, M., White, N., and Vaux, D. (1997). Interphase nuclei of many mammalian cell types contain deep, dynamic, tubular membrane-bound invaginations of the nuclear envelope. *J Cell Biol* 136(3)**,** 531-44.

Funk, A., Mhamdi, M., Lin, L., Will, H., and Sirma, H. (2004). Itinerary of hepatitis B viruses: delineation of restriction points critical for infectious entry. *J Virol* 78(15)**,** 8289-300.

Gao, G., Vandenberghe, L. H., Alvira, M. R., Lu, Y., Calcedo, R., Zhou, X., and Wilson, J. M. (2004). Clades of Adeno-associated viruses are widely disseminated in human tissues. *J Virol* 78(12)**,** 6381-8.

Gao, G. P., Alvira, M. R., Wang, L., Calcedo, R., Johnston, J., and Wilson, J. M. (2002). Novel adeno-associated viruses from rhesus monkeys as vectors for human gene therapy. *Proc Natl Acad Sci U S A* 99(18)**,** 11854-9.

Girod, A., Ried, M., Wobus, C., Lahm, H., Leike, K., Kleinschmidt, J., Deleage, G., and Hallek, M. (1999). Genetic capsid modifications allow efficient re-targeting of adeno-associated virus type 2. *Nat Med* 5(9)**,** 1052-6.

Girod, A., Wobus, C. E., Zadori, Z., Ried, M., Leike, K., Tijssen, P., Kleinschmidt, J. A., and Hallek, M. (2002). The VP1 capsid protein of adeno-associated virus type 2 is carrying a phospholipase A2 domain required for virus infectivity. *J Gen Virol* 83(Pt 5)**,** 973-8.

Glotzer, J. B., Michou, A. I., Baker, A., Saltik, M., and Cotten, M. (2001). Microtubule-independent motility and nuclear targeting of adenoviruses with fluorescently labeled genomes. *J Virol* 75(5)**,** 2421-34.

Greber, U. F., and Fornerod, M. (2005). Nuclear import in viral infections. *Curr Top Microbiol Immunol* 285**,** 109-38.

Griffin, B. A., Adams, S. R., and Tsien, R. Y. (1998). Specific covalent labeling of recombinant protein molecules inside live cells. *Science* 281(5374)**,** 269-72.

Grifman, M., Trepel, M., Speece, P., Gilbert, L. B., Arap, W., Pasqualini, R., and Weitzman, M. D. (2001). Incorporation of tumor-targeting peptides into recombinant adeno-associated virus capsids. *Mol Ther* 3(6)**,** 964-75.

Grimm, D., Kern, A., Pawlita, M., Ferrari, F., Samulski, R., and Kleinschmidt, J. (1999). Titration of AAV-2 particles via a novel capsid ELISA: packaging of genomes can limit production of recombinant AAV-2. *Gene Ther* 6(7)**,** 1322-30.

Grimm, D., and Kleinschmidt, J. A. (1999). Progress in adeno-associated virus type 2 vector production: promises and prospects for clinical use. *Hum Gene Ther* 10(15)**,** 2445-50.

Hacein-Bey-Abina, S., von Kalle, C., Schmidt, M., Le Deist, F., Wulffraat, N., McIntyre, E., Radford, I., Villeval, J. L., Fraser, C. C., Cavazzana-Calvo, M., and Fischer, A. (2003). A serious adverse event after successful gene therapy for X-linked severe combined immunodeficiency. *N Engl J Med* 348(3)**,** 255-6.

Hacker, U. T., Gerner, F. M., Buning, H., Hutter, M., Reichenspurner, H., Stangl, M., and Hallek, M. (2001). Standard heparin, low molecular weight heparin, low molecular weight heparinoid, and recombinant hirudin differ in their ability to inhibit transduction by recombinant adeno-associated virus type 2 vectors. *Gene Ther* 8(12)**,** 966-8.

Hacker, U. T., Wingenfeld, L., Kofler, D. M., Schuhmann, N. K., Lutz, S., Herold, T., King, S. B., Gerner, F. M., Perabo, L., Rabinowitz, J., McCarty, D. M., Samulski, R. J., Hallek, M., and Buning, H. (2005). Adeno-associated virus serotypes 1 to 5 mediated tumor cell directed gene transfer and improvement of transduction efficiency. *J Gene Med* 7(11)**,** 1429-38.

Handa, A., Muramatsu, S., Qiu, J., Mizukami, H., and Brown, K. E. (2000). Adeno-associated virus (AAV)-3-based vectors transduce haematopoietic cells not susceptible to transduction with AAV-2-based vectors. *J Gen Virol* 81(Pt 8)**,** 2077-84.

Hansen, J., Qing, K., and Srivastava, A. (2001a). Adeno-associated virus type 2-mediated gene transfer: altered endocytic processing enhances transduction efficiency in murine fibroblasts. *J Virol* 75(9)**,** 4080-90.

Hansen, J., Qing, K., and Srivastava, A. (2001b). Infection of purified nuclei by adeno-associated virus 2. *Mol Ther* 4(4)**,** 289-96.

Heilbronn, R., Schlehofer, J. R., Yalkinoglu, A. O., and Zur Hausen, H. (1985). Selective DNA-amplification induced by carcinogens (initiators): evidence for a role of proteases and DNA polymerase alpha. *Int J Cancer* 36(1)**,** 85-91.

Hermonat, P. L. (1989). The adeno-associated virus Rep78 gene inhibits cellular transformation induced by bovine papillomavirus. *Virology* 172(1)**,** 253-61.

Hoque, M., Ishizu, K., Matsumoto, A., Han, S. I., Arisaka, F., Takayama, M., Suzuki, K., Kato, K., Kanda, T., Watanabe, H., and Handa, H. (1999). Nuclear transport of the major capsid protein is essential for adeno-associated virus capsid formation. *J Virol* 73(9)**,** 7912-5.

Huttner, N. A., Girod, A., Schnittger, S., Schoch, C., Hallek, M., and Buning, H. (2003). Analysis of site-specific transgene integration following co-transduction with recombinant adeno-associated virus and a rep encoding plasmid. *J Gene Med* 5(2)**,** 120-9.

Im, D. S., and Muzyczka, N. (1990). The AAV origin binding protein Rep68 is an ATP-dependent site-specific endonuclease with DNA helicase activity. *Cell* 61(3)**,** 447-57.

Ingber, D. E. (2003). Mechanosensation through integrins: cells act locally but think globally. *Proc Natl Acad Sci U S A* 100(4)**,** 1472-4.

Jaffe, E. A., Nachman, R. L., Becker, C. G., and Minick, C. R. (1973). Culture of human endothelial cells derived from umbilical veins. Identification by morphologic and immunologic criteria. *J Clin Invest* 52(11)**,** 2745-56.

Kaludov, N., Brown, K. E., Walters, R. W., Zabner, J., and Chiorini, J. A. (2001). Adeno-associated virus serotype 4 (AAV4) and AAV5 both require sialic acid binding for hemagglutination and efficient transduction but differ in sialic acid linkage specificity. *J Virol* 75(15)**,** 6884-93.

Kaplitt, M. G., Leone, P., Samulski, R. J., Xiao, X., Pfaff, D. W., O'Malley, K. L., and During, M. J. (1994). Long-term gene expression and phenotypic correction using adeno-associated virus vectors in the mammalian brain. *Nat Genet* 8(2)**,** 148-54.

Kashiwakura, Y., Tamayose, K., Iwabuchi, K., Hirai, Y., Shimada, T., Matsumoto, K., Nakamura, T., Watanabe, M., Oshimi, K., and Daida, H. (2005). Hepatocyte growth factor receptor is a coreceptor for adeno-associated virus type 2 infection. *J Virol* 79(1)**,** 609-14.

Kern, A., Schmidt, K., Leder, C., Muller, O. J., Wobus, C. E., Bettinger, K., Von der Lieth, C. W., King, J. A., and Kleinschmidt, J. A. (2003). Identification of a heparin-binding motif on adeno-associated virus type 2 capsids. *J Virol* 77(20)**,** 11072-81.

Khleif, S. N., Myers, T., Carter, B. J., and Trempe, J. P. (1991). Inhibition of cellular transformation by the adeno-associated virus rep gene. *Virology* 181(2)**,** 738-41.

King, J. A., Dubielzig, R., Grimm, D., and Kleinschmidt, J. A. (2001). DNA helicase-mediated packaging of adeno-associated virus type 2 genomes into preformed capsids. *Embo J* 20(12)**,** 3282-91.

Koivunen, E., Wang, B., and Ruoslahti, E. (1995). Phage libraries displaying cyclic peptides with different ring sizes: ligand specificities of the RGD-directed integrins. *Biotechnology (N Y)* 13(3)**,** 265-70.

Kotin, R. M., Siniscalco, M., Samulski, R. J., Zhu, X. D., Hunter, L., Laughlin, C. A., McLaughlin, S., Muzyczka, N., Rocchi, M., and Berns, K. I. (1990). Site-specific integration by adeno-associated virus. *Proc Natl Acad Sci U S A* 87(6)**,** 2211-5.

Kotin, R. M., Linden, R. M., and Berns, K. I. (1992). Characterization of a preferred site on human chromosome 19q for integration of adeno-associated virus DNA by non-homologous recombination. *Embo J* 11(13)**,** 5071-8.

Kramer, R. M., and Sharp, J. D. (1997). Structure, function and regulation of Ca2+-sensitive cytosolic phospholipase A2 (cPLA2). *FEBS Lett* 410(1)**,** 49-53.

Kronenberg, S., Bottcher, B., von der Lieth, C. W., Bleker, S., and Kleinschmidt, J. A. (2005). A conformational change in the adeno-associated virus type 2 capsid leads to the exposure of hidden VP1 N termini. *J Virol* 79(9)**,** 5296-303.

Kronenberg, S., Kleinschmidt, J. A., and Bottcher, B. (2001). Electron cryo-microscopy and image reconstruction of adeno-associated virus type 2 empty capsids. *EMBO Rep* 2(11)**,** 997-1002.

Kyostio, S. R., Owens, R. A., Weitzman, M. D., Antoni, B. A., Chejanovsky, N., and Carter, B. J. (1994). Analysis of adeno-associated virus (AAV) wild-type and mutant Rep proteins for their abilities to negatively regulate AAV p5 and p19 mRNA levels. *J Virol* 68(5)**,** 2947-57.

Labow, M. A., and Berns, K. I. (1988). The adeno-associated virus rep gene inhibits replication of an adeno-associated virus/simian virus 40 hybrid genome in cos-7 cells. *J Virol* 62(5)**,** 1705-12.

Lakadamyali, M., Rust, M. J., Babcock, H. P., and Zhuang, X. (2003). Visualizing infection of individual influenza viruses. *Proc Natl Acad Sci U S A* 100(16)**,** 9280-5.

Lauvrak, S. U., Torgersen, M. L., and Sandvig, K. (2004). Efficient endosome-to-Golgi transport of Shiga toxin is dependent on dynamin and clathrin. *J Cell Sci* 117(Pt 11)**,** 2321-31.

Linden, R. M., Ward, P., Giraud, C., Winocour, E., and Berns, K. I. (1996). Site-specific integration by adeno-associated virus. *Proc Natl Acad Sci U S A* 93(21)**,** 11288-94.

Loiler, S. A., Conlon, T. J., Song, S., Tang, Q., Warrington, K. H., Agarwal, A., Kapturczak, M., Li, C., Ricordi, C., Atkinson, M. A., Muzyczka, N., and Flotte, T. R. (2003). Targeting recombinant adeno-associated virus vectors to enhance gene transfer to pancreatic islets and liver. *Gene Ther* 10(18)**,** 1551-8.

Lusby, E. W., and Berns, K. I. (1982). Mapping of the 5' termini of two adeno-associated virus 2 RNAs in the left half of the genome. *J Virol* 41(2)**,** 518-26.

Lux, K., Goerlitz, N., Schlemminger, S., Perabo, L., Goldnau, D., Endell, J., Leike, K., Kofler, D. M., Finke, S., Hallek, M., and Buning, H. (2005). Green fluorescent protein-tagged adeno-associated virus particles allow the study of cytosolic and nuclear trafficking. *J Virol* 79(18)**,** 11776-87.

Mani, B., Baltzer, C., Valle, N., Almendral, J. M., Kempf, C., and Ros, C. (2006). Low pH-dependent endosomal processing of the incoming parvovirus minute virus of mice virion leads to externalization of the VP1 N-terminal sequence (N-VP1), N-VP2 cleavage, and uncoating of the full-length genome. *J Virol* 80(2)**,** 1015-24.

Maniatis, T., Fritsch, E. F. und Sambrook, J. (1989). Molecular Cloning: A Laboratory Manual. Cold Spring Harbor Laboratory, Cold Spring Harbor, New York.

Mayor, H. D., Houlditch, G. S., and Mumford, D. M. (1973). Influence of adeno-associated satellite virus on adenovirus-induced tumours in hamsters. *Nat New Biol* 241(106)**,** 44-6.

Mayor, H. D. J., R. M.; Jordan, L. E. und Melnick, J. L. (1965). Structure and Composition of a Small Particle Prepared from a Simian Adenovirus. *Journal of Bacteriology* 90(1)**,** 235 - 242.

McCarty, D. M., Pereira, D. J., Zolotukhin, I., Zhou, X., Ryan, J. H., and Muzyczka, N. (1994). Identification of linear DNA sequences that specifically bind the adeno-associated virus Rep protein. *J Virol* 68(8)**,** 4988-97.

McDonald, D., Vodicka, M. A., Lucero, G., Svitkina, T. M., Borisy, G. G., Emerman, M., and Hope, T. J. (2002). Visualization of the intracellular behavior of HIV in living cells. *J Cell Biol* 159(3)**,** 441-52.

McLaughlin, S. K., Collis, P., Hermonat, P. L., and Muzyczka, N. (1988). Adeno-associated virus general transduction vectors: analysis of proviral structures. *J Virol* 62(6)**,** 1963-73.

Mizukami, H., Young, N. S., and Brown, K. E. (1996). Adeno-associated virus type 2 binds to a 150-kilodalton cell membrane glycoprotein. *Virology* 217(1)**,** 124-30.

Mori, S., Wang, L., Takeuchi, T., and Kanda, T. (2004). Two novel adeno-associated viruses from cynomolgus monkey: pseudotyping characterization of capsid protein. *Virology* 330(2)**,** 375-83.

Moskalenko, M., Chen, L., van Roey, M., Donahue, B. A., Snyder, R. O., McArthur, J. G., and Patel, S. D. (2000). Epitope mapping of human anti-adeno-associated virus type 2 neutralizing antibodies: implications for gene therapy and virus structure. *J Virol* 74(4)**,** 1761-6.

Mouw, M. B., and Pintel, D. J. (2000). Adeno-associated virus RNAs appear in a temporal order and their splicing is stimulated during coinfection with adenovirus. *J Virol* 74(21)**,** 9878-88.

Muzyczka, N. (1992). Use of adeno-associated virus as a general transduction vector for mammalian cells. *Curr Top Microbiol Immunol* 158**,** 97-129.

Nicklin, S. A., Buening, H., Dishart, K. L., de Alwis, M., Girod, A., Hacker, U., Thrasher, A. J., Ali, R. R., Hallek, M., and Baker, A. H. (2001). Efficient and selective AAV2-mediated gene transfer directed to human vascular endothelial cells. *Mol Ther* 4(3)**,** 174-81.

Norkin, L. C., and Kuksin, D. (2005). The caveolae-mediated sv40 entry pathway bypasses the golgi complex en route to the endoplasmic reticulum. *Virol J* 2**,** 38.

Opie, S. R., Warrington, K. H., Jr., Agbandje-McKenna, M., Zolotukhin, S., and Muzyczka, N. (2003). Identification of amino acid residues in the capsid proteins of adeno-associated virus type 2 that contribute to heparan sulfate proteoglycan binding. *J Virol* 77(12)**,** 6995-7006.

Pajusola, K., Gruchala, M., Joch, H., Luscher, T. F., Yla-Herttuala, S., and Bueler, H. (2002). Cell-type-specific characteristics modulate the transduction efficiency of adeno-associated virus type 2 and restrain infection of endothelial cells. *J Virol* 76(22)**,** 11530-40.

Parker, J. S., and Parrish, C. R. (2000). Cellular uptake and infection by canine parvovirus involves rapid dynamin-regulated clathrin-mediated endocytosis, followed by slower intracellular trafficking. *J Virol* 74(4)**,** 1919-30.

Pasqualini, R., Koivunen, E., Kain, R., Lahdenranta, J., Sakamoto, M., Stryhn, A., Ashmun, R. A., Shapiro, L. H., Arap, W., and Ruoslahti, E. (2000). Aminopeptidase N is a receptor for tumor-homing peptides and a target for inhibiting angiogenesis. *Cancer Res* 60(3)**,** 722-7.

Pelkmans, L., Kartenbeck, J., and Helenius, A. (2001). Caveolar endocytosis of simian virus 40 reveals a new two-step vesicular-transport pathway to the ER. *Nat Cell Biol* 3(5)**,** 473-83.

Perabo, L., Buning, H., Kofler, D. M., Ried, M. U., Girod, A., Wendtner, C. M., Enssle, J., and Hallek, M. (2003). In vitro selection of viral vectors with modified tropism: the adeno-associated virus display. *Mol Ther* 8(1)**,** 151-7.

Perabo, L., Endell, J., King, S., Lux, K., Goldnau, D., Hallek, M., and Buning, H. (2006). Combinatorial engineering of a gene therapy vector: directed evolution of adeno-associated virus. *J Gene Med* 8(2)**,** 155-62.

Pereira, D. J., McCarty, D. M., and Muzyczka, N. (1997). The adeno-associated virus (AAV) Rep protein acts as both a repressor and an activator to regulate AAV transcription during a productive infection. *J Virol* 71(2)**,** 1079-88.

Philpott, N. J., Giraud-Wali, C., Dupuis, C., Gomos, J., Hamilton, H., Berns, K. I., and Falck-Pedersen, E. (2002a). Efficient integration of recombinant adeno-associated virus DNA vectors requires a p5-rep sequence in cis. *J Virol* 76(11)**,** 5411-21.

Philpott, N. J., Gomos, J., Berns, K. I., and Falck-Pedersen, E. (2002b). A p5 integration efficiency element mediates Rep-dependent integration into AAVS1 at chromosome 19. *Proc Natl Acad Sci U S A* 99(19)**,** 12381-5.

Qing, K., Mah, C., Hansen, J., Zhou, S., Dwarki, V., and Srivastava, A. (1999). Human fibroblast growth factor receptor 1 is a co-receptor for infection by adeno-associated virus 2. *Nat Med* 5(1)**,** 71-7.

Qiu, J., and Brown, K. E. (1999). A 110-kDa nuclear shuttle protein, nucleolin, specifically binds to adeno-associated virus type 2 (AAV-2) capsid. *Virology* 257(2), 373-82.

Rabinowitz, J. E., Rolling, F., Li, C., Conrath, H., Xiao, W., Xiao, X., and Samulski, R. J. (2002). Cross-packaging of a single adeno-associated virus (AAV) type 2 vector genome into multiple AAV serotypes enables transduction with broad specificity. *J Virol* 76(2), 791-801.

Rabinowitz, J. E., Xiao, W., and Samulski, R. J. (1999). Insertional mutagenesis of AAV2 capsid and the production of recombinant virus. *Virology* 265(2), 274-85.

Raj, K., Ogston, P., and Beard, P. (2001). Virus-mediated killing of cells that lack p53 activity. *Nature* 412(6850), 914-7.

Redemann, B. E., Mendelson, E., and Carter, B. J. (1989). Adeno-associated virus rep protein synthesis during productive infection. *J Virol* 63(2), 873-82.

Ren, M., Xu, G., Zeng, J., De Lemos-Chiarandini, C., Adesnik, M., and Sabatini, D. D. (1998). Hydrolysis of GTP on rab11 is required for the direct delivery of transferrin from the pericentriolar recycling compartment to the cell surface but not from sorting endosomes. *Proc Natl Acad Sci U S A* 95(11), 6187-92.

Ried, M. U., Girod, A., Leike, K., Buning, H., and Hallek, M. (2002). Adeno-associated virus capsids displaying immunoglobulin-binding domains permit antibody-mediated vector retargeting to specific cell surface receptors. *J Virol* 76(9), 4559-66.

Ros, C., Baltzer, C., Mani, B., and Kempf, C. (2006). Parvovirus uncoating in vitro reveals a mechanism of DNA release without capsid disassembly and striking differences in encapsidated DNA stability. *Virology* 345(1), 137-47.

Russell, D. W., Miller, A. D., and Alexander, I. E. (1994). Adeno-associated virus vectors preferentially transduce cells in S phase. *Proc Natl Acad Sci U S A* 91(19), 8915-9.

Saint-Pol, A., Yelamos, B., Amessou, M., Mills, I. G., Dugast, M., Tenza, D., Schu, P., Antony, C., McMahon, H. T., Lamaze, C., and Johannes, L. (2004). Clathrin adaptor epsinR is required for retrograde sorting on early endosomal membranes. *Dev Cell* 6(4), 525-38.

Sampaio, K. L., Cavignac, Y., Stierhof, Y. D., and Sinzger, C. (2005). Human cytomegalovirus labeled with green fluorescent protein for live analysis of intracellular particle movements. *J Virol* 79(5), 2754-67.

Samulski, R. J., Chang, L. S., and Shenk, T. (1987). A recombinant plasmid from which an infectious adeno-associated virus genome can be excised in vitro and its use to study viral replication. *J Virol* 61(10), 3096-101.

Sandvig, K., Garred, O., Prydz, K., Kozlov, J. V., Hansen, S. H., and van Deurs, B. (1992). Retrograde transport of endocytosed Shiga toxin to the endoplasmic reticulum. *Nature* 358(6386), 510-2.

Sanlioglu, S., Benson, P. K., Yang, J., Atkinson, E. M., Reynolds, T., and Engelhardt, J. F. (2000). Endocytosis and nuclear trafficking of adeno-associated virus type 2 are controlled by rac1 and phosphatidylinositol-3 kinase activation. *J Virol* 74(19), 9184-96.

Seisenberger, G., Ried, M. U., Endress, T., Buning, H., Hallek, M., and Brauchle, C. (2001). Real-time single-molecule imaging of the infection pathway of an adeno-associated virus. *Science* 294(5548), 1929-32.

Shi, W., Arnold, G. S., and Bartlett, J. S. (2001). Insertional mutagenesis of the adeno-associated virus type 2 (AAV2) capsid gene and generation of AAV2 vectors targeted to alternative cell-surface receptors. *Hum Gene Ther* 12(14), 1697-711.

Shi, W., and Bartlett, J. S. (2003). RGD inclusion in VP3 provides adeno-associated virus type 2 (AAV2)-based vectors with a heparan sulfate-independent cell entry mechanism. *Mol Ther* 7(4), 515-25.

Snyder, R. O., Im, D. S., and Muzyczka, N. (1990). Evidence for covalent attachment of the adeno-associated virus (AAV) rep protein to the ends of the AAV genome. *J Virol* 64(12), 6204-13.

Snyder, R. O., Miao, C. H., Patijn, G. A., Spratt, S. K., Danos, O., Nagy, D., Gown, A. M., Winther, B., Meuse, L., Cohen, L. K., Thompson, A. R., and Kay, M. A. (1997). Persistent and therapeutic concentrations of human factor IX in mice after hepatic gene transfer of recombinant AAV vectors. *Nat Genet* 16(3), 270-6.

Sodeik, B., Ebersold, M. W., and Helenius, A. (1997). Microtubule-mediated transport of incoming herpes simplex virus 1 capsids to the nucleus. *J Cell Biol* 136(5), 1007-21.

Sonnichsen, B., De Renzis, S., Nielsen, E., Rietdorf, J., and Zerial, M. (2000). Distinct membrane domains on endosomes in the recycling pathway visualized by multicolor imaging of Rab4, Rab5, and Rab11. *J Cell Biol* 149(4), 901-14.

Srivastava, A., Lusby, E. W., and Berns, K. I. (1983). Nucleotide sequence and organization of the adeno-associated virus 2 genome. *J Virol* 45(2), 555-64.

Suikkanen, S., Aaltonen, T., Nevalainen, M., Valilehto, O., Lindholm, L., Vuento, M., and Vihinen-Ranta, M. (2003). Exploitation of microtubule cytoskeleton and dynein during parvoviral traffic toward the nucleus. *J Virol* 77(19), 10270-9.

Summerford, C., Bartlett, J. S., and Samulski, R. J. (1999). AlphaVbeta5 integrin: a co-receptor for adeno-associated virus type 2 infection. *Nat Med* 5(1), 78-82.

Summerford, C., and Samulski, R. J. (1998). Membrane-associated heparan sulfate proteoglycan is a receptor for adeno-associated virus type 2 virions. *J Virol* 72(2)**,** 1438-45.

Suomalainen, M., Nakano, M. Y., Keller, S., Boucke, K., Stidwill, R. P., and Greber, U. F. (1999). Microtubule-dependent plus- and minus end-directed motilities are competing processes for nuclear targeting of adenovirus. *J Cell Biol* 144(4)**,** 657-72.

Theiss, H. D., Kofler, D. M., Buning, H., Aldenhoff, A. L., Kaess, B., Decker, T., Baumert, J., Hallek, M., and Wendtner, C. M. (2003). Enhancement of gene transfer with recombinant adeno-associated virus (rAAV) vectors into primary B-cell chronic lymphocytic leukemia cells by CpG-oligodeoxynucleotides. *Exp Hematol* 31(12)**,** 1223-9.

Vafaie, J., and Schwartz, R. A. (2004). Parvovirus B19 infections. *Int J Dermatol* 43(10)**,** 747-9.

Vailhe, B., Vittet, D., and Feige, J. J. (2001). In vitro models of vasculogenesis and angiogenesis. *Lab Invest* 81(4)**,** 439-52.

Vihinen-Ranta, M., Kalela, A., Makinen, P., Kakkola, L., Marjomaki, V., and Vuento, M. (1998). Intracellular route of canine parvovirus entry. *J Virol* 72(1)**,** 802-6.

Ward, B. M. (2004). Pox, dyes, and videotape: making movies of GFP-labeled vaccinia virus. *Methods Mol Biol* 269**,** 205-18.

Warrington, K. H., Jr., Gorbatyuk, O. S., Harrison, J. K., Opie, S. R., Zolotukhin, S., and Muzyczka, N. (2004). Adeno-associated virus type 2 VP2 capsid protein is nonessential and can tolerate large peptide insertions at its N terminus. *J Virol* 78(12)**,** 6595-609.

Weitzman, M. D., Kyostio, S. R., Kotin, R. M., and Owens, R. A. (1994). Adeno-associated virus (AAV) Rep proteins mediate complex formation between AAV DNA and its integration site in human DNA. *Proc Natl Acad Sci U S A* 91(13)**,** 5808-12.

Wistuba, A., Kern, A., Weger, S., Grimm, D., and Kleinschmidt, J. A. (1997). Subcellular compartmentalization of adeno-associated virus type 2 assembly. *J Virol* 71(2)**,** 1341-52.

Wistuba, A., Weger, S., Kern, A., and Kleinschmidt, J. A. (1995). Intermediates of adeno-associated virus type 2 assembly: identification of soluble complexes containing Rep and Cap proteins. *J Virol* 69(9)**,** 5311-9.

Wobus, C. E., Hugle-Dorr, B., Girod, A., Petersen, G., Hallek, M., and Kleinschmidt, J. A. (2000). Monoclonal antibodies against the adeno-associated virus type 2 (AAV-2) capsid: epitope mapping and identification of

capsid domains involved in AAV-2-cell interaction and neutralization of AAV-2 infection. *J Virol* 74(19)**,** 9281-93.

Wolfstein, A., Nagel, C. H., Radtke, K., Dohner, K., Allan, V. J., and Sodeik, B. (2006). The inner tegument promotes herpes simplex virus capsid motility along microtubules in vitro. *Traffic* 7(2)**,** 227-37.

Wu, P., Xiao, W., Conlon, T., Hughes, J., Agbandje-McKenna, M., Ferkol, T., Flotte, T., and Muzyczka, N. (2000). Mutational analysis of the adeno-associated virus type 2 (AAV2) capsid gene and construction of AAV2 vectors with altered tropism. *J Virol* 74(18)**,** 8635-47.

Xiao, W., Chirmule, N., Berta, S. C., McCullough, B., Gao, G., and Wilson, J. M. (1999). Gene therapy vectors based on adeno-associated virus type 1. *J Virol* 73(5)**,** 3994-4003.

Xiao, W., Chirmule, N., Schnell, M. A., Tazelaar, J., Hughes, J. V., and Wilson, J. M. (2000). Route of administration determines induction of T-cell-independent humoral responses to adeno-associated virus vectors. *Mol Ther* 1(4)**,** 323-9.

Xiao, W., Warrington, K. H., Jr., Hearing, P., Hughes, J., and Muzyczka, N. (2002). Adenovirus-facilitated nuclear translocation of adeno-associated virus type 2. *J Virol* 76(22)**,** 11505-17.

Xiao, X., Li, J., and Samulski, R. J. (1996). Efficient long-term gene transfer into muscle tissue of immunocompetent mice by adeno-associated virus vector. *J Virol* 70(11)**,** 8098-108.

Xiao, X., Li, J., and Samulski, R. J. (1998). Production of high-titer recombinant adeno-associated virus vectors in the absence of helper adenovirus. *J Virol* 72(3)**,** 2224-32.

Xie, Q., Bu, W., Bhatia, S., Hare, J., Somasundaram, T., Azzi, A., and Chapman, M. S. (2002). The atomic structure of adeno-associated virus (AAV-2), a vector for human gene therapy. *Proc Natl Acad Sci U S A* 99(16)**,** 10405-10.

Yakobson, B., Hrynko, T. A., Peak, M. J., and Winocour, E. (1989). Replication of adeno-associated virus in cells irradiated with UV light at 254 nm. *J Virol* 63(3)**,** 1023-30.

Yakobson, B., Koch, T., and Winocour, E. (1987). Replication of adeno-associated virus in synchronized cells without the addition of a helper virus. *J Virol* 61(4)**,** 972-81.

Yalkinoglu, A. O., Zentgraf, H., and Hubscher, U. (1991). Origin of adeno-associated virus DNA replication is a target of carcinogen-inducible DNA amplification. *J Virol* 65(6)**,** 3175-84.

Yan, Z., Zak, R., Luxton, G. W., Ritchie, T. C., Bantel-Schaal, U., and Engelhardt, J. F. (2002). Ubiquitination of both adeno-associated virus type 2 and 5 capsid

proteins affects the transduction efficiency of recombinant vectors. *J Virol* 76(5)**,** 2043-53.

Yang, Q., Mamounas, M., Yu, G., Kennedy, S., Leaker, B., Merson, J., Wong-Staal, F., Yu, M., and Barber, J. R. (1998). Development of novel cell surface CD34-targeted recombinant adenoassociated virus vectors for gene therapy. *Hum Gene Ther* 9(13)**,** 1929-37.

Zádori, Z., Szelei, J., Lacoste, M. C., Li, Y., Gariepy, S., Raymond, P., Allaire, M., Nabi, I. R., and Tijssen, P. (2001). A viral phospholipase A2 is required for parvovirus infectivity. *Dev Cell* 1(2)**,** 291-302.

Zolotukhin, S., Byrne, B. J., Mason, E., Zolotukhin, I., Potter, M., Chesnut, K., Summerford, C., Samulski, R. J., and Muzyczka, N. (1999). Recombinant adeno-associated virus purification using novel methods improves infectious titer and yield. *Gene Ther* 6(6)**,** 973-85.

7. Supplemental information on CD-Rom

7.1 Movies

Movie 1: supplement of chapter 2.1.4

Movies 2-4: supplement of chapter 2.1.10

For detailed movie legend and links to the movies please refer to the HTML document on CD-Rom. (The CD-Rom is attached to the last page of the thesis.)

7.2 PDF files from publications

Lux et al. 2005: "Green flourescent protein-tagged adeno-associated virus particles allow the study of cytosolic and nuclear trafficking"

Perabo and Endell et al. 2006: "Combinatorial engineering of a gene therapy vector: directed evolution of adeno-associated virus"

7.3 PDF file from PhD thesis

Curriculum Vitae

Kerstin Lux

Persönliche Daten

Geburtsdatum:	20. Mai 1977
Geburtsort:	Würzburg
Familienstand:	ledig
Staatsangehörigkeit:	deutsch

Schulausbildung und Studium

1987 - 1996	Feodor-Lynen-Gymnasium in Planegg Abschluss: Allgemeine Hochschulreife
1996 - 2003	Studium der Biologie an der LMU München
1999 - 2000	DAAD Stipendium für einen einjährigen Studienaufenthalt an der Universidad de Concepción, Chile
2002 - 2003	Diplomarbeit im Arbeitskreis von Prof. Dr. Michael Hallek mit dem Titel: „Etablierung von Markierungsmethoden für fluoreszenz-mikroskopische Untersuchung der AAV2-Infektionsbiologie unter besonderer Betrachtung der intrinsischen Phospholipase A2-Aktivität"
Februar 2003	Diplom der Biologie
2003 - 2006	Promotionsarbeit am Genzentrum der LMU München in der Arbeitsgruppe von Prof. Dr. Michael Hallek mit dem Titel: „Visualization of the intracellular trafficking of incoming Adeno-associated virus type 2"

Publikationen

Lux K., Goerlitz N., Schlemminger S., Perabo L., Goldnau D., Endell J., Leike K., Kofler D. M., Finke S., Hallek M., and Büning H. (2005). Green fluorescent protein-tagged adeno-associated virus particles allow the study of cytosolic and nuclear trafficking. *J Virol* 79(18)**,** 11776-87.

Perabo L., Endell J., King S., **Lux K.,** Goldnau D., Hallek M., and Büning H. (2006). Combinatorial engineering of a gene therapy vector: directed evolution of adeno-associated virus. *J Gene Med* 8(2)**,** 155-62.

Teilnahme an nationalen und internationalen Kongressen

Gesellschaft für Virologie joint meeting with Società Italiana di Virologia, Tübingen (2004)
  Posterpräsentation: Incorporation of the green fluorescent protein into the adeno-associated type 2 capsid

11. Jahrestagung der Deutschen Gesellschaft für Gentherapie and 2. workshop „viral vectors" der Gesellschaft für Virologie, Frankfurt (2004)
  Vortrag: Incorporation of the green fluorescent protein into the adeno-associated type 2 capsid

8th annual meeting of the American Society of Gene Therapy, St. Louis, USA (2005)
  Posterpräsentation: GFP-tagged adeno-associated virus particles allow the study of cytosolic and nuclear traffic

Jahrestagung der Gesellschaft für Virologie, München (2006)
  Vortrag: Uncoating takes place before or during nuclear entry